



HAL
open science

A contribution to the multi-link propagation channel modeling for 4G radio mobile relaying systems

Quang Hien Chu

► **To cite this version:**

Quang Hien Chu. A contribution to the multi-link propagation channel modeling for 4G radio mobile relaying systems. Networking and Internet Architecture [cs.NI]. Télécom ParisTech, 2011. English. NNT: . pastel-00683133

HAL Id: pastel-00683133

<https://pastel.hal.science/pastel-00683133>

Submitted on 27 Mar 2012

HAL is a multi-disciplinary open access archive for the deposit and dissemination of scientific research documents, whether they are published or not. The documents may come from teaching and research institutions in France or abroad, or from public or private research centers.

L'archive ouverte pluridisciplinaire **HAL**, est destinée au dépôt et à la diffusion de documents scientifiques de niveau recherche, publiés ou non, émanant des établissements d'enseignement et de recherche français ou étrangers, des laboratoires publics ou privés.



EDITE - ED 130

Doctorat ParisTech

THÈSE

pour obtenir le grade de docteur délivrée par

TELECOM ParisTech

Spécialité « **Électronique et Communications** »

présentée et soutenue publiquement par

Quang Hien CHU

le 8 décembre 2011

A contribution to the multi-link propagation channel modeling for 4G radio mobile relaying systems

Directeur de thèse : **Jean-Christophe COUSIN**
Co-encadrement de la thèse : **Jean-Marc CONRAT**

Jury

Mme. Martine LIÉNARD , Professeur, Université de Lille 1	Rapporteur
M. Claude OESTGES , Professeur, Université Catholique de Louvain	Rapporteur
M. Aziz BENLARBI-DELAÏ , Professeur, Université Pierre et Marie Curie	Examineur
M. David CARSENAT , Enseignant Chercheur, Université de Limoges	Examineur
M. Bernard HUYART , Professeur, Télécom ParisTech	Examineur
M. Jean-Christophe COUSIN , Maître de Conférences, Télécom ParisTech	Directeur de thèse
M. Jean-Marc CONRAT , Ingénieur de Recherche, Orange Labs Belfort	Co-encadrant de thèse

*To my parents,
to my wife and my daughter,
to my nephews and nieces,
and to my great family.*

–Belfort, 2011–

Acknowledgements

The PhD programme is one of the greatest and the most enjoyable challenges I have ever had. After three hard working years, I find myself stronger by facing to problems and learning how to overcome them. However, despite all my efforts, it would not have been possible to write this doctoral thesis without the help and support of many people, to only some of whom I can give particular mention here.

Above all, I would like to express my deepest gratitude to my parents and my wife for their endless loves and supports, as always, for which my mere expressions of gratitude are not enough. Besides, my beloved young daughter has always been there with her smiles giving me powers to go until the end of this adventure. At this moment I am also thinking about my family in Vietnam : my brothers and my sisters are my endless supports, my nephews and nieces are my endless joys, my grandfather is waiting for me coming home with the doctoral degree. This doctoral thesis is dedicated to them.

This thesis would not have been possible without the guidance and support of my supervisor in Orange Labs Belfort, Mr Jean-Marc Conrat. His availability, patience, help and permanent encouragement in both academical and personal life are invaluable to me, for which I am extremely grateful. I would like also to thank my supervisor in Télécom ParisTech, Mr Jean-Christophe Cousin. His advices, support and friendship are indispensable for the success of this thesis.

I am very grateful to Mr Aziz Benlarbi-Delaiï, Mr David Carsenat, Mr Bernard Huyart, Mme Martine Liénard and Mr Claude Oestges for accepting to take part in my dissertation committee. Their precious remarks and advices are greatly useful for me and for the improvements of this thesis.

I would like to acknowlegde France Télécom R&D - Orange Labs and its staffs for providing me the financial and logistic support during the whole three years of my PhD programme. I really appreciate the efficient cooperation and the warm friendship that the staff members of laboratory WEP (Wireless Engineering Propagation) - Orange Labs Belfort have given to me. Especially, I would like to thank Mr Pierre Dekyndt and Mr Daniel Milli for welcoming

me in their laboratory. I would like also present my acknowledgment to Mr Laurent Cartier, Mr Philippe Brun and the measurement team for their great help and contribution to the measurement campaigns.

I would like to dedicate a special thank to the Toinens, especially Ann-mie and Christian, for all the wonderful things they have done for me. They will always rest in my heart as the most beautiful souvenir that I have during my four unforgettable years in France.

Thank you Laurent for the excellent friendship that you've given to us. I'll never forget the trips in Alsace and Ardèche that we made together.

My three years in Belfort would not have been so enjoyable without my friends. Thank you Philippe, Edgard, Ali, Michel, Ramzi, Mathieu and others for nice moments that we have shared together. I would like also to thank my vietnamese friends in France (Hieu, Minh, Tuan, Nam, Thai, Chi, Hai) and elsewhere for always supporting me.

Finally, I would like to thank everyone who is not mentioned here but has contributed to the fulfilment of this thesis.

Résumé

Les progrès technologiques pour les réseaux radiomobiles ont augmenté régulièrement l'efficacité spectrale au cours des dernières années. Cependant, cet accroissement de performance ne représente que l'augmentation du débit maximal théorique. En effet, les performances crêtes ne sont obtenues que pour des conditions de propagation très favorables, typiquement lorsque l'utilisateur est relativement proche de la station de base (BS). Depuis quelques années, de nombreux travaux proposent des solutions permettant de réduire les écarts de débit entre utilisateurs sur une cellule (technique à relais, coopération de station de base, annulation d'interférence, ...). Dans le cadre de cette thèse, nous nous intéressons aux techniques à relais telles qu'elles ont été définies pour le LTE-Advanced dans le cadre du 3GPP.

L'évaluation des performances des nouvelles technologies radio s'effectuent généralement grâce à des simulations qui nécessitent une modélisation du canal de propagation. L'objectif de cette thèse est d'améliorer les modèles de canaux de propagation dédiés aux scénarios à relais en insistant sur les modèles de path loss, la corrélation de shadowing et l'impact de la hauteur du relais. Pour cela, une campagne de mesures avec relais a été effectuée dans des environnements urbains.

Quelques modèles de path loss existants tels que les modèles WINNER, 3GPP et COST-231 WI ont été comparés et confrontés aux résultats de mesures, particulièrement pour le lien entre la station de base et le relais (RS).

Concernant l'impact de la hauteur du relais, une augmentation de puissance sur le lien BS-RS a été observée lorsque la hauteur du relais s'accroît. Cette tendance n'a pas été mise en évidence sur le lien entre le relais et le mobile (MS). La variation de puissance en fonction de la hauteur dépend des positions des relais et de la position du mobile par rapport au relais. Cette diversité pourrait être due aux particularités de l'environnement local entourant les relais.

La corrélation de shadowing entre les liens BS-MS/RS-MS ou RS-MS/RS-MS dans un système avec relais a été étudiée et modélisée. Ce travail a démontré la relation entre la corrélation de shadowing et plusieurs paramètres physiques tels que la hauteur du relais, la distance de séparation des émetteurs (BS ou RS) et l'angle entre deux émetteurs vu depuis le mobile.

Finalement, les aspects cohérence des canaux de propagation ont été succinctement abordés en prenant le modèle WINNER comme exemple.

Mots-clés : *4G, propagation, relais, modèles de path loss, corrélation de shadowing, hauteur d'antenne de relais*

Abstract

Advanced technologies in radio mobile systems have steadily increased the spectral efficiency over years. However, these technologies greatly increase only the peak data rate but not the cell-edge one. Indeed, the peak data rate can only be obtained in the most favorable propagation conditions, typically when users are relatively close to the Base Station (BS). Much research has been carried out for several years in order to reduce the performance differences among users in a cell. Several technical solutions have been proposed such as relays, base station cooperation, interference cancellation, etc. As part of this thesis, we focus on the relaying technology which is one of the key features of 3GPP LTE-Advanced.

The performance of latest technologies has generally been evaluated by system simulations which require a reliable propagation channel model. This thesis aims to improve existing channel models dedicated to relaying scenarios with a particular focus on path loss models, shadow fading correlation and relay antenna height impact. To this end, a multi-link measurement campaign with relays has been carried out in outdoor urban areas.

The existing path loss models proposed by WINNER, 3GPP and COST-231 WI have been compared with our measurement data. A particular attention has been paid for the link between the BS and relay station (RS) which has not been adequately studied yet.

Concerning the relay antenna height impact, an increasing trend of BS-RS link received powers has been observed when the relay antenna height has been raised. However, this trend has not been shown in RS-MS link. The dependence of the received power on the relay height varies among relay locations and depends also on the RS-MS distance. This diversity could be due to the particularities of the local environments surrounding the relay. Further investigations are necessary in order to clarify this issue.

The correlation of shadow fading between BS-MS/RS-MS links or between two RS-MS links in a relaying system has also been studied and modeled. This study has demonstrated the relationship between the shadow fading correlation and several parameters such as the relay antenna height, the separation distance between transmitters and the angle between two transmitters viewed from the mobile station.

Finally, the consistent aspects of path loss propagation channels have been briefly discussed.

Keywords: *4G, propagation, relay, path loss model, shadow fading correlation, relay antenna height*

Contents

Acknowledgements	i
Résumé	iii
Abstract	iv
List of Figures	ix
List of Tables	xiii
List of Abbreviations	xv
Introduction	1
1 Relaying technology in 4G radio mobile systems	7
1.1 Evolution of radio mobile systems	7
1.2 New technology features for LTE-Advanced	12
1.2.1 The challenges	12
1.2.2 Bandwidth extension	13
1.2.3 Enhanced MIMO schemes	14
1.2.4 Coordinated Multi-point Transmission/Reception (CoMP)	15
1.2.5 Relaying	16
1.2.5.1 Overview	16
1.2.5.2 Relaying technologies in 3GPP LTE-Advanced standards	19
1.3 Conclusion	21
2 Wireless propagation channels	23
2.1 Radio wave propagation fundamentals	23
2.1.1 Multipath propagation	23
2.1.2 Three scales of propagation signal variation	25
2.1.2.1 Path loss	25

	2.1.2.2	Shadow Fading	27
	2.1.2.3	Fast fading	27
2.2		Path loss models	29
	2.2.1	Overview	29
	2.2.2	Okumura-Hata model	30
	2.2.3	COST-231 model	31
	2.2.3.1	COST-231 Hata model	31
	2.2.3.2	COST-231 Walfish-Ikegami model	32
	2.2.4	ITU-R P.1411 models	35
	2.2.4.1	Path loss model for LOS urban areas	35
	2.2.4.2	Path loss model for NLOS urban area with over-rooftop propagation	36
	2.2.4.3	Path loss model for NLOS urban areas with propagation within street canyons for frequency range from 800 MHz to 2000 MHz	39
	2.2.5	WINNER models	40
	2.2.5.1	Supported scenarios	41
	2.2.5.2	Path loss models	42
	2.2.6	IEEE 802.16j models	44
	2.2.6.1	Type E path loss model	44
	2.2.6.2	Type F path loss model	44
	2.2.6.3	Type H path loss model	47
	2.2.7	3GPP models	47
	2.2.8	Summary and discussion	49
2.3		Shadow fading models	53
	2.3.1	Shadow fading correlation models for traditional radio mobile network	54
	2.3.1.1	Angle-only models	54
	2.3.1.2	Angle-distance models	55
	2.3.1.3	Angle-distance ratio models	56
	2.3.1.4	Saunders model	57
	2.3.2	Shadow fading correlation models for relay-based radio mobile network	57
2.4		Conclusion	58
3		Measurement campaign	59
	3.1	Measurement scenario	59
	3.2	System construction	60
	3.3	Measurement operation	62
	3.3.1	Measurement phase I	62
	3.3.2	Measurement phase II	65

3.4	Data processing	66
3.4.1	Measurement route localization	66
3.4.2	Data averaging	67
3.4.3	Measurement route synchronization	70
3.5	Measurement validation	75
3.5.1	Antenna validation	75
3.5.2	Localization validation	76
3.5.3	Total measurement validation	78
3.5.4	Discussion	80
3.6	Conclusion	80
4	Multi-link characterization and modeling	81
4.1	BS-RS link characterization and modeling	81
4.1.1	Introduction	81
4.1.2	Relay antenna height impacts on BS-RS link path loss	82
4.1.3	Extended research on the impact of relay antenna height	84
4.1.3.1	Measurement descriptions	85
4.1.3.2	Received power dependence on floor level . .	87
4.1.3.3	Conclusion	89
4.1.4	Path loss models for BS-RS propagation link	89
4.1.4.1	Validation of existing path loss models	89
4.1.4.2	Proposed path loss model	92
4.2	BS-MS link characterization and modeling	94
4.3	RS-MS link characterization and modeling	97
4.3.1	Propagation condition classification	97
4.3.2	RS-MS link characterization in NLOS conditions	98
4.3.2.1	RS antenna height impact on RS-MS NLOS link path loss	99
4.3.2.2	RS-MS NLOS link path loss characterization	101
4.3.2.3	Discussions	102
4.3.3	RS-MS link characterization in LOS conditions	103
4.3.3.1	RS antenna height impact on RS-MS LOS link path loss	103
4.3.3.2	RS-MS LOS link path loss characterization .	106
4.4	Shadow fading correlation characterization and modeling . . .	107
4.4.1	Shadow fading characterization	107
4.4.2	Shadow fading correlation characterization	109
4.4.2.1	General characterization	109
4.4.2.2	Dependence of shadow fading correlation on the angle (θ)	111
4.5	Path loss consistency	114

4.6 Conclusion	114
Conclusion and Perspectives	117
A LOS/OLOS/NLOS classification for all RS-MS links	121
B RS-MS link path loss in NLOS conditions	131
C RS-MS link path loss in LOS conditions	135
Personal publications	141
Bibliography	155

List of Figures

1.1	Evolution of radio mobile systems	8
1.2	Cell-edge problem in radio mobile systems	13
1.3	LTE-Advanced key features	13
1.4	A continuous carrier aggregation example	14
1.5	SU-MIMO and MU-MIMO examples	15
1.6	An example of CoMP with 3 collaborating cells	17
1.7	Fixed Relay vs Mobile Relay	19
2.1	Basic propagation mechanisms	24
2.2	Multipath propagation	25
2.3	Three scales of radio mobile signal variation	26
2.4	Rayleigh pdf with different values of σ	28
2.5	Rice pdf with different values of K	29
2.6	Parameters of COST-231 Walfish-Ikegami model	32
2.7	Street orientation definition	33
2.8	ITU-R P.1411 propagation scenarios	35
2.9	Parameter definitions for propagation within street canyons	40
2.10	Definition of d_1 and d_2 for B1 path loss model	41
2.11	Street geometry used for Berg model	46
2.12	Shadow fading definition	53
2.13	Shadow fading correlation parameters	55
3.1	Measurement scenario	60
3.2	BS, RS and MS equipments	61
3.3	Isolation problem at RS	62
3.4	Radio configuration at BS, RS and MS	63
3.5	RS locations at Train Station area	64
3.6	RS locations at Old Town area	64
3.7	RS locations and measurement route at Train Station area	65
3.8	RS locations and measurement route at Old Town area	66
3.9	Data processing steps for BS-MS/RS-MS measurements	67

3.10	A localization procedure example	68
3.11	Averaging procedure of measurement signal	69
3.12	Averaged data with different W and D in comparison with raw measurement data	70
3.13	A measurement section performed with RS4 and its 3 antenna heights	71
3.14	An example of erroneous section removal	72
	(a) Before	72
	(b) After	72
3.15	Pairing procedure illustration	73
3.16	MS antenna measured path loss displayed against RS antenna measured one	76
3.17	15 processed data of BS-MS links in Train Station area	77
3.18	15 processed data of BS-MS links in Old Town area	77
3.19	An shifting problem example	78
3.20	Histogram of <i>diff_all</i> and <i>diff_point</i>	79
4.1	Impact of RS antenna height on BS-RS path loss	83
4.2	Empirical CDF of measured path loss at different RS antenna height	83
4.3	Histogram of path loss difference between RS antenna heights	84
4.4	Measurement campaign environment	85
4.5	Photos of Tx antenna and Rx set-up with rotating device	86
4.6	Measurement positions at the ground level	87
4.7	Received power dependence on floor level	88
4.8	Aerial photos showing reception building facades with different propagation conditions.	89
4.9	Received power dependence on floor level	90
4.10	Path loss predicted by WINNER B5f, 3GPP Relay and COST-231 WI models in comparison with the measurements	91
4.11	Proposed path loss model prediction in comparison with the measurements	93
4.12	Proposed path loss model prediction in comparison with the measurements at facade 2 in the additional measurement campaign	94
4.13	Path loss predicted by the COST-231 WI, 3GPP Urban Macro, 3GPP BS-MS Relay and WINNER Urban Macro in comparison with the measurements in Train Station area	95
4.14	Path loss predicted by the COST-231 WI, 3GPP Urban Macro, 3GPP BS-MS Relay and WINNER Urban Macro in comparison with the measurements in Old Town area	96

4.15	An example of LOS/OLOS/NLOS classification	98
4.16	An example of LOS/OLOS/NLOS points displayed on the satellite photo	99
4.17	RS2-MS NLOS path loss with 3 relay antenna heights	100
4.18	RS7-MS NLOS path loss with 3 RS antenna heights	100
4.19	RS1-MS NLOS path loss with 3 RS antenna heights	101
4.20	RS1-MS LOS path loss with 3 RS antenna heights	103
4.21	Antenna radiation pattern effects on path loss	104
4.22	Simulation of Antenna radiation pattern and propagation dis- tance effects on path loss	105
4.23	RS7-MS LOS path loss with 3 RS antenna heights	106
4.24	Measured SF distribution	108
4.25	SF of RS1-MS link measured with 3 antenna heights	110
4.26	Dependence of SF correlation on the transmitter separation distance	112
4.27	Angular groups for SF correlation calculation	113
4.28	Measured SF correlation vs. angle θ	114
A.1	LOS/OLOS/NLOS classification for RS1-MS link	122
A.2	RS1-MS LOS/OLOS/NLOS measurement points	122
A.3	LOS/OLOS/NLOS classification for RS2-MS link	123
A.4	RS2-MS LOS/OLOS/NLOS measurement points	123
A.5	LOS/OLOS/NLOS classification for RS4-MS link	124
A.6	RS4-MS LOS/OLOS/NLOS measurement points	124
A.7	LOS/OLOS/NLOS classification for RS5-MS link	125
A.8	RS5-MS LOS/OLOS/NLOS measurement points	125
A.9	LOS/OLOS/NLOS classification for RS6-MS link	126
A.10	RS6-MS LOS/OLOS/NLOS measurement points	126
A.11	LOS/OLOS/NLOS classification for RS7-MS link	127
A.12	RS7-MS LOS/OLOS/NLOS measurement points	127
A.13	LOS/OLOS/NLOS classification for RS8-MS link	128
A.14	RS8-MS LOS/OLOS/NLOS measurement points	128
A.15	LOS/OLOS/NLOS classification for RS9-MS link	129
A.16	RS9-MS LOS/OLOS/NLOS measurement points	129
A.17	LOS/OLOS/NLOS classification for RS10-MS link	130
A.18	RS10-MS LOS/OLOS/NLOS measurement points	130
B.1	RS3-MS NLOS path loss with 3 RS antenna heights	131
B.2	RS4-MS NLOS path loss with 3 RS antenna heights	132
B.3	RS5-MS NLOS path loss with 3 RS antenna heights	132
B.4	RS6-MS NLOS path loss with 3 RS antenna heights	133

B.5	RS8-MS NLOS path loss with 3 RS antenna heights	133
B.6	RS9-MS NLOS path loss with 3 RS antenna heights	134
B.7	RS10-MS NLOS path loss with 3 RS antenna heights	134
C.1	RS2-MS LOS path loss with 3 RS antenna heights	135
C.2	RS3-MS LOS path loss with 3 RS antenna heights	136
C.3	RS4-MS LOS path loss with 3 RS antenna heights	136
C.4	RS5-MS LOS path loss with 3 RS antenna heights	137
C.5	RS6-MS LOS path loss with 3 RS antenna heights	137
C.6	RS8-MS LOS path loss with 3 RS antenna heights	138
C.7	RS9-MS LOS path loss with 3 RS antenna heights	138
C.8	RS10-MS LOS path loss with 3 RS antenna heights	139

List of Tables

1.1	Overview of the principal 3GPP radio mobile systems	11
1.2	Types of 3GPP Release 10 LTE-Advanced relay	21
2.1	Path loss exponents	27
2.2	Summary of IEEE 802.16 Path loss models	45
2.3	3GPP relaying path loss models	49
2.4	NLOS path loss model summary	51
2.5	LOS path loss model summary	52
2.6	Shadow fading correlation model proposed by Zayana et al.	57
3.1	Details of measurement routes with RS4	71
3.2	BS-MS measurement data	74
4.1	Prediction error statistics of COST-231 WI model	91
4.2	Prediction error statistics of proposed model	92
4.3	BS-MS model prediction error statistics in comparison with measurements	96
4.4	Typical models for LOS and NLOS radio mobile channels	97
4.5	Measured path loss error mean (μ) and standard deviation (σ) in comparison with the linear fit	102
4.6	Measured σ_{SF} in comparison with model-proposed ones	109
4.7	Shadow fading correlation between different links in Tran Sta- tion area	111
4.8	Shadow fading correlation between different links in Old Town area	111

List of Abbreviations

1xEVDO	Evolution-Data Optimized
3GPP	Third Generation Global Partnership Project
8PSK	Eight-Phase Shift Keying
A	
AF	Amplify and Forward
AMPS	Advanced Mobile Phone Service
ARIB	Association of Radio Industries and Businesses
ATIS	Alliance for Telecommunications Industry Solutions
B	
BS	Base Station
C	
CCSA	China Communications Standards Association
CDF	Cumulative Distribution Function
CDMA	Code Division Multiple Access
CoMP	Coordinated Multi Point Transmission /Reception
COST	European Cooperation in Science and Technology
D	
DL	Down Link
DF	Decode and Forward
E	
EDGE	Enhanced Data Rates for Global Evolution
eNB	Evolution Node B
ETSI	European Telecommunications Standards Institute

F

FDD	Frequency Division Duplex
FDMA	Frequency Division Multiple Access
FRN	Fixed Relay Node

G

GMSK	Gaussian Minimum Shift Keying
GPRS	General Packet Radio Services
GSM	Global System for Mobile Communications

H

HSDPA	High Speed Downlink Packet Access
HSPA	High Speed Packet Access
HSUPA	High Speed Uplink Packet Access

I

ICI	Inter-cell Interference
IEEE	Institute of Electrical and Electronics Engineers
IMT	International Mobile Telecommunication
IMT-A	International Mobile Telecommunications - Advanced
ITU	International Telecommunication Union

L

LOS	Line-of-Sight
LTE-A	Long Term Evolution - Advanced

M

MIMO	Multi-Input-Multi-Output
MPC	Multi Path Component
MRN	Mobile Relay Node
MS	Mobile Station
MU-MIMO	Multi-User Multi-Input-Multi-Output

N

NLOS	Non-Line-of-Sight
NMT	Nordic Mobile Telephone

O

OFDMA	Orthogonal Frequency Division Multiple Access
OLOS	Obstructed-Line-of-Sight

P

pdf Probability Density Function

Q

QAM Quadrature Amplitude Modulation

QoS Quality of Service

QPSK Quadrature Phase Shift Keying

R

RS Relay Station

Rx Receiver

S

SC-FDMA Single Carrier-Frequency Division Multiple Access

SINR Signal to Interference plus Noise Ratio

SIR Signal to Interference Ratio

SU-MIMO Singer-User Multi-Input-Multi-Output

T

TACS Total Access Communication System

TDD Time Division Duplex

TDMA Time Division Multiple Access

Tx Transmitter

U

UE User Equipment

UMTS Universal Mobile Telecommunications System

UL Up Link

UTRAN UMTS Terrestrial Radio Access Network

UTRA Universal Terrestrial Radio Access

V

VoD Video on Demand

W

WCDMA Wideband Code Division Multiple Access

WiMAX Worldwide Interoperability for Microwave Access

WINNER Wireless World Initiative New Radio

Introduction

The world over the last twenty years witnesses the remarkable development of radio mobile communication systems. While the early systems e.g. GSM (*Global System for Mobile Communications*) or cdmaOne (*Code Division Multiple Access - One*) are only capable of providing data rates on the order of few ten kbps, the recent evolutions such as 3GPP LTE (*The 3rd Generation Partnership Project - Long Term Evolution*) or WIMAX (*Worldwide Interoperability for Microwave Access*) provide a data rate of up to several hundred Mbps. With increasing demands for various data and multimedia services, future mobile communication systems should be able to provide even higher data rates over a limited spectrum bandwidth.

Some advanced radio transmission techniques, including MIMO (*Multiple-Input-Multiple-Output*) and OFDM (*Orthogonal Frequency Division Multiplex*) have been proposed to improve the spectrum efficiency of mobile cellular systems. While these advanced technologies greatly increase the peak data rate, that in the cell-edge area can only be slightly improved. Indeed, the peak data rate can only be obtained in the most favorable propagation conditions, typically when users are relatively close to the Base Station (BS). When users move far away from BS to the cell-edge area, the actual achievable data rate rapidly decreases. The gap between the peak and cell-edge data rates could be up to hundreds of times [1]. This performance degradation is essentially due to the severe path loss and the inter-cell interference. The cell edge problem will be even more serious in future mobile communications, because radio frequency higher than 2 GHz will be exploited [2]. This explains why much research has been carried out for the last few years in order to reduce the performance differences among users in a cell. Several technical solutions have been proposed such as relays, base station cooperation, interference cancellation, etc. As part of this thesis, we focus on the relaying technology.

Relaying technologies have received much interest from standardization bodies for next generation (4G) radio mobile communication systems such as 3GPP LTE-Advanced, IEEE 802.16m, etc. They have also been widely

investigated by both academic and industrial researchers [3–37]. A large number of papers focusing on technical aspects of relays can be found in the literature. The capacity benefits of relays have been analyzed in [6, 16–18, 21, 25, 27, 38]. References [3, 7, 13, 18, 21, 23, 38] consider the coverage extension obtained with relay deployments. Throughput and data rate enhancements have been discussed in [4, 5, 9, 29]. The interference management in a relay-based network have been studied in [12, 15, 32, 35, 36, 39, 40]. In conclusion, relays have been shown as a greatly attractive solution not only to solve the cell-edge problem but also improve the overall network performance.

However, most of these studies use theoretical analyses and simulations which take into account many different assumptions. To the author’s knowledge, very few measurement-based researches for outdoor urban macro-cell environment can be found in the literature. Therefore, the relay performance in a practical deployment has yet to be thoroughly validated.

Moreover, the real contribution of relays must be evaluated through simulation systems that incorporate a realistic propagation model. Many propagation channels have been defined by European projects and standardization bodies such as WINNER (*Wireless World Initiative New Radio*), 3GPP, ITU (*International Telecommunication Union*), IEEE (*Institute of Electrical and Electronics Engineers*), COST (*European Cooperation in Science and Technology*), etc. However, very few models are really dedicated to relaying scenarios. Furthermore, these models are essentially based on relatively limited data sets and/or specific assumptions and approximations.

In this context, Orange Labs has initiated since 2010 research activities concerning the relaying technologies. As part of these activities, this thesis has been carried out in order to assess the validation of the existing propagation models and provide new ones which are dedicated to relaying scenarios. These new models in addition to the data gathered with measurement campaigns will be used to evaluate the real contribution of relays in terms of cellular data rate and coverage homogeneousness.

This thesis aims to tackle the following concrete objectives:

- **Characterization and modeling of path loss and path loss model consistency:**

Relaying systems are expected to be deployed in various scenarios from improving the reliability of cellular networks to achieving high throughput in cell-edge area or to providing coverage extension [8, 22, 41]. Reliable propagation channel models for all links in a relay-based network i.e. BS-RS (Base Station - Relay Station), RS-MS (Relay Station - Mobile Station) and BS-MS are then necessary in order to design such systems. A number of propagation models have recently been suggested by 3GPP [41], WINNER project [42] and IEEE 802.16j task

group [43]. However, these models are basically derived from previous work and their validation in a realistic environment is yet to be fully examined.

Furthermore, the propagation channels in relaying systems should be coherent with each other. This consistency is crucial because an unbalance of channel models could lead to a wrong evaluation of relays' contribution. To the author knowledge, there is still no publication covering this channel consistency issue.

- **Investigation of relay antenna height impact on path loss models:**

The antenna height is a practical deployment parameter which has been actively studied for many years. In relaying scenarios, relays can be deployed in different heights varying from 5 meters e.g. lamppost to above 10 meters e.g. building wall. The challenge is to find the optimal relay antenna height in order to maximize the potential relay contributions. If the relay antenna height is enough high to create a "good" BS-RS radio link, it is more likely to cause more interference to adjacent cells. On the contrary, if the relay antenna is low, the interference may be reduced but the backhaul link capacity may not be sufficient causing the bottleneck problem. However, to the author's knowledge, the research concerning antenna height impacts concentrates principally on the impact of BS antenna height on BS-MS link [44, 45] in a conventional cellular network. To the author's knowledge, very few studies concern the link BS-RS in a relaying deployment. One of the rare papers can be found in [46] where Webb *et al.* presents a measurement-based study related to BS-RS link. This study proposes an antenna height correction factor modelled by the log-linear function. Nevertheless, the relay antenna height varies only in the range from 2 m to 5 m with 1 m steps. These heights are considered to be low compared to the proposed relaying scenarios [41, 42]. Reference [47] examines the path loss predicted by different models for IEEE Fixed Wireless Systems with two levels of receive antenna height. The analysis result demonstrates a 10 - 20 dB path loss reduction when the receive antenna is raised from 6 m to 10 m. Another research work concerning the impact of receive antenna height on link path loss is to be found in [48]. This paper reports that the path loss exponent reduces as the receive antenna height increases towards average rooftop level. However, only receive antenna height from 3 m to 7 m is considered in this study. Reference [49] shows the dependence of excess path loss on floor level but this study concentrates principally on the problem of outdoor to indoor penetration.

- **Shadow fading correlation characterization and modeling:**

In a relaying network, the shadow fading of a BS-MS link and a RS-MS link or between two RS-MS links may be strongly correlated. This correlation can significantly affect the system performance [50]. Therefore, it is of great important to characterize and model the shadow fading correlation between links in relaying systems.

Some work has been recently carried out by WINNER project [42], IEEE 802.16j Relay Task Group [43] or 3GPP [41] in order to predict the shadow fading correlation in a relaying deployment. Unfortunately, there is currently no well-agreed model. While 3GPP assumes a constant correlation coefficient equal to 0.5 for all scenarios, WINNER specifies zero correlation due to the limited amount of measurement data. Regarding IEEE 802.16j Task Group, only the model for shadowing correlation between two BSs which is based on the Saunders work [50] is proposed. However, this model is not feasible in every case as proved in [51]. The correlation models for the shadowing between BS-MS and RS-MS links or between two RS-MS links are still for further study.

Moreover, the angle seen from the MS to the transmitters (θ) is recognized as an important parameter which has a significant impact on the shadow fading correlation [50–55]. It was reported a strong correlation on the order of 0.6 to 0.8 with small θ . This correlation was observed to decrease toward zero when θ becomes greater. Although this angular property has been discussed in many papers for the traditional radio mobile network i.e. without the presence of RS, this issue has not yet been adequately studied in the relaying deployment.

This thesis is divided into 4 chapters:

- **Chapter 1:** This chapter aims to draw the general context over which this thesis is carried out. Firstly, the radio mobile communication evolution will be briefly presented with particular focus on 3GPP LTE-Advanced systems. Then, LTE-Advanced key technical enhancements including relaying technology will be described. The challenge which initiates the development of these enhancements will also be investigated.
- **Chapter 2:** This chapter will describe the fundamentals of wireless propagation channel including the multi-path phenomena, basic propagation mechanisms, three scales of signal variation, etc. A particular attention will be paid to investigate the existing path loss and shadow fading correlation models. This investigation reveals advantages as well as disadvantages of these models allow defining the most relevant ones for relaying systems.

- **Chapter 3:** A multi-link outdoor urban measurement campaign with relays will be presented in this chapter. The measurement data processing will also be described. The potential errors caused by different factors such as antenna, data processing or channel non-stationarity will be examined.
- **Chapter 4:** This chapter is dedicated to the analysis results concerning the multi-link propagation channel characterization and modeling. The path losses of BS-MS, BS-RS and RS-MS links will be characterized in both LOS and NLOS conditions. Furthermore, the relay antenna height impact on path loss, especially with the BS-RS link, will be investigated. An additional measurement campaign dedicated to analyze this impact on extended environments and frequencies will be presented. Moreover, different suitable existing path loss models determined from Chapter 2 will be evaluated with the measurement data. The correlations between the shadow fading of BS-MS/RS-MS links or between two RS-MS links will also be characterized and modeled. Finally, the path loss model consistency issue will be briefly discussed.

Chapter 1

Relaying technology in 4G radio mobile systems

This chapter describes the general context in which this thesis has been carried out. Firstly, the evolution of mobile communication systems will be presented. The main characteristics of principal systems will be briefly recalled. Then, LTE-Advanced, the latest evolution of mobile communication systems proposed by the 3GPP, will be described. Considered as one of the key features of LTE-Advanced, relaying technology will be discussed in the next part of this chapter. Finally, a state-of-the-art in relay technology in 3GPP LTE-Advanced context will also be provided.

1.1 Evolution of radio mobile systems

Radio mobile systems have undergone a remarkable development since the apparition of the first mobile communication generation in the 1980s. There was no dominant standard but several competing ones such as NMT (*Nordic Mobile Telephone*), TACS (*Total Access Communication System*) and AMPS (*Advanced Mobile Phone Service*) [56]. These systems were based on the analog technology and designed only for the voice services. Since then, radio mobile systems have been constantly evolving in order to satisfy the increasing customers demands. This development has been contributed and realized by a number of different organizations. Among them, the 3GPP and the WIMAX Forum have been emerged as two major actors. Figure 1.1 illustrates the worldwide mobile communication landscape with different systems and standardization bodies.

The 3GPP is currently the worldwide dominating systems with the participation of many standardization bodies, such as ETSI (*European Telecom-*

communications Standards Institute) in Europe, the ARIB (*Association of Radio Industries and Businesses*) in Japan, the CCSA (*China Communications Standards Association*) in China and the ATIS (*Alliance for Telecommunications Industry Solutions*) in the United State. It can also be found in 3GPP many major manufacturers and operators in telecommunication industry [57].

At the technology level, the first mobile communication system in 3GPP family was GSM - the most successful and widely used second-generation (2G) system. Although adopting the digital technology, GSM systems were still designed for the narrow-band voice and limited data services which were restricted at 9.6 Kbps data rate. GPRS (*General Packet Radio Services*) is an upgraded solution which was proposed to increase the low data rate provided by GSM systems. The first commercial launch for GPRS took place in 2001. With this technology, the data rates can theoretically be pushed up to 115 Kbps. The next improvement to GSM is EDGE (*Enhanced Data Rates for Global Evolution*). The key enhancement of EDGE is a new modulation scheme called 8PSK (*Eight-Phase Shift Keying*). It increases the data rate of standard GSM up to 384 Kbps [56].

The next remarkable system developed within the 3GPP program given in Release 99 is UMTS (*Universal Mobile Telecommunications System*). Considered as the third mobile communication generation (3G) [56], UMTS employs W-CDMA (*Wideband Code Division Multiple Access*) radio access technology to offer greater spectral efficiency to mobile network operators. UMTS specifies a complete network system, covering the radio access net-

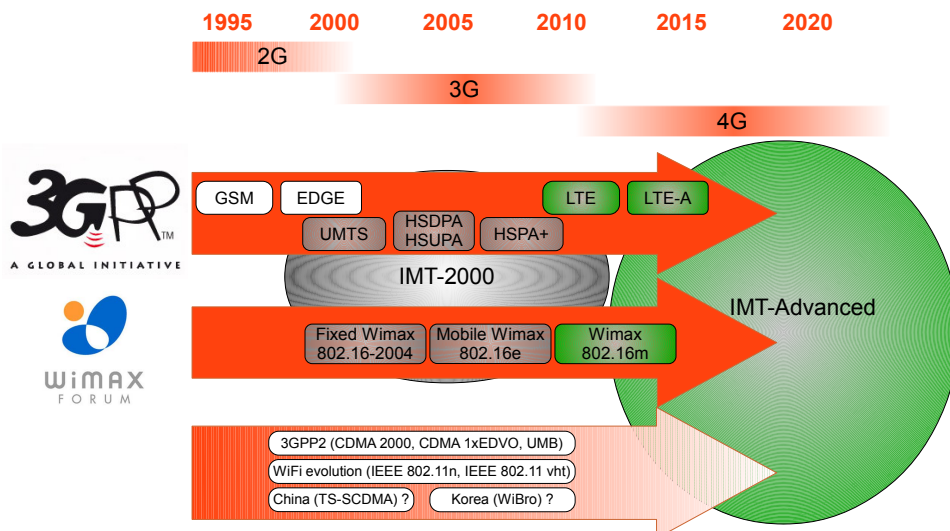


Figure 1.1: Evolution of radio mobile systems

work (*UMTS Terrestrial Radio Access Network* or UTRAN) and the core network (*Mobile Application Part*, or MAP). UMTS supports data rates of up to 2 Mbps over a new wideband air interface.

HSPA (*High-Speed Packet Access*) [56] is the upgrade developed within 3GPP in order to improve the UMTS performance. The peak data rates of 14 Mbps in the Downlink (DL) and 5.8 Mbps in the Uplink (UL) can respectively be achieved with HSDPA (*High-Speed Downlink Packet Access*) (Release 5) and HSUPA (*High-Speed Uplink Packet Access*) (Release 6) [56]. HSPA improvements in UMTS are obtained through a new modulation (16QAM - *16 Quadrature Amplitude Modulation*), reduced radio frame lengths and new functionalities within radio networks. HSPA+, an evolution of HSPA given in Release 7, adds MIMO antenna capability and 16QAM (for UL)/ 64QAM (for DL) modulations. These enhancements allow achieving UL speeds of up to 11 Mbps and DL speeds of up to 42 Mbps.

UMTS, HSPA and HSPA+ belong to the IMT-2000 family (*International Mobile Telecommunication - 2000*) which is a term defined by the ITU to indicate all mobile systems fulfilling 3G specifications. It is foreseen that the development of IMT-2000 will reach a limit of around 30 Mbps. In the vision of the ITU, there may be a need for a new wireless access capable of supporting even higher data rates with high mobility, which could be widely deployed around the year 2015 in some countries. Therefore, ITU introduced a new concept called IMT-Advanced to define the mobile communication systems with enhanced capabilities compared to that of IMT-2000. The new capabilities of these IMT-Advanced systems are envisaged to handle a wide range of supported data in multi-user environments with target peak data rates of up to 100 Mbps for high mobility and up to 1 Gbps for low mobility users.

The first mobile system initiated by 3GPP which can be placed in IMT-Advanced family is *Long Term Evolution* (LTE) [57]. LTE is described in 3GPP Release 8 and then in Release 9 with small enhancements. LTE project focused on enhancing the UTRA (*Universal Terrestrial Radio Access*) and optimizing 3GPP's radio access architecture. OFDM was selected for the DL and SC-FDMA (*Single Carrier-Frequency Division Multiple Access*) for the UL. The supporting data modulation schemes for DL are the QPSK, 16QAM, and 64QAM. Those for UL are the BPSK, QPSK, 8PSK and 16QAM. The LTE radio access uses flexibly channel bandwidths defined between 1.25 MHz and 20 MHz [57]. Targets were to have average user throughput of 300 Mbps for DL and 75 Mbps for UL.

The work toward the evolution of LTE called LTE-Advanced is the response of 3GPP to the ITU-R Circular Letter requesting candidate submissions for IMT-Advanced radio interface technologies. With LTE-Advanced,

the 3GPP aims to fulfill and even go beyond all IMT-Advanced requirements [58]. In order to achieve these objectives, a set of new features have been discussed by 3GPP. The initial version of LTE-Advanced was completed and described in Release 10. Release 11 is under discussion within the 3GPP framework. Details of some key features will be discussed in Section 1.2 of this chapter.

Table 1.1 summarizes the key features of 3GPP principal radio mobile systems from GSM to LTE-Advanced.

In addition to 3GPP, the second major technology family which has an important influence on the global telecommunication landscape is the WiMAX [59]. This evolution conducted by IEEE and WiMAX Forum has received mainly the support from industrial companies and several mobile operators. The early version of WiMAX was based on the IEEE 802.16-2004 standard, also known as 802.16d [60]. This standard targeted the fixed network and was sometimes referred to as “Fixed WiMAX”. The next version was the mobile WiMAX Release 1.0 which was based on the 802.16e or 802.16-2005 standard [61] and targeted the mobile utilization. This system was based on OFDMA and enabled DL and UL MIMO as well as beamforming features. The release 1.0 system was defined only for the TDD operation mode and focused on 5 and 10 MHz bandwidths in several frequency bands such as 2.3 GHz, 2.5 GHz and 3.5 GHz. These versions of WiMAX are also members of the IMT-2000 family.

The more recent amendment of WiMAX evolution is 802.16j [62] which enhances the coverage, throughput and system capacity by introducing multi-hop relay capacity. The latest version of WiMAX is 802.16m which has been developing in the 16m technical group (TGM) [63]. WiMAX 802.16m is very similar to the 3GPP LTE-Advanced from parameter and performance point of view. It targets major enhancements in spectrum efficiency, latency and scalability of the access technology with wider bandwidths in challenging spectrum environments [59]. Like 3GPP LTE-Advanced, WiMAX 802.16m forms the basis of a proposal for IMT-Advanced family.

Besides the 3GPP and WiMAX, there are several smaller technical families which have been developed by other standardization groups or countries such as 3GPP2 with CDMA2000 and 1xEVDO (*Evolution-Data Optimized*) or IEEE’s WiFi evolution for the short-range systems. China and Korea develop also their own technologies. Because this thesis work is carried out in 3GPP LTE-Advanced context, no further discussion about WiMAX evolution and other standards such as 3GPP2, WiFi, etc. will be given in the rest of this thesis.

Table 1.1: Overview of the principal 3GPP radio mobile systems

	GSM	UMTS	HSPA	LTE	LTE-Advanced
3GPP Release		Rel' 99	Rel' 5 for HSDPA Rel' 6 for HSUPA Rel' 7 for HSPA+	Rel' 8 and 9	Rel' 10
Operating bands	850 MHz 900 MHz 1800 MHz 1900 MHz	Around 2 GHZ	Around 2 GHz	Wide range of operating bands	Will be deployed as an evolution of LTE and on new bands
Access Scheme	FDMA/TDMA	WCDMA	WCDMA	OFDMA (DL) SC-FDMA (UL) MIMO	Evolution of LTE, Higher order MIMO with CoMP and Relay
Modulation	GMSK	QPSK	16QAM	QPSK, 16QAM, 64QAM	Evolution of LTE
Channel bandwidth	200 kHz	5 MHz	5 MHz	Variable 1.4, 3, 5, 10, 15 and 20 MHz	Up to 100 MHz with bandwidth aggregation
Switching Technology	Circuit	Circuit	Packet	Packet	Packet
Peak Data rate	9.6 kbps	Up to 2 Mbps	Up to 14 Mbps (DL) Up to 5.8 Mbps (UL)	Up to 300 Mbps (DL) Up to 75 Mbps (UL)	Up to 1 Gbps

1.2 New technology features for LTE-Advanced

This section discusses about the 3GPP LTE-Advanced system and its new key technology components. After defining the challenges of current radio mobile systems, we will describe the most remarkable features of LTE-Advanced with focus on relaying technology.

1.2.1 The challenges

User traffic in radio mobile systems has rapidly increased. This traffic in 1G and 2G systems was relatively low with only voice and short-message services. However, the current Internet explosion and the introduction of smart-phones leads to the emergence of multimedia applications and services such as VoD (*Video on Demand*), Mobile Internet, Mobile TV, etc. These applications in turn require dramatically increasing throughput and data rate. Facing to this challenge, radio mobile systems have adopted many technical enhancements such as the higher bandwidth, the higher modulation scheme, the MIMO, etc. The recent radio mobile systems such as LTE or WiMAX promise the data rate of several hundreds of Mbps.

However, challenges of radio mobile systems are not only to provide a high data rate but also to distribute it uniformly over the covered area and among users. Unfortunately, it is not yet the case with current systems. The data rate achieved by a user in a mobile system depends strongly on the radio propagation conditions as well as the position of the user in the cell. The theoretical peak data rate underlined in promoting documents can only be achieved in very good conditions, even only when the MS is close to the BS. This peak data rate is generally ten times higher than the average one that a user may have in the cell. When the MS goes far away from the BS to the cell-edge area, the worse propagation condition is no longer allowing the utilization of optimal modulation schemes. Moreover, interference coming from adjacent cells reduces rapidly the system performance. Consequently, the data rate experienced by a user in the cell-edge area is usually ten times lower than the average throughput of the cell. Technologies like MIMO, OFDM and advanced error control codes enhance the per-link throughput but do not inherently mitigate the effects of interference. Cell edge problem is more crucial as cellular systems employ higher carrier frequencies [30]. This so-called cell-edge problem is illustrated in Figure 1.2.

In order to overcome the aforementioned challenges, many new technology components have currently been adopted or discussed by 3GPP for LTE-Advanced. The principal ones consist of the bandwidth extension, the enhanced MIMO scheme, the CoMP (*Coordinated Multipoint Transmission or*

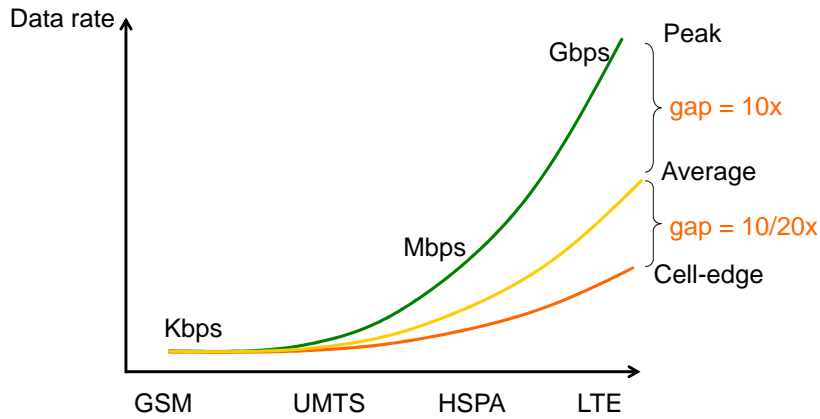


Figure 1.2: Cell-edge problem in radio mobile systems

Reception) and the relaying (Figure 1.3) [41]. These technologies are briefly described in the following sections with focus on relaying which is the main research object of this thesis.

1.2.2 Bandwidth extension

In order to achieve up to 1 Gbps data rate in future IMT-Advanced mobile systems, wider frequency bandwidths are required. A bandwidth of up to 100 MHz has been discussed in the context of LTE-Advanced. At the same time, such a bandwidth extension should be done while preserving the

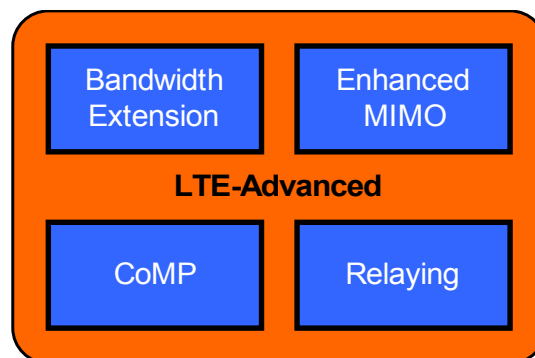


Figure 1.3: LTE-Advanced key features

backward compatibility to legacy systems. In other words, LTE-Advanced should be able to be deployed in the spectrum already occupied by LTE with no impact on existing LTE terminals. This requirement can be fulfilled with a technique called carrier aggregation where multiple LTE components are aggregated on the physical layer to provide the necessary bandwidth [19]. Figure 1.4 presents an example of the contiguous component carriers. To a LTE terminal, each component carrier will appear as an LTE carrier, while a LTE-Advanced terminal can use the total aggregated bandwidth.

Nevertheless, accessing to large amount of contiguous spectrum to obtain the total bandwidth of 100 MHz is not always possible. Therefore, LTE-Advanced could also allow for aggregation of non-contiguous component carriers in separate spectrum to handle situations where large amounts of contiguous spectrum are not available. However, the aggregation of non-contiguous spectrum is challenging from an implementation perspective, especially concerning the terminal support.

1.2.3 Enhanced MIMO schemes

Fundamentally, MIMO techniques use multiple antennas at the transmitter (Tx) and the receiver (Rx) to enable a higher throughput and/or improved link reliability with the same system bandwidth and transmitter power [19, 28, 64]. Multi-antenna technologies including beam-forming and spatial multiplexing are key features which have already been proposed for LTE. These technologies continue to play an even more important role in LTE-Advanced.

In Release 10 the configurations of up to 4x4 MIMO (i.e. 4 Tx antennas and 4 Rx antennas) for the UL and up to 8x8 MIMO for the DL have been proposed. Spatial multiplexing allows several independent data streams

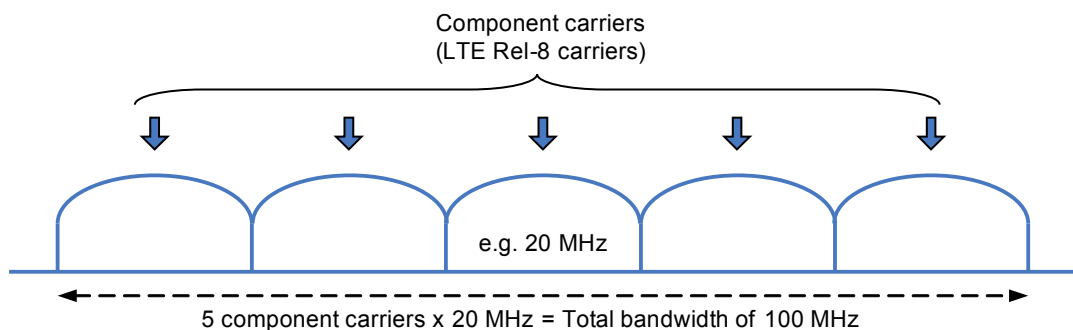


Figure 1.4: A continuous carrier aggregation example

(called spatial layers in 3GPP) to be transmitted over the same time and frequency resources. When all the spatial layers are allocated to the same user, this scheme is called SU-MIMO (*Single-User MIMO*). Alternatively, the layers can be split among several (typically two) users, which can then be served on the same resources, provided that they can be separated in space. This scheme is called MU-MIMO (*Multi-User MIMO*). Nevertheless, spatial multiplexing is only applicable in good radio conditions and under specific channel properties [56].

The principle of SU- and MU-MIMO is illustrated in Figure 1.5 (for the particular case of two spatial layers).

1.2.4 Coordinated Multi-point Transmission/Reception (CoMP)

A major performance limiting factor of before-LTE-Advanced systems is the heavy co-channel (inter-cell) interference. In order to mitigate this problem and thereby enhance the cell-edge performance, CoMP have been investigating for LTE-Advanced [19, 28, 65].

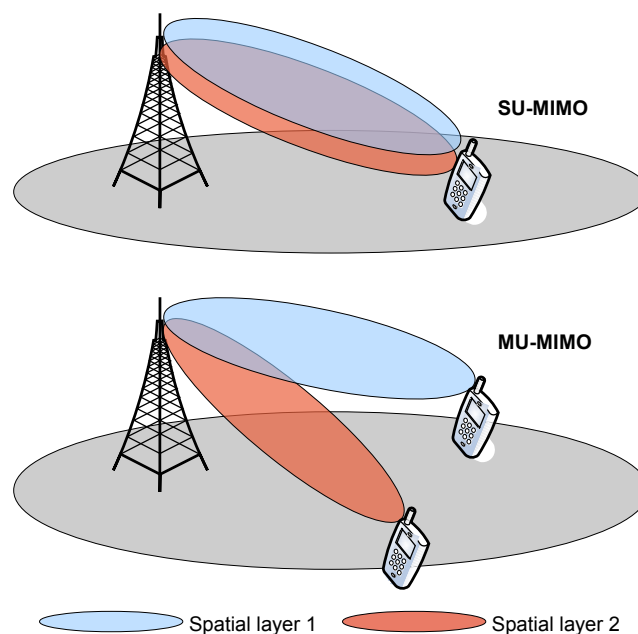


Figure 1.5: SU-MIMO and MU-MIMO examples

The main idea of CoMP is as follows: when a MS is in the cell-edge region, it may be able to receive signals from multiple cell sites. If the system can take advantage of this multiple transmission/reception by coordinating them, the overall performance can significantly be improved. Both DL CoMP and UL CoMP are considered for LTE-Advanced [41, 64].

Two classes of CoMP schemes have been identified by 3GPP:

Coordinated scheduling or Beamforming (CBF): In this category, only one point transmits the data while the other ones are coordinated to reduce interference (e.g. by avoiding beam collisions for CB).

Joint Processing/Joint Transmission (JP/JT): For JP/JT, the transmission to a single MS is simultaneously executed from multiple transmission points, across cell sites. The multi-point transmissions will be coordinated as a single transmitter with antennas that are geographically separated. This scheme is potential to provide higher performance compared to coordination only in the scheduling but needs more stringent requirements on backhaul communication.

An example of CoMP is given in Figure 1.6.

Although CoMP is considered as a potential tool to improve coverage, cell-edge throughput, and/or system efficiency, the implementation of this technique must overcome some serious constraints and challenges. First, the network needs to be time-synchronized with the same accuracy as for TDD (*Time Division Duplexing*). Second, for DL techniques the network needs to acquire the channel knowledge between the MS and all coordinated cells. This increases the measurement load at the MS as well as the feedback overhead. Finally, CoMP technique requires the considerable increase on the backhaul network because of the need to exchange information between coordinated entities. Therefore, despite of the high theoretical performance gain of cooperative transmission schemes, CoMP was considered not to be mature enough to be integrated in Release 10. Nevertheless, it is currently being studied thoroughly for potential inclusion in Release 11.

1.2.5 Relaying

1.2.5.1 Overview

(a) *Basic concepts:*

A classical relaying network is composed of a BS (*Base Station*), a RS (*Relay Station*) and a MS (*Mobile Station*). The RS acts as an intermediate node to receive, process and forward the signal between the BS (called *donor BS*) and the MSs that it serves. The MS can receive the

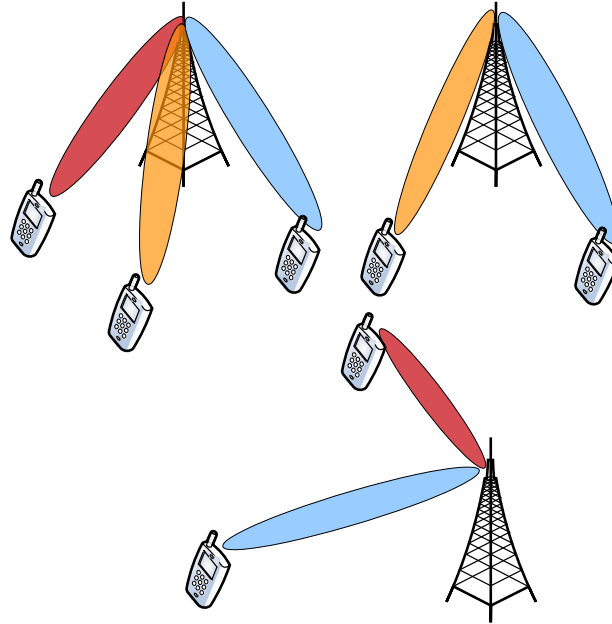


Figure 1.6: An example of CoMP with 3 collaborating cells

signal from the donor BS via two paths: the two-hop relaying link and the one-hop direct link. In the two-hop relaying link the physical channel between the BS and the RS is called the *backhaul link* and that between the RS and the MS is called the *access link* [22, 41].

(b) *Advantages:*

It is well known that at a given power and carrier frequency, the available data rate decreases if the distance from a BS increases whereas the quality of end-user experience (QoE) must not depend on the user location. Hence, the deployment of a conventional cellular radio network, including the enhancements made by signal processing, advanced coding and smart antenna techniques would require a very high density of BSs to achieve satisfactory radio coverage, capacity and service quality. Consequently, the total expense of broadband radio mobile systems will increase dramatically, resulting in very high cost per delivered bit.

To meet the goal of low-cost radio network deployment, the deployment concept based on relay nodes appears to be one of the most promising solutions [22].

Wireless relays help overcoming the current dependence on wired back-

bones and enable cost-effective enhancement of coverage, throughput and system capacity. In fact, relay nodes do not need a wired (e.g. copper or fiber) backbone access by using a wireless connection. This feature helps not only reducing deployment costs but also offering high flexibility in placing relays, allowing fast network rollout and adaptive traffic capacity engineering.

(c) *Relaying types:*

In the literature, two different types of relaying network have been investigated [8]. The first one called Mobile Relay proposes to use other user's terminals to relay the traffic. The second one called Fixed Relay introduces a new element i.e. relay station into existing network infrastructure. These two relay types are illustrated in Figure 1.7. In a Mobile Relay network, the non-active MSs are potential to relay the traffic between the BS and other MSs in less favorable conditions. The principal advantage is that no additional network elements are presented. However, there are some fatal problems related to the mobile relay terminal such as increased energy consumption (fast battery draining), additional hardware and functionality, security issues, mobile availability, etc. Most of above problems can be solved when fixed relays are used. Currently, standardization documents of 3GPP consider that relaying will be performed through fixed relays, at least in the early phase of 4G deployments. Therefore, in this document, only fixed relaying type is considered.

(d) *Relaying scenarios:*

Thanks to its installation flexibility, relays are expected to be deployed in some typical scenarios such as: urban outdoor hotspot (to provide high throughput or to achieve coverage for shadowed area), urban indoor (to indoor coverage), rural coverage (to achieve ubiquitous coverage with the reduced deployment cost) or emergency and temporary network deployment [64].

(e) *Transmission schemes:*

Several relay transmission schemes have been proposed to establish two-hop communication between a BS and a MS through a RS. Among these has emerged two main transmission schemes [29]:

- Amplify and Forward (AF): The RS receives the signal from the source (BS or MS) at the first phase. It amplifies this received signal before forwarding it to the destination (MS or BS) at the second phase. This Amplify and Forward (AF) scheme is very simple and has very short delay but it also amplifies noise.
- Decode and Forward (DF): In DF schemes, the RS regenerates the sig-

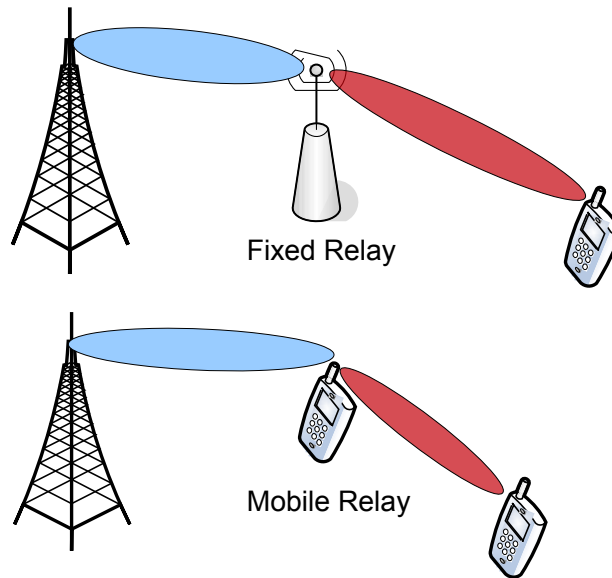


Figure 1.7: Fixed Relay vs Mobile Relay

nal received from the BS (or MS) by fully decoding and re-encoding it before retransmitting it. This scheme can effectively avoid propagation error but it adds the delay due to the signal processing time.

(f) *Operation modes:*

- Full-duplex: the RS can simultaneously communicate with its donor BS and MSs that it serves over one carrier frequency.
- Half-duplex: over one carrier frequency, the RS communicates with its BS and MSs using different time intervals.

1.2.5.2 Relaying technologies in 3GPP LTE-Advanced standards

The relay node is wirelessly connected to the radio-access network via a donor cell. With respect to the relay node's usage of spectrum, its operation can be classified into in-band or out-band. A relay operation is called in-band if the BS-RS link shares the same carrier frequency with RS-MS links. In contrast, the BS-RS link does not operate in the same carrier frequency as RS-MS links in out-band case.

For both in-band and out-band relaying, it shall be possible to operate the BS-RS link on the same carrier frequency as BS-MS links.

With respect to the knowledge of MS, relays can be classified into “transparent” or “non-transparent”. If the MS is not aware of whether or not it communicates with the network via the relay, the relaying network is called “transparent”. It is called “non-transparent” if the MS is aware of whether or not it communicates with the network via the relay.

In the 3GPP standardization documents, several relay types have been defined [41]. They distinguish from each other by the following characteristics:

- A type 1 relay is a half-duplex in-band one. It appears to a MS as a separate cell with its own Physical cell ID (*Identification*) and distinct from the donor cell. Type 1 relays are backward compatible to LTE terminals and supported in Release 10.
- A type 1a relay has the same characteristics as Type 1 relay, except that it is an out-band relay. Type 1a is also supported in Release 10.
- Type 1b is defined as an in-band full-duplex relay. This relay type is not agreed to be supported in Rel'10. Type 1b relays have to be equipped with adequately isolated antennas to allow the full duplex operation, which can be achieved by placing the antennas used to communicate with the BS and the MSs far apart, e.g. one indoors and the other outdoors. Additional signal processing (e.g. interference cancellation) should be used to further enhance the antennas isolation.
- Type 2 relays do not have a separate Physical Cell ID and thus would not create any new cells. Besides, it is transparent to LTE user equipment. This type of relay is not agreed to be supported in 3GPP Rel'10.

Table 1.2 summaries the relay types which are supported in Rel'10 LTE-Advanced.

Table 1.2: Types of 3GPP Release 10 LTE-Advanced relay

Class	Cell ID	Inband/Outband	Supported in Rel'10
Type1	YES	Inband, Half-duplex	YES
Type1a	YES	Outband	YES
Type1b	YES	Inband, Full-duplex	NO
Type2	NO	Inband	NO

1.3 Conclusion

This chapter presented the general context in which this thesis was carried out. The landscape of radio mobile communication systems was given with a particular focus on the 3GPP evolution. The cell-edge problem, one of the main challenges for recent radio mobile systems, was described. Relaying technology, the promising solution to overcome the cell-edge problem, was presented. The state-of-the-art of this technology within LTE-Advanced standards was also given.

Chapter 2

Wireless propagation channels

A wireless propagation channel is the medium linking the Tx and the Rx. Its properties determine the wireless communication performance and also determine how specific wireless systems behave. It is thus essential that the wireless propagation channel is understood and modeled. This chapter intends to describe the basic phenomena behind the wireless propagation channel which are necessary to understand the following chapters of this thesis. Multi-path and basic propagation mechanisms will be presented. Existing path loss and shadow fading correlation models for outdoor urban environments will be particularly investigated.

2.1 Radio wave propagation fundamentals

2.1.1 Multipath propagation

Unlike wired channels that are stationary and predictable, radio channels are extremely variable and not easy to analyze. When the Tx and the Rx have a clear, unobstructed Line-of-Sight (LOS) path between them, the electromagnetic wave propagates in the free space to the Rx. The received signal strength is predicted by the Friis free space equation [66]:

$$P_r(d) = \frac{P_t G_t G_r \lambda^2}{(4\pi)^2 d^2} \quad (2.1)$$

where P_t is the transmitted power (in Watts), $P_r(d)$ is the received power (in Watts), G_t and G_r are the Tx and Rx antenna gain respectively, d is the distance in meters between the Tx and the Rx, λ is the signal wavelength.

However, a clear and unobstructed line-of-sight path between the Tx and the Rx seldom happens in a real communication system. Instead, the electromagnetic wave interacts with obstacles and objects presented in propagation

path such as buildings, mountains, trees and other obstructions before reaching the Rx.

The mechanisms behind these interactions are diverse but they can generally be attributed to the reflection, the diffraction and the scattering (Figure 2.1).

Reflection occurs when a propagating electromagnetic wave hits an object which has very large dimensions compared to the wavelength (e.g. earth surface, building facades, walls, etc.).

Diffraction happens when electromagnetic waves are bended around the obstacle edge or spread after passing through an opening. This phenomenon forms secondary waves in the geometrical shadowed area behind the obstacle even when a LOS path does not exist between the Tx and the Rx.

Scattering occurs when the medium through which the wave travels consists of objects with dimensions that are small compared to the wavelength and the number of obstacles per unit volume is large. Scattering causes energy from a Tx to be reradiated in many different directions. Foliage is an example of objects which induces scattering in urban mobile communication systems.

As a result of the aforementioned phenomena, the received signal is not only a simple attenuated and delayed wave but the summation of many copies of the transmitted signal having various complex amplitudes, delays and direction of departure/arrival(Figure 2.2). Such multi-path propagation

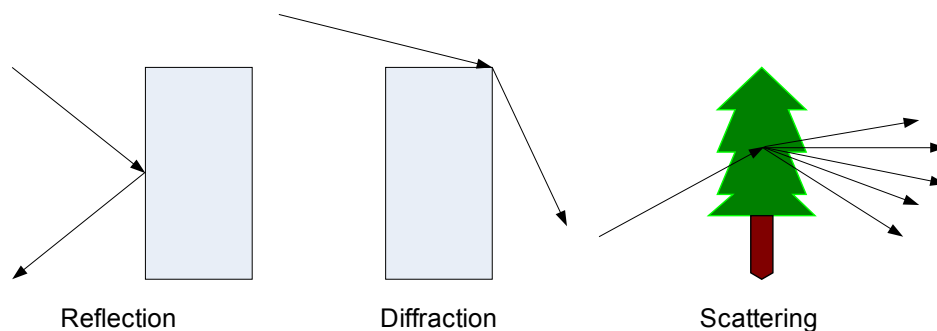


Figure 2.1: Basic propagation mechanisms

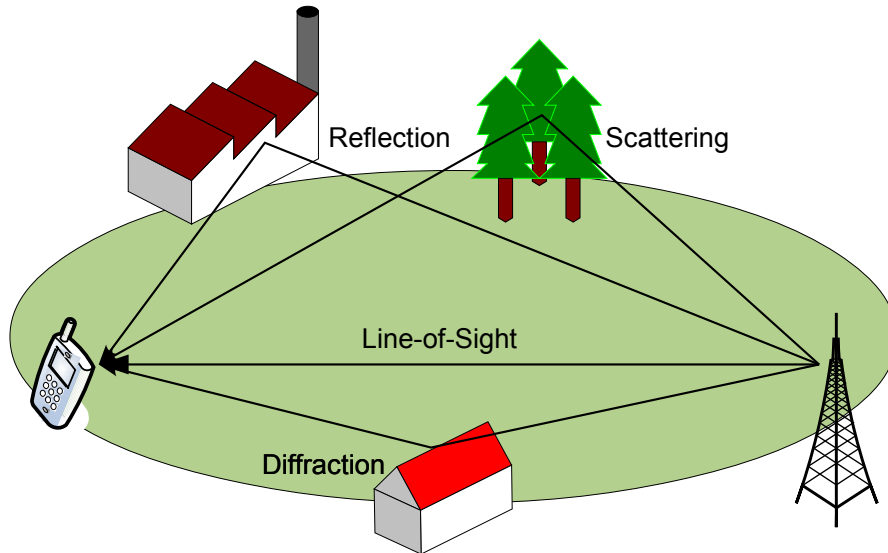


Figure 2.2: Multipath propagation

is particularly significant in urban environments where buildings and street surfaces provide strong reflections.

2.1.2 Three scales of propagation signal variation

In radio mobile communication systems, the interactions of electromagnetic waves with the environment cause variations in the transmitted signal over time and distance. These variations are divided into three scales i.e. the path loss, the shadowing and the fast fading (Figure 2.3).

2.1.2.1 Path loss

Path loss is an average decrease of the received signal strength due to the propagation distance. It is generally expressed in dB.

The path loss for free-space model when antenna gains are excluded is given by:

$$PL(dB) = 10 \log \frac{P_t}{P_r} = -10 \log \left[\frac{\lambda^2}{(4\pi)^2 d^2} \right] \quad (2.2)$$

This model is only valid for far field conditions when the Tx-Rx distance is greater than *Fraunhofer distance*. The Fraunhofer distance is defined as:

$$d_R = \frac{2L_a^2}{\lambda} \quad (2.3)$$

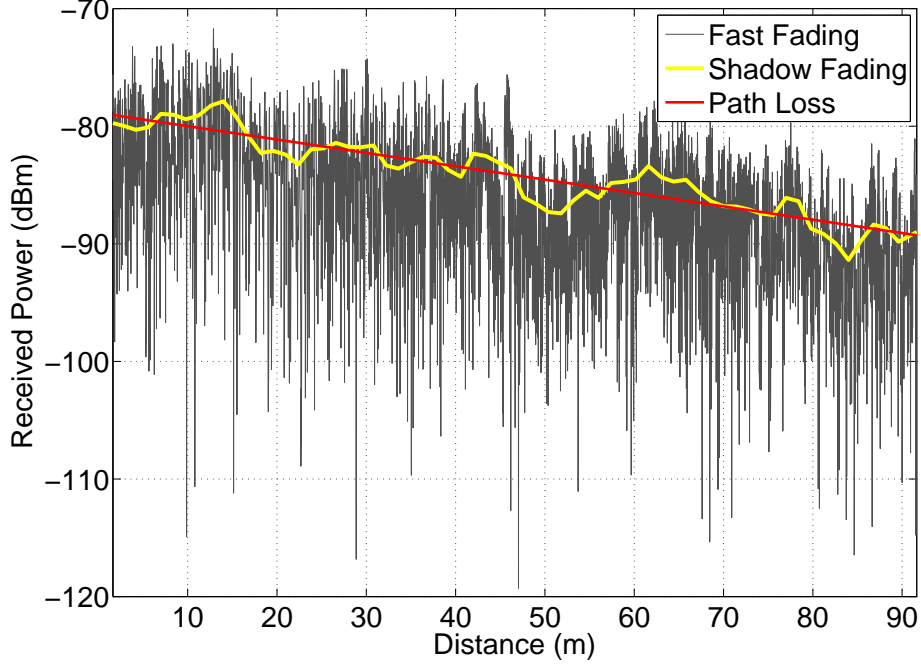


Figure 2.3: Three scales of radio mobile signal variation

where L_a is the largest dimension of the antenna. Moreover, the far field requires $d \gg \lambda$ and $d \gg L_a$.

A convenient way to express the free-space path loss is:

$$PL(dB) = 20 \log_{10}(f) + 20 \log_{10}(d) + 32.4 \quad (2.4)$$

where f is the operating frequency measured in MHz, d is the propagation distance in Km.

However, the free space propagation rarely happens in real radio mobile systems. Instead of free space model, a general path loss (PL) model is normally used. This model is expressed as [67]

$$PL(dB) = PL(d_0) + 10n \log_{10}(d/d_0) \quad (2.5)$$

where d_0 is a reference distance. It is typically 1 km for large urban mobile systems, 100 m for microcell systems and 1 m for indoor systems. Path loss exponent n denotes the relationship between distance and received power. Table 2.1 below presents value of n in some typical environments.

Table 2.1: Path loss exponents [67]

Environment	Path loss exponent (n)
Free space	2
Urban area	2.7 to 3.5
Severe urban area	3 to 5

2.1.2.2 Shadow Fading

Shadow fading or large-scale fading is the medium term variation (over hundreds of λ) of the received signal strength around the path loss level.

In fact, the general path loss model in Equation 2.5 does not take into account the effects caused by surrounding environmental obstacles such as hill or building. With the same propagation distance, the obstructions are vastly different from each other. Consequently, the measured signals at different location having the same Tx-Rx distance fluctuate over the average value predicted by Equation 2.5. This phenomenon is called shadow fading. Measurements have shown that at any distance d this fluctuation measured in dB is random and have a zero mean Gaussian (normal) distribution.

2.1.2.3 Fast fading

Fast fading or small-scale fading is the short-term fluctuations (a few λ) of the received signal strength due to multi-path interference.

Fast fading is normally modeled by the Rayleigh or Rice distributions.

When radio signals are scattered by many objects in the environment and does not content a dominant component, the fast fading is widely described by the Rayleigh distribution.

The Rayleigh distribution has a probability density function (pdf) given by:

$$p(x) = \begin{cases} \frac{x}{\sigma^2} \exp\left(-\frac{x^2}{2\sigma^2}\right) & 0 \leq x \leq \infty \\ 0 & x < 0 \end{cases} \quad (2.6)$$

where σ and $2\sigma^2$ are respectively the rms value and the time-average power of the received signal. Figure 2.4 shows Rayleigh pdf with several different values of σ .

When there is a dominant stationary signal component, such us a line-of-sight propagation path, the small-scale fading envelope distribution is Ricean.

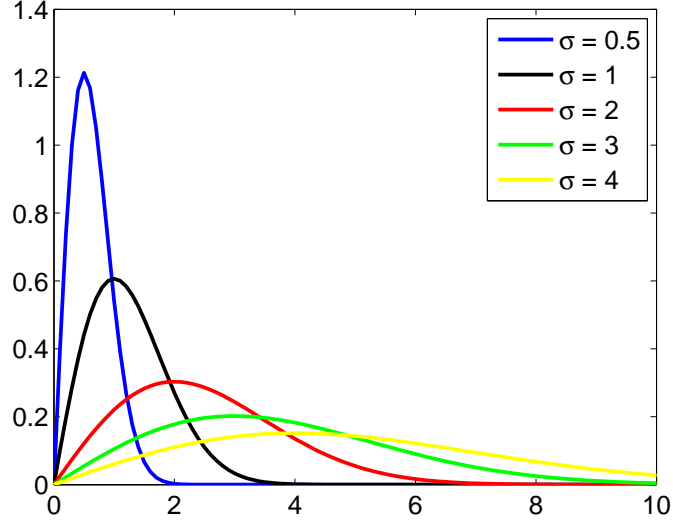


Figure 2.4: Rayleigh pdf with different values of σ

The Ricean distribution is given by:

$$p(r) = \begin{cases} \frac{r}{\sigma^2} e^{-\frac{r^2+A^2}{2\sigma^2}} I_0\left(\frac{Ar}{\sigma^2}\right) & A \geq 0, r \geq 0 \\ 0 & r < 0 \end{cases} \quad (2.7)$$

where A denotes the peak amplitude of the dominant signal and $I_0()$ is the modified Bessel function of the first kind and zero order. The Ricean distribution is often described in terms of a parameter K , also known as the Ricean factor, which is defined as the signal power ratio between the dominant component and scattered component. K is given by:

$$K(\text{dB}) = 10 \log_{10}\left(\frac{A^2}{2\sigma^2}\right) \quad (2.8)$$

As $A \rightarrow 0$ and $K \rightarrow -\infty$ dB (the dominant path decreases) the Ricean distribution degenerates to a Rayleigh distribution. Figure 2.5 shows the Ricean pdf with different K values.

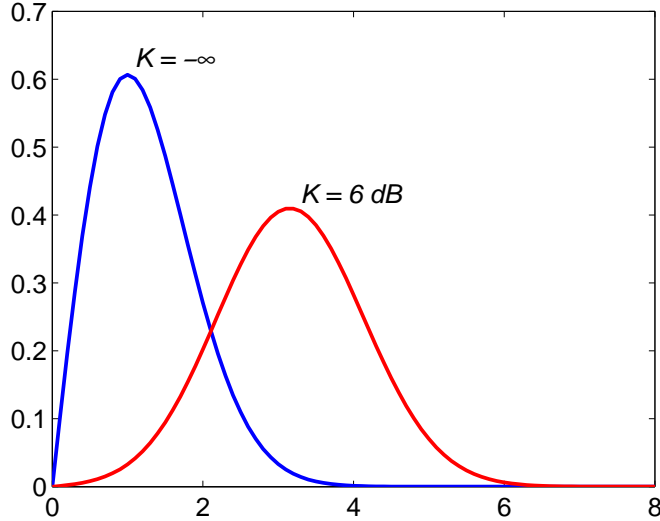


Figure 2.5: Rice pdf with different values of K

2.2 Path loss models

2.2.1 Overview

Path loss prediction is a crucial element in the first step of network planning. In relaying systems, path loss models should be defined for three links which are BS-RS, RS-MS and BS-MS. Furthermore, each relay applied scenario such as urban outdoor, urban indoor, rural, emergency or temporary network deployment, etc. requires a more specific path loss model. In this thesis, we focus our research only to the urban outdoor scenarios where relays are expected to extend the coverage and combat the cell-edge problem.

The BS-MS link in relaying deployments is considered similar to the BS-MS link in a classical macro-cellular radio mobile network. The BS antenna height is above the surrounding rooftops and MS antenna height is about 1-2 m. Much research has been studied this link. Consequently, the proposed path loss models are abundant. Several widely used models are given by Okumura-Hata [68, 69], COST-231 Hata [70], COST-231 Walfish-Ikegami [70], ITU-R P.1411 [71], etc.

Concerning the BS-RS link, an important parameter is the effective RS antenna height. Simulation results obtained in 3GPP have shown that the backhaul link is the bottleneck of the relay-enhanced performance [64]. Therefore, it is necessary to favor as much as possible a good BS-RS link in order to provide it a sufficient capacity. This can be achieved by using directive

antenna at RS and placing the it in good radio locations. To this end, RS antenna height should be high enough such as on top of buildings in order to achieve LOS or nearly LOS condition to the donor BS. However, this deployment requires some site planning for the operator and potential additional installation expenses. One of the expected advantages of relays is their ease of deployment as well as their operation and maintenance. In order to achieve these advantages, a promising solution is to install relays with medium antenna heights of about 4-12 m such as lamppost, etc. Indeed, 3GPP and WINNER suppose a relay antenna height of 5 m [41, 42]. Some efforts to develop path loss models for this scenario have been carried out by WINNER [42], IEEE 802.16 [72], 3GPP [41]. However, these models are not validated yet in a realistic deployment. Moreover, when the relay antenna height varies, it has probably certain impacts on path loss models. Once again, this issue is not adequately studied yet.

With the aforementioned relay antenna height, the RS-MS link can be considered as traditional micro-cellular deployment. Path loss models for this scenario have been studied and proposed by some studies [70, 73–78].

Although the path loss models for different links in relaying systems have been more or less dealt in certain studies, these models are proposed in an independent way. Consequently, their consistency is not valid yet. However, in relaying systems, three links are strongly related to each other. The potential enhancement contributed by relays can only be correctly evaluated if suitable path loss models taking into account their consistency are available. Therefore, a part of this thesis will be dedicated to this issue.

The following sections describe the most widely used path loss models in urban outdoor scenarios.

2.2.2 Okumura-Hata model

In 1968, Okumura has conducted measurements of BS-MS link in Tokyo and introduced empirical plots [68]. Later, in 1980, Hata developed a closed-form expression from Okumura's data [69]. This model is called Okumura-Hata model and given by:

$$PL(dB) = 69.55 + 26.16 \log_{10}(f) - 13.82 \log_{10}(h_{BS}) - a(h_{MS}) \\ + (44.9 - 6.55 \log_{10}(h_{BS})) \log_{10}(d) \quad (2.9)$$

where f is the frequency (in MHz) which varies from 150 MHz to 1500 MHz, h_{BS} and h_{MS} are the effective BS and MS antenna heights, d is the Tx-Rx separation (in km) and $a(h_{MS})$ is the correction factor for the mobile unit.

For a small to medium size cities, the mobile antenna correction factor is given by:

$$a(h_{MS}) = [1.1 \log_{10}(f_c) - 0.7] h_{MS} - 1.56 \log_{10}(f_c) - 0.8 \quad (2.10)$$

And for large city, it is given by:

$$a(h_{MS}) = 8.28 [\log_{10}(1.54h_{MS})]^2 - 1.1 \quad \text{for } f_c \leq 300 \text{ MHz} \quad (2.11)$$

$$a(h_{MS}) = 3.2 [\log_{10}(11.75h_{MS})]^2 - 4.97 \quad \text{for } f_c > 300 \text{ MHz} \quad (2.12)$$

2.2.3 COST-231 model

The European Cooperation in Science and Technology (COST) formed the COST-231 action to identify the most likely migration paths from current cellular networks towards next generation universal systems [70]. One important output of COST-231 is the development of outdoor propagation models for urban areas at 900 and 1800 MHz bands. Based on extensive measurement campaigns in European cities, COST-231 has investigated different existing models and has created new propagation models. These models, valid for flat terrain, are based on the approaches of Walfisch-Bertoni [79], Ikegami [80] and Hata [69].

2.2.3.1 COST-231 Hata model

COST-231 has extended Hata model [69] to the 1500 MHz - 2000 MHz frequency band by analyzing Okumura propagation curves in the upper frequency band. This combination is called COST-231 Hata model and is given by [70]:

$$PL(dB) = 49.3 + 33.9 \log_{10}(f) - 13.82 \log_{10}(h_{BS}) - a(h_{MS}) \\ + (44.9 - 6.55 \log_{10}(h_{BS})) \log_{10}(d) + C_m \quad (2.13)$$

where $a(h_{MS})$ is defined in Equation 2.10 and 2.12 and

$$C_m = \begin{cases} 0 \text{ dB,} & \text{for medium sized cities and suburban areas} \\ 3 \text{ dB,} & \text{for metropolitan centers} \end{cases} \quad (2.14)$$

The COST-231 Hatal model is restricted to the following range of parameters:

$$\begin{aligned}
 f: & \quad 1500 \text{ MHz to } 2000 \text{ MHz} \\
 h_{BS}: & \quad 30 \text{ m to } 200 \text{ m} \\
 h_{MS}: & \quad 1 \text{ m to } 10 \text{ m} \\
 d: & \quad 1 \text{ km to } 20 \text{ km}
 \end{aligned}$$

2.2.3.2 COST-231 Walfish-Ikegami model

The COST-231 proposes also a combination of Walfish [79] and Ikegami [80] models. It is called the COST-231 Walfish-Ikegami (COST-231 WI) model. This model improves the path loss prediction by considering more data to describe the urban environment. These data include the average building heights h_r , the road width w , the building separation b (Figure 2.6) and the road orientation with respect to the direct radio path φ (Figure 2.7).

The parameters presented in Figure 2.6 are:

h_r : average height of building (m)

w : street width (m)

b : average building separation (m)

φ : street orientation with respect to the direct path (degrees)

h_{BS} : BS antenna height (m)

h_{MS} : MS antenna height (m)

l : length of the path covered by building (m)

d : distance from BS to MS

The COST-231 WI model distinguishes between LOS and NLOS (*Non-Line-of-Sight*) situations.

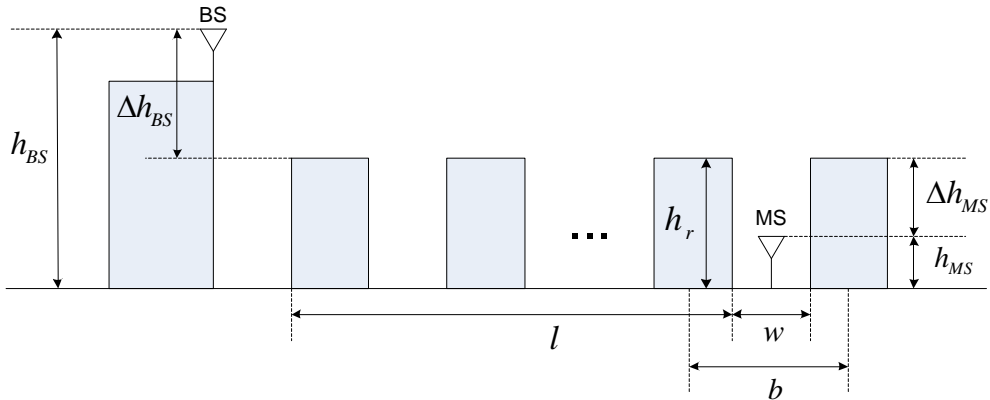


Figure 2.6: Parameters of COST-231 Walfish-Ikegami model

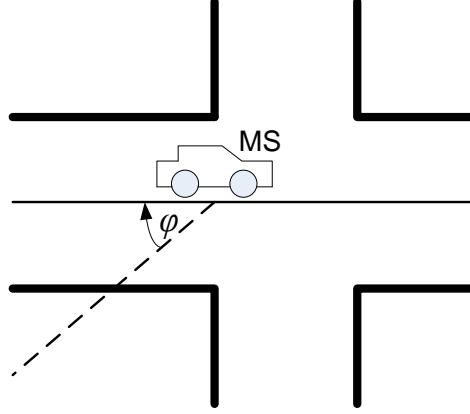


Figure 2.7: Street orientation defination

In the **LOS case**, the path loss formula is described by:

$$L_b(dB) = 42.6 + 26 \log_{10}(d/[Km]) + 20 \log_{10}(f/[MHz]) \quad \text{for } d \geq 20m \quad (2.15)$$

In the **NLOS case**, the basic transmission loss is composed of the free space loss L_0 , the multiple screen diffraction loss L_{msd} and the rooftop-to-street diffraction and scatter loss L_{rts} .

$$L_b = \begin{cases} L_0 + L_{rts} + L_{msd} & \text{for } L_{msd} + L_{rts} > 0 \\ L_0 & \text{for } L_{msd} + L_{rts} \leq 0 \end{cases} \quad (2.16)$$

where the free-space loss is given by Equation 2.4.

The term L_{rts} describes the coupling of the wave propagating along the multiple-screen path into the street where the mobile station is located.

$$L_{rts} = -16.9 - 10 \log_{10}(w) + 10 \log_{10}(f) + 20 \log_{10}(\Delta h_{MS}) + L_{Ori} \quad (2.17)$$

and:

$$\Delta h_{MS} = h_r - h_{MS} \quad (2.18)$$

is the difference between the average building height h_r , and the mobile antenna height, h_{MS} .

L_{Ori} is given by:

$$L_{Ori} = \begin{cases} -10 + 0.354\varphi & \text{if } 0^\circ \leq \varphi \leq 35^\circ \\ 2.5 + 0.075(\varphi - 35) & \text{if } 35^\circ \leq \varphi \leq 55^\circ \\ 4.0 - 0.114(\varphi - 35) & \text{if } 55^\circ \leq \varphi \leq 90^\circ \end{cases} \quad (2.19)$$

The multiple screen diffraction loss L_{msd} is given by:

$$L_{msd} = L_{bsh} + k_a + k_d \log_{10}(d) + k_f \log_{10}(f) - 9 \log_{10}(b) \quad (2.20)$$

The term k_a represents loss for the case in which BS antennas below the roof tops of the adjacent building.

With the definition

$$\Delta h_{BS} = h_{BS} - h_r \quad (2.21)$$

L_{bsh} and k_a are given by:

$$L_{bsh} = \begin{cases} -18 \log(1 + \Delta h_{BS}) & \text{if } h_{BS} > h_r \\ 0 & \text{if } h_{BS} \leq h_r \end{cases} \quad (2.22)$$

and

$$k_a = \begin{cases} 54 & \text{if } h_{BS} > h_r \\ 54 - 0.8\Delta h_{BS} & \text{if } d \geq 0.5 \text{ km and } h_{BS} \leq h_r \\ 54 - 1.6\Delta h_{BS} & \text{if } d < 0.5 \text{ km and } h_{BS} \leq h_r \end{cases} \quad (2.23)$$

The terms k_d and k_f control the dependence of the multi-screen diffraction loss versus distance and radio frequency, respectively. They are given by:

$$k_d = \begin{cases} 18 & \text{if } h_{BS} > h_r \\ 18 - 15 \frac{\Delta h_{BS}}{h_r} & \text{if } h_{BS} \leq h_r \end{cases} \quad (2.24)$$

and

$$k_f = -4 + \begin{cases} 0.7 \left(\frac{f}{925} - 1 \right) & \text{for medium-sized cities} \\ & \text{and suburban centers} \\ & \text{with moderate tree densities.} \\ 1.5 \left(\frac{f}{925} - 1 \right) & \text{for metropolitan centers.} \end{cases} \quad (2.25)$$

If the data on the structure of buildings and streets are unknown, the following default values are recommended:

$$h_r = 3 \times (\text{number of floors}) + \text{roof-height (m)}$$

$$\text{roof-height} = \begin{cases} 3 \text{ (m)} & \text{for pitched roofs} \\ 0 \text{ (m)} & \text{for flat roofs} \end{cases}$$

$$w = b/2$$

$$b = 20 \text{ to } 50 \text{ m}$$

$$\varphi = 35^\circ$$

The COST-WI model is restricted to:

$$\begin{aligned}
 f &= 800 \text{ MHz to } 2000 \text{ MHz} \\
 h_{BS} &= 4 \text{ to } 50 \text{ m} \\
 h_{MS} &= 1 \text{ to } 3 \text{ m} \\
 d &= 20 \text{ m to } 5 \text{ km}
 \end{aligned}$$

The path loss prediction of COST-231 WI is reported to be well agreed with measurements for base station antenna heights above rooftop level. However, the prediction error becomes large for $\Delta h_{BS} \approx h_r$. The model performance is poor when $\Delta h_{BS} < h_r$ or the propagation terrain is not flat and homogeneous [70].

2.2.4 ITU-R P.1411 models

ITU-R Recommendation P.1411-5 [71] describes a set of path loss models for several urban outdoor scenarios. These scenarios are depicted in Figure 2.8.

Base station BS1 is mounted above rooftop level. The corresponding cell is a macro-cell. Propagation from this BS is mainly over the rooftops. Base station BS2 is mounted below rooftop level and defines a dense urban micro- or pico-cellular environment. In these cell types, propagation is mainly within street canyons.

2.2.4.1 Path loss model for LOS urban areas

This path loss model is used for LOS situations within street canyons which are the BS1-MS2 and BS2-MS4 cases in the Figure 2.8. This model is

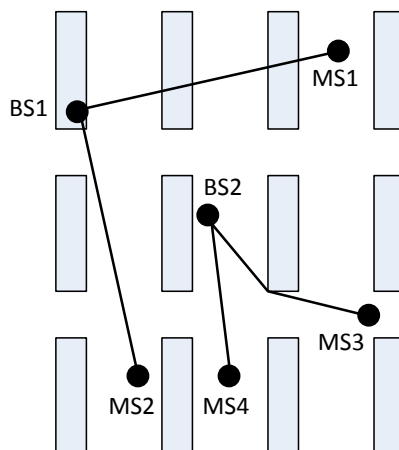


Figure 2.8: ITU-R P.1411 propagation scenarios

defined by two slopes and a single breakpoint. An approximate lower bound is given by:

$$L_{LOS,l}(dB) = L_{bp} + \begin{cases} 20\log_{10}\left(\frac{d}{R_{bp}}\right) & \text{for } d \leq R_{bp} \\ 40\log_{10}\left(\frac{d}{R_{bp}}\right) & \text{for } d > R_{bp} \end{cases} \quad (2.26)$$

where R_{bp} is the break point distance given by:

$$R_{bp} \approx \frac{4h_{BS}h_{MS}}{\lambda} \quad (2.27)$$

where λ is the wavelength (m).

An approximate upper bound is given by:

$$L_{LOS,u}(dB) = L_{bp} + 20 + \begin{cases} 25\log_{10}\left(\frac{d}{R_{bp}}\right) & \text{for } d \leq R_{bp} \\ 40\log_{10}\left(\frac{d}{R_{bp}}\right) & \text{for } d > R_{bp} \end{cases} \quad (2.28)$$

where L_{bp} is the basic transmission loss at the break point, defined as:

$$L_{bp} = \left| 20\log_{10}\left(\frac{\lambda^2}{8\pi h_{BS}h_{MS}}\right) \right| \quad (2.29)$$

A median value is given by:

$$L_{LOS,m}(dB) = L_{bp} + 6 + \begin{cases} 20\log_{10}\left(\frac{d}{R_{bp}}\right) & \text{for } d \leq R_{bp} \\ 40\log_{10}\left(\frac{d}{R_{bp}}\right) & \text{for } d > R_{bp} \end{cases} \quad (2.30)$$

2.2.4.2 Path loss model for NLOS urban area with over-rooftop propagation

This model uses the same parameters and is very similar to the COST-231 WI model (Figure 2.6). It is applied for the BS1-MS1 case in Figure 2.8 and is expressed as:

$$L_{NLoS} = \begin{cases} L_{bf} + L_{rts} + L_{msd} & \text{for } L_{rts} + L_{msd} > 0 \\ L_{bf} & \text{for } L_{rts} + L_{msd} \leq 0 \end{cases} \quad (2.31)$$

Where L_{bf} , L_{rts} and L_{msd} are respectively the free-space loss, the diffraction loss from rooftop to street and the loss due to multiple screen diffraction past rows of buildings.

The free-space loss is given in Equation 2.4.

The diffraction loss from rooftop to street L_{rts} is refined by:

$$L_{rts} = -8.2 - 10\log_{10}(w) + 10\log_{10}(f) + 20\log_{10}(\Delta h_{MS}) + L_{Ori} \quad (2.32)$$

with L_{Ori} is defined in Equation 2.19.

The multiple screen diffraction loss is given by defining a new parameter - the ‘‘settled field distance’’, d_s :

$$d_s = \frac{\lambda d^2}{\Delta h_{BS}^2} \quad (2.33)$$

where

$$\Delta h_{BS} = h_{BS} - h_r \quad (2.34)$$

The overall multiple screen diffraction loss is given by:

$$L_{msd} = \begin{cases} -\tanh\left(\frac{\log(d) - \log(d_{bp})}{\chi}\right) (L1_{msd}(d) - L_{mid}) + L_{mid} & \text{for } l > d_s, \\ \tanh\left(\frac{\log(d) - \log(d_{bp})}{\chi}\right) (L1_{msd}(d) - L_{mid}) + L_{mid} & \text{for } l \leq d_s, \\ L2_{msd}(d) & \text{for } dh_{bp} > 0 \\ L1_{msd}(d) - \tanh\left(\frac{\log(d) - \log(d_{bp})}{\xi}\right) (L_{upp} - L_{mid}) - L_{upp} + L_{mid} & \text{for } l > d_s, \\ L2_{msd}(d) + \tanh\left(\frac{\log(d) - \log(d_{bp})}{\xi}\right) (L_{mid} - L_{low}) + L_{mid} - L_{low} & \text{for } l \leq d_s, \end{cases} \quad (2.35)$$

where

$$dh_{bp} = L_{upp} - L_{low} \quad (2.36)$$

$$\xi = (L_{upp} - L_{low}) \cdot v \quad (2.37)$$

$$L_{mid} = \frac{(L_{upp} + L_{low})}{2} \quad (2.38)$$

$$L_{upp} = L1_{msd}(d_{bp}) \quad (2.39)$$

$$L_{low} = L2_{msd}(d_{bp}) \quad (2.40)$$

and

$$d_{bp} = \left| \Delta h_{BS} \sqrt{\frac{l}{\lambda}} \right| \quad (2.41)$$

$$v = [0.0417] \quad (2.42)$$

$$\chi = [0.1] \quad (2.43)$$

The individual losses, $L1_{msd}(d)$ and $L2_{msd}(d)$, are defined as follows

$$L1_{msd}(d) = L_{bsh} + k_a + k_d \log_{10} \frac{d}{1000} + k_f \log_{10}(f) - 9 \log_{10}(b) \quad (2.44)$$

where

$$L_{bsh} = \begin{cases} -18 \log_{10}(1 + \Delta h_{BS}) & \text{for } h_{BS} > h_r \\ 0 & \text{for } h_{BS} \leq h_r \end{cases} \quad (2.45)$$

$$k_a = \begin{cases} 71.4 & \text{for } h_{BS} > h_r, f > 2000 \text{ MHz} \\ 73 - 0.8 \Delta h_{BS} & \text{for } h_{BS} \leq h_r, f > 2000 \text{ MHz and } d \geq 500 \text{ m} \\ 73 - 1.6 \Delta h_{BS} \frac{d}{1000} & \text{for } h_{BS} \leq h_r, f > 2000 \text{ MHz and } d < 500 \text{ m} \\ 54 & \text{for } h_{BS} > h_r, f \leq 2000 \text{ MHz} \\ 54 - 0.8 \Delta h_{BS} & \text{for } h_{BS} \leq h_r, f \leq 2000 \text{ MHz and } d \geq 500 \text{ m} \\ 54 - 1.6 \Delta h_{BS} \frac{d}{1000} & \text{for } h_{BS} \leq h_r, f \leq 2000 \text{ MHz and } d < 500 \text{ m} \end{cases} \quad (2.46)$$

$$k_d = \begin{cases} 18 & \text{for } h_{BS} > h_r \\ 18 - 15 \frac{\Delta h_{BS}}{h_r} & \text{for } h_{BS} \leq h_r \end{cases} \quad (2.47)$$

$$k_f = \begin{cases} -8 & \text{for } f > 2000 \text{ MHz} \\ -4 + 0.7 \left(\frac{f}{925} - 1 \right) & \text{for medium sized city and suburban centers} \\ & \text{and } f \leq 2000 \text{ MHz} \\ -4 + 1.5 \left(\frac{f}{925} - 1 \right) & \text{for metropolitan centers} \\ & \text{and } f \leq 2000 \text{ MHz} \end{cases} \quad (2.48)$$

$L2_{msd}(d)$ is given as by:

$$L2_{msd}(d) = -10 \log_{10}(Q_M^2) \quad (2.49)$$

where:

$$Q_M = \begin{cases} 2.35 \left(\frac{\Delta h_{BS}}{d} \sqrt{\frac{b}{\lambda}} \right)^{0.9} & \text{for } h_{BS} > h_r + \delta h_u \\ \frac{b}{d} & \text{for } h_{BS} \leq h_r + \delta h_u \text{ and } h_{BS} \geq h_r + \delta h_l \\ \frac{b}{2\pi d} \sqrt{\frac{\lambda}{\rho}} \left(\frac{1}{\theta} - \frac{1}{2\pi + \theta} \right) & \text{for } h_{BS} < h_r + \delta h_l \end{cases} \quad (2.50)$$

and

$$\theta = \arctan\left(\frac{\Delta h_{BS}}{b}\right) \quad (2.51)$$

$$\rho = \sqrt{\Delta h_{BS}^2 + b^2} \quad (2.52)$$

$$\delta h_u = 10^{-\log_{10}\left(\sqrt{\frac{b}{\lambda}}\right) - \frac{\log_{10}(d)}{9} + \frac{10}{9}\log_{10}\left(\frac{b}{2.35}\right)} \quad (2.53)$$

$$\delta h_l = \frac{0.00023b^2 - 0.1827b - 9.4978}{(\log_{10}(f))^{2.938}} + 0.000781b + 0.06923 \quad (2.54)$$

This ITU-R P.1411 model is valid for:

$$\begin{aligned} f: & \quad 800 \text{ MHz to } 5000 \text{ MHz} \\ & \quad 2 \text{ to } 16 \text{ GHz for } h_{BS} < h_r \text{ and } w < 10 \text{ m} \\ h_{BS}: & \quad 4 \text{ m to } 50 \text{ m} \\ h_{MS}: & \quad 1 \text{ m to } 3 \text{ m} \\ d: & \quad 20 \text{ m to } 5 \text{ km} \end{aligned}$$

2.2.4.3 Path loss model for NLOS urban areas with propagation within street canyons for frequency range from 800 MHz to 2000 MHz

For the situations where both antennas are below roof-top level, diffracted and reflected waves at the street corners have to be considered (see Figure 2.9).

The relevant parameters for this situation are:

- w_1 : street width at the position of the BS (m)
- w_2 : street width at the position of the MS (m)
- x_1 : distance BS to street crossing (m)
- x_2 : distance MS to street crossing (m)
- α : is the corner angle (rad).

In this case, the path loss is given by:

$$L_{NLoS} = -10\log_{10}(10^{-L_r/10} + 10^{-L_d/10}) \quad (2.55)$$

where L_r is the reflection loss defined by:

$$L_r = 20\log_{10}(x_1 + x_2) + x_1x_2\frac{f(\alpha)}{w_1w_2} + 20\log_{10}\frac{4\pi}{\lambda} \quad (2.56)$$

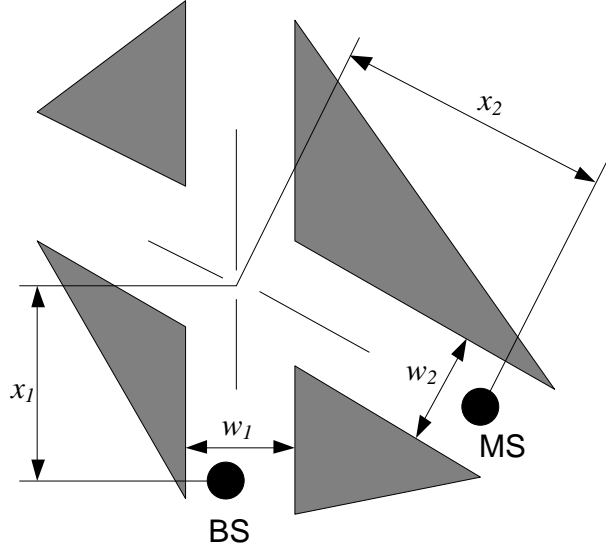


Figure 2.9: Parameter definitions for propagation within street canyons

where

$$f(\alpha) = \frac{3.86}{\alpha^{3.5}} (\text{dB}), \quad 0.6 < \alpha [\text{rad}] < \pi \quad (2.57)$$

Diffraction loss is defined by:

$$L_d = 10 \log_{10} [x_1 x_2 (x_1 + x_2)] + 2D_a - 0.1 \left(90 - \alpha \frac{180}{\pi} \right) + 20 \log_{10} \frac{4\pi}{\lambda} \quad (2.58)$$

where

$$D_a = \frac{40}{2\pi} \left[\arctan\left(\frac{x_2}{w_2}\right) + \arctan\left(\frac{x_1}{w_1}\right) - \frac{\pi}{2} \right] \quad (2.59)$$

2.2.5 WINNER models

The Wireless World Initiative New Radio (WINNER) project is an international research project under Framework Program 6 (FP6) of the European Commission. This project was a initiative joining the efforts of major industrial and academic players in radio mobile communication world. The main objective is to develop a new radio interface for systems beyond 3G [81]. Phases I and II of the WINNER project contributed to the deployment, integration and assessment of new mobile network techniques. Some of these techniques are now in the 3GPP LTE and IEEE 802.16 (WiMAX) standards, while others are under consideration for LTE-Advanced and 802.16m [82].

2.2.5.1 Supported scenarios

WINNER channel models cover a large frequency range (2 to 6 GHz) and wide scope of propagation scenarios including indoor-to-outdoor, outdoor-to-indoor, urban macro and micro-cell, suburban and rural, etc. Furthermore, several scenarios with relay are also included [42]. The models for outdoor urban and relaying scenarios are discussed below:

– **Urban micro-cell scenario (B1):**

In urban micro-cell scenarios, both BS and MS antenna heights are assumed to be well below the tops of surrounding buildings. Both antennas are assumed to be outdoors in an area where streets are laid out in a Manhattan-like grid. This scenario is defined for both the LOS and the NLOS cases. The NLOS path loss model for scenario B1 is dependent on two distances d_1 and d_2 . These distances are defined with respect to a rectangular street grid, as illustrated in Figure 2.10, where the MS is shown moving along a street perpendicular to the street on which the BS is located (the LOS street). d_1 is the distance from the BS to the centre of the perpendicular street, and d_2 is the distance of the MS along the perpendicular street, measured from the centre of the LOS street.

– **Urban macro-cell scenario (C2):**

In typical urban macro-cell, MS is located outdoors at street level and BS is clearly above surrounding building heights. As for propagation conditions, non- or obstructed line-of-sight is a common case, since

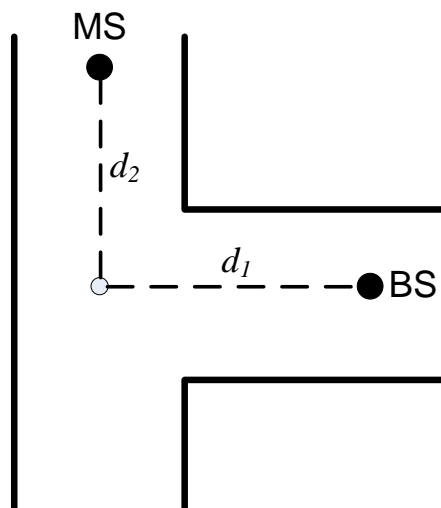


Figure 2.10: Definition of d_1 and d_2 for B1 path loss model

street level is often reached by a single diffraction over the rooftop. The building blocks can form either a regular Manhattan type of grid, or have more irregular locations. Buildings height and density in typical urban macro-cell are mostly homogenous.

– **Relay scenario (B5):**

WINNER considers only the BS-RS link that they call “stationary feeder link”. This scenario is divided into 4 categories:

- *B5a (LOS stationary feeder: rooftop to rooftop):*

The signal in B5a can be assumed to consist of a strong LOS signal and single bounce reflection. The connection is almost like in free space, so that the path-loss does not depend noticeably on the antenna heights.

- *B5b (LOS stationary feeder: street level to street level):*

In B5b it is assumed that both the Tx and Rx have many surrounding scatterers. In addition there can also be long echoes from the ends of the street. There is a LOS ray between the Tx and Rx and when this path is strong, the contribution from all the scatters is small.

- *B5c (LOS stationary feeder: below rooftop to street level):*

Scenarios B5c can be considered as the LOS case of B1 scenario. The only difference in environment is the assumed antenna height of the mobile/relay.

- *B5f:*

B5f scenario consists of the cases in which relay antennas are some meters over the roof-top or some meters below the roof-top. The WINNER approach is that the desired BS-RS link can be planned to be LOS or OLOS (Obstructed Line of Sight), or at least “good” links. In B5f it is assumed that the RS is shadowed due to some obstacles. The proposed model is based on literature and formed from the B5a LOS fixed relay model by attenuating artificially its direct component by 15 dB in average and summing to it a normally distributed random decibel number with standard deviation 8 dB. The model B5f can also be understood as NLOS part of the model B5a.

2.2.5.2 Path loss models

Path loss models for various WINNER scenarios have been developed based on carried-out measurements results as well as results from the open literature. These path loss models are typically given by [42]:

$$PL_{WINNER} = A \log_{10}(d[m]) + B + C \log_{10}\left(\frac{f_c[GHz]}{5}\right) + X \quad (2.60)$$

where d is Tx-Rx distance in [m], f_c is the system frequency in [GHz], parameter A includes the path-loss exponent, parameter B is the intercept and C describes the path loss frequency dependence. X is an optional, environment-specific term. These parameters for each scenario are completely described in the reference [42].

Several models for outdoor urban areas are described below:

– **Urban micro-cell (B1) LOS models:**

If $10 \text{ m} < d_1 < d'_{bp}$ where $d'_{bp} = \frac{h'_{BS}h'_{MS}f_c}{c}$ with $h'_{BS} = h_{BS} - 1$ and $h'_{MS} = h_{MS} - 1$, the path loss model is given in Equation 2.60 with $A = 22.7$, $B = 41$ and $C = 20$.

If $d'_{bp} < d_1 < 5 \text{ km}$, the path loss model is:

$$PL = 40 \log_{10}(d_1) + 9.45 - 17.3 \log_{10}(h'_{BS}) - 17.3 \log_{10}(h'_{MS}) + 2.7 \log_{10}\left(\frac{f_c}{5}\right) \quad (2.61)$$

These models assume $h_{BS} = 10 \text{ m}$, $h_{MS} = 1.5 \text{ m}$.

– **Urban micro-cell (B1) NLOS models**

This model is given as:

$$PL = \min(PL(d_1, d_2), PL(d_2, d_1)) \quad (2.62)$$

where

$$PL(d_k, d_l) = PL_{LOS}(d_k) + 20 - 12.5n_j + 10n_j \log_{10}(d_l) + 3 \log_{10}\left(\frac{f_c}{5}\right) \quad (2.63)$$

and $n_j = \max(2.8 - 0.0024d_k, 1.84)$, $k, l \in \{1, 2\}$.

PL_{LOS} is the B1 LOS path loss.

The model applicability range includes: $10 \text{ m} < d_1 < 5 \text{ km}$, $w/2 < d_2 < 2 \text{ km}$, $w = 20 \text{ m}$, $h_{BS} = 10 \text{ m}$ and $h_{MS} = 1.5 \text{ m}$. When $0 < d_2 < w/2$, the B1 LOS path loss is used.

– **Urban macro-cell (C2) LOS model:**

If $10 \text{ m} < d < d'_{bp}$, the path loss model is given in Equation 2.60 with $A = 26$, $B = 39$ and $C = 20$.

If $d'_{bp} < d < 5 \text{ km}$, the path loss model is:

$$PL = 40 \log_{10}(d) + 13.47 - 14 \log_{10}(h'_{BS}) - 14 \log_{10}(h'_{MS}) + 6 \log_{10}\left(\frac{f_c}{5}\right) \quad (2.64)$$

It is assumed that $h_{BS} = 25 \text{ m}$, $h_{MS} = 1.5 \text{ m}$.

– **Urban macro-cell (C2) NLOS model:**

This model is expressed as:

$$PL = (44.9 - 6.55 \log_{10}(h_{BS})) \log_{10}(d) + 33.46 + 5.83 \log_{10}(h_{BS}) + 23 \log_{10}\left(\frac{f_c}{5}\right) \quad (2.65)$$

This model is applicable for $50 \text{ m} < d < 5 \text{ km}$ and $h_{BS} = 25 \text{ m}$, $h_{MS} = 1.5 \text{ m}$.

– **LOS stationary feeder - rooftop to rooftop (B5a):**

This model is given as the general forms in Equation 2.60 with $A = 23.5$, $B = 42.5$ and $C = 20$. The model application range is $30 \text{ m} < d < 8 \text{ km}$ and $h_{BS} = 25 \text{ m}$, $h_{RS} = 25 \text{ m}$

– **LOS stationary feeder - below rooftop to street level (B5c):**

This model is the same as B1 LOS model excepting for the antenna height. In this case, $h_{BS} = 25 \text{ m}$ and $h_{RS} = 5 \text{ m}$.

– **B5f model:** This model is given as the general forms in Equation 2.60 with $A = 23.5$, $B = 57.5$ and $C = 23$. The model application range is $30 \text{ m} < d < 1.5 \text{ km}$ and $h_{BS} = 25 \text{ m}$, $h_{RS} = 15 \text{ m}$

2.2.6 IEEE 802.16j models

IEEE Working Group 802.16 has been working actively to develop the technical standards for fixed wireless access systems. Path loss model has been proposed for different environment such as urban, suburban, rural, etc. Summary of these models is presented in Table 2.2. Details of these modes can be found in [43].

Here we focus on the models for outdoor urban macro-cell environments.

2.2.6.1 Type E path loss model

This path loss model type is applied for BS-RS or RS-RS links in NLOS urban macro-cell environments. In these cases, COST-231 WI is recommended with the following parameters: building separation $b = 60 \text{ [m]}$, street width $w = 12 \text{ [m]}$, street orientation $\varphi = 90 \text{ [degree]}$, average rooftop height $h_r = 25 \text{ [m]}$.

2.2.6.2 Type F path loss model

This scenario is applied for RS-RS or RS-MS link.

- **LOS scenario:** This scenario assumes that both antennas are located below the rooftop and in the same street. The model is given as follow:

$$PL = 20 \log_{10} \left(\frac{e^{sr} 4\pi D(r)}{\lambda} \right) \quad (2.66)$$

Table 2.2: Summary of IEEE 802.16 Path loss models

Category	Description	
Type A	Macro-cell, suburban, ART ¹ to BRT ² for hilly terrain with moderate to heavy tree densities	LOS/NLOS
Type B	Macro-cell, suburban, ART to BRT for intermediate path-loss condition	LOS/NLOS
Type C	Macro-cell, suburban, ART to BRT for flat terrain with light tree densities	LOS/NLOS
Type D	Macro-cell, suburban, ART to ART	LOS
Type E	Macro-cell, urban, ART to BRT	NLOS
Type F	Urban or suburban, BRT to BRT	LOS/NLOS
Type G	Indoor office	LOS/NLOS
Type H	Macro-cell, urban, ART to BRT	LOS
Type J	Outdoor to Indoor	NLOS

where:

r is Tx-Rx distance.

e^{sr} is the visibility factor ($s = 0.002$).

λ is the wavelength.

and

$$D(r) = \begin{cases} 1 & r \leq r_{bp} \\ \frac{r}{r_{bp}} & r > r_{bp} \end{cases} \quad (2.67)$$

$$r_{bp} = \frac{4(h_t - h_0)(h_r - h_0)}{\lambda} \quad (2.68)$$

h_t is the Tx height above ground.

h_r is the Rx height above ground.

h_0 is the effective road height (1 m).

In the case where the Tx-Rx distance is less than 10 m, the free-space path loss model is used.

- **NLOS scenario:** This scenario assumes that both antenna heights are below roof top and located in different streets. The model takes the minimum of an over-the-rooftop component and a round-the-streets component. The round-the-streets component is based on Berg model [83], although it has been modified to be compatible with the advanced LOS such that the inclusion of the visibility factor and the effective

1. Above Roof Top

2. Below Roof Top

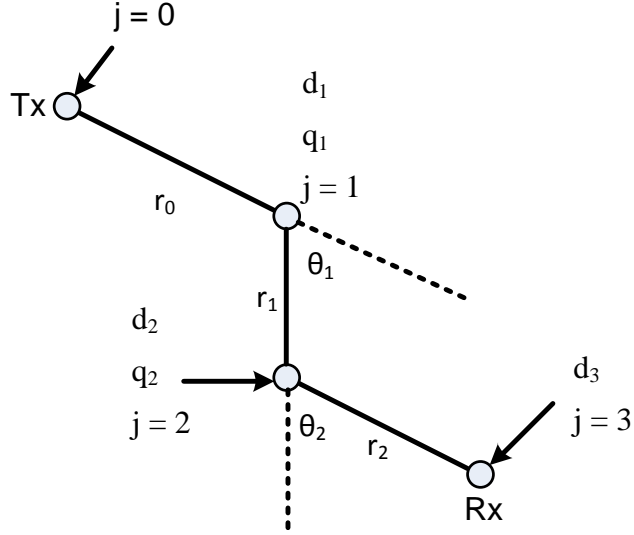


Figure 2.11: Street geometry used for Berg model

road height. The street geometry used for Berg model is shown in Figure 2.11. The path loss model is defined as:

$$PL(dB) = \min(PL_{Berg}(dB), PL_{over-roof-top}(dB)) \quad (2.69)$$

where

$$PL_{over-roof-top}(dB) = 24 + 45 \log_{10}(r_{Eu}) \quad (2.70)$$

r_{Eu} is the Euclidean distance between Tx and Rx. and

$$PL_{Berg}(dB) = 20 \log_{10} \left(\frac{4\pi d_n D(R) \prod_{j=1}^n e^{sr_{j-1}}}{\lambda} \right) \quad (2.71)$$

$R = \sum_{j=1}^n r_{j-1}$ is the distance along streets between Tx and Rx. r_j is the street length between nodes j and $j+1$ (there are totally $n+1$ nodes).

$$r_{bp} = \begin{cases} r_0 & \text{if } r_0 \leq \frac{4(h_t - h_0)(h_r - h_0)}{\lambda} \\ \frac{4(h_t - h_0)(h_r - h_0)}{\lambda} & \text{if } r_0 > \frac{4(h_t - h_0)(h_r - h_0)}{\lambda} \end{cases} \quad (2.72)$$

$$D(R) = \begin{cases} 1 & \text{if } R \leq r_{bp} \\ \frac{R}{r_{bp}} & R > r_{bp} \end{cases} \quad (2.73)$$

The distance d_n is the imaginary distance defined by the following recursive expression:

$$k_j = k_{(j-1)} + d_{(j-1)}q_{(j-1)} \quad (2.74)$$

$$d_j = k_j r_{(j-1)} + d_{(j-1)} \quad (2.75)$$

With $k_0 = 1$ and $d_0 = 0$ and:

$$q_j(\theta_j) = \left(\theta_j \frac{q_{90}}{90} \right)^{1.5} \quad (2.76)$$

θ_j is the angle between streets at junction j and $q_{90} = 0.5$.

2.2.6.3 Type H path loss model

This model is based on COST-231 WI model but excluding the rooftop-to-street diffraction loss. Therefore, type H path loss model consists of the free space loss (L_0) plus the multi-screen diffraction loss (L_{msd}).

$$PL(dB) = L_0 + L_{msd} \quad (2.77)$$

L_0 and L_{msd} are the same as in Section 2.2.3.2.

2.2.7 3GPP models

Within 3GPP standardization process, path loss models for the various propagation scenarios have been developed based on measurement as well as literature results[41]. The models can be applied in the frequency range of 2 - 6 GHz and for different antenna heights. Most of models proposed by 3GPP are based and strongly similar to WINNER models. These models are included in ITU-R Report 2135 which presents the guidelines for evaluation of radio interface technologies for IMT-Advanced. Moreover, 3GPP introduce also a set of path loss models dedicated to relaying systems.

The 3GPP path loss models [41] for urban macro- and micro-cell as well as relaying scenarios are described below.

– 3GPP Urban micro-cell LOS models:

If $10 \text{ m} < d_1 < d'_{bp}$ where $d'_{bp} = \frac{h'_{BS} h'_{MS} f_c}{c}$ with $h'_{BS} = h_{BS} - 1$ and $h'_{MS} = h_{MS} - 1$, the path loss model is given as:

$$PL = 22 \log_{10}(d) + 28 + 20 \log_{10}(f_c) \quad (2.78)$$

f_c and d are respectively frequency given in GHz and propagation distance given in meters. Parameter d_1 is defined in the same way as in WINNER models (Figure 2.10)

If $d'_{bp} < d_1 < 5$ km, the path loss model is:

$$PL = 40 \log_{10}(d) + 7.8 - 18 \log_{10}(h'_{BS}) - 18 \log_{10}(h'_{MS}) + 2 \log_{10}(f_c) \quad (2.79)$$

These models assume $h_{BS} = 10$ m, $h_{MS} = 1.5$ m.

– **3GPP Urban micro-cell NLOS models:**

This model is the same as the WINNER urban micro-cell (B1) NLOS model which is described earlier.

– **3GPP Urban macro-cell LOS model:**

In this case, proposed path loss models is the same as for micro LOS scenarios excepting the assuming BS antenna height. It is assumed that $h_{BS} = 25$ m.

– **3GPP Urban macro-cell NLOS model:**

This model is expressed as:

$$\begin{aligned} PL = & 161.04 - 7.1 \log_{10}(w) + 7.5 \log_{10}(h_r) \\ & - (24.37 - 3.7 \left(\frac{h_r}{h_{BS}}\right)^2) \log_{10}(h_{BS}) \\ & + (43.42 - 3.1 \log_{10}(h_{BS})) (\log_{10}(d) - 3) \\ & + 20 \log_{10}(f_c) - (3.2 (\log_{10}(11.75 h_{MS})))^2 - 4.97 \end{aligned} \quad (2.80)$$

This model is applicable for:

$$\begin{aligned} 10 \text{ m} & < d < 5000 \text{ m} \\ 5 \text{ m} & < h_r < 50 \text{ m} \\ 5 \text{ m} & < w < 50 \text{ m} \\ 10 \text{ m} & < h_{BS} < 150 \text{ m} \\ 1 \text{ m} & < h_{MS} < 10 \text{ m} \end{aligned}$$

- **3GPP relaying models:** These models, which are proposed for 2GHz operating systems, are summarized in Table 2.3 with distance d given in [km]:

Table 2.3: 3GPP relaying path loss models

Link	Path loss models
BS-MS	$PL_{LOS} = 103.4 + 24.2 \log_{10}(d)$ $PL_{NLOS} = 131.1 + 42.8 \log_{10}(d)$
BS-RS	$PL_{LOS} = 100.7 + 23.5 \log_{10}(d)$ $PL_{NLOS} = 125.2 + 36.3 \log_{10}(d)$
RS-MS	$PL_{LOS} = 103.8 + 20.9 \log_{10}(d)$ $PL_{NLOS} = 145.4 + 37.5 \log_{10}(d)$

2.2.8 Summary and discussion

The aforementioned path loss models for LOS and NLOS conditions are respectively summarized in Table 2.4 and 2.5. The models which may be applied for each propagation link in relaying systems are presented with focus on their simplicity and the received antenna height correction factor. As analyzed earlier, relay antenna height is an important parameter in relaying systems. Furthermore, from engineering point of view, the simplicity is essential to the applicability of a model. For instance, propagation models described by few simple equations will greatly improve its applicability. On the contrary, models including many conditional statements given in several pages are obviously difficult to be applied in practical conditions.

It can be learnt from the above tables that BS-MS path loss models are abundant in both NLOS and LOS scenarios. The antenna height correction factor is included in several models such as COST-231 Hata, COST-231 WI, etc. The simplicity is various among models.

Path loss models for RS-MS link which are considered similar to traditional micro-cellular models are also quite numerous. Most of these models in NLOS scenarios such as WINNER B1, 802.16j Type F and 3GPP Urban Micro models assume Manhattan-like or street canyon environment. However, the implementation of this grid is quite challenging in practical cases. In the case of LOS scenarios, the proposed models are given in much simpler forms.

Concerning the BS-RS link, few path loss models are given. For NLOS scenarios, the 802.16j model is actually the COST-231 WI model given with predefined parameter values. The WINNER and 3GPP models are very simple but do not provide an antenna height correction factor. The similar observation is found with models for LOS scenarios. Otherwise, several models such as COST-231 Hata, COST-231 WI may be used for BS-RS link if the received antenna height parameter is extend to 4-12 meters.

In conclusion, 3GPP and WINNER provide the most complete path loss

models which cover all of BS-MS, BS-RS and RS-MS links. Although these models do not take into account the relay antenna height impact, they are very simple and then easy to use. COST-231 WI is given in a quite complicated form which requires detail knowledge of propagation environments. However, this model is reported to be coherent with many measurement data. Many models such as ITU-R P.1411 or 802.16j are derived from this model. An antenna height correction factor is also provided. Furthermore, 3GPP, WINNER and COST-231 WI models are all well-known. They are largely accessible and used by both academic and industrial researchers. Therefore, we consider that 3GPP and WINNER models, in addition to COST-231 WI model, are the most appropriate to evaluate the relay contribution in relaying systems. The analysis and discussion given in this thesis will be based on these models.

Table 2.4: NLOS path loss model summary

Models	Applicable link			Antenna height correction factor	Simplicity	Note
	BS-MS	BS-RS	RS-MS			
Okumura-Hata	✓			$ah_{MS} + b$ for small and medium city $a(\log_{10} h_{MS})^2 + b$ for large city	Simple	
COST-231 Hata	✓			The same as Okumura-Hata model	Simple	Based on Okumura-Hata model
COST-231 WI	✓			$\log_{10}(h_r - h_{MS})$	Complicated	
ITU-R P.1411	✓			The same as COST-231 WI	Very complicated	Based on COST-231 WI model
WINNER C2	✓			Not provided	Simple	
WINNER B5f		✓		Not provided	Very simple	
WINNER B1			✓	Not provided	Simple	Based on Manhattan grid
802.16j Type E	✓			COST-231 WI is recommended		
802.16j Type F			✓	$\log_{10}(ah_{MS})$	Very complicated	
3GPP Urban Macro	✓			$\log_{10}(h_{MS})$	Simple	
3GPP Urban Micro		✓		The same as WINNER		
3GPP Relay BS-MS	✓			Not provided	Very simple	
3GPP Relay BS-RS		✓		Not provided	Very simple	
3GPP Relay BS-RS			✓	Not provided	Very simple	

Table 2.5: LOS path loss model summary

Models	Applicable link			Antenna height correction factor	Simplicity	Note
	BS-MS	BS-RS	RS-MS			
ITU-R P.1411	✓			$\log_{10}(1/h_{MS})$	Simple	
WINNER C2	✓			$\log_{10}(h_{MS})$	Simple	
WINNER B1			✓	$\log_{10}(h_{MS})$	Simple	
WINNER B5a		✓		Not provided	Very simple	
WINNER B5c		✓		The same as WINNER B1 excepting the antenna height (5 m against 1 m)		
802.16j Type F			✓	$\log_{10}(h_{MS} - a)$	Simple	
802.16j Type H		✓		The same as COST-231 WI without the multi-screen diffraction loss		
3GPP Urban Macro	✓			$\log_{10}(h_{MS})$	Simple	Very similar to WINNER C2
3GPP Urban Macro			✓	$\log_{10}(h_{MS})$	Simple	Very similar to WINNER B1
3GPP Relay BS-MS	✓			Not provided	Very simple	
3GPP Relay BS-RS		✓		Not provided	Very simple	
3GPP Relay RS-MS			✓	Not provided	Very simple	

2.3 Shadow fading models

The shadow fading correlation between different links in a radio mobile network is an important element which can significantly affect the system performance [50]. Therefore, this issue has been studied for many years [5, 51, 53–55, 84–88]. We distinguish two correlation types which are auto-correlation and cross-correlation. To illustrate these correlations, let consider the situation depicted in Figure 2.12. The Rx moves in the coverage area of two transmitters Tx1 and Tx2. At the drive path length l_0 , the shadow fading of Tx1-Rx(l_0) and Tx2-Tx(l_0) links are respectively S_{11} and S_{21} . At the drive path length $l_0 + \Delta l$, the shadow fading of Tx1-Rx($l_0 + \Delta l$) and Tx2-Rx($l_0 + \Delta l$) links at this new location are S_{12} and S_{22} . As aforementioned in Section 2.1.2.2, S_{11} , S_{12} , S_{21} and S_{22} have Gaussian distributions with zero means.

- **Auto-correlation** is defined as the correlation between shadow fading of a same Tx-Rx link at two different locations in the moving path of Rx. Correlation between S_{11} and S_{12} or between S_{21} and S_{22} are examples of this case. The auto-correlation is defined as:

$$\rho_{auto} = \frac{(\varepsilon[S_{11}S_{12}])}{(\sigma_{11}\sigma_{12})} \quad (2.81)$$

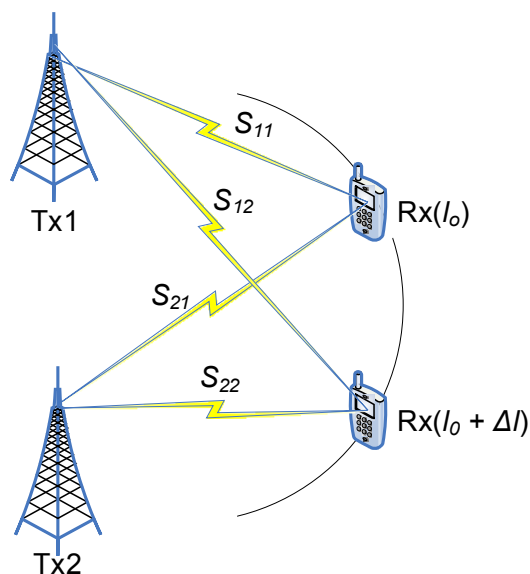


Figure 2.12: Shadow fading definition

where σ_{11} and σ_{12} are standard deviations of S_{11} and S_{12} . ε is the expected operator.

It is reasonable to assume here that σ_{11} and σ_{12} are equal because the two Rx locations are typically sufficiently close together so that they encounter the same general category of environment. The above equation is therefore rewritten as:

$$\rho_{auto} = \frac{(\varepsilon[S_{11}S_{12}])}{(\sigma^2)} \quad (2.82)$$

- **Cross-correlation** is the correlation between two links from two different Tx at the same Rx location such as between S_{11} and S_{21} or between S_{12} and S_{22} . Cross-correlation is given as:

$$\rho = \frac{(\varepsilon[S_{12}S_{22}])}{(\sigma_{12}\sigma_{22})} \quad (2.83)$$

The shadow fading auto-correlation is characterized by the decorrelation distance. This is the distance where the normalized correlation falls to e^{-1} . This distance is typically a few tens or hundreds of meters and corresponds to the building width or other obstructions which surround the receiver. A well-agreed model for shadow fading auto-correlation is given in [84]. Furthermore, the auto-correlation can be assumed negligible if receivers' locations are far enough. Therefore, this subject will not be discussed further in this thesis. In the following, when the term "shadow fading correlation" is used, it means cross-correlation.

2.3.1 Shadow fading correlation models for traditional radio mobile network

Although much research has been carried out for many years, there is currently no well-agreed model for predicting shadow fading correlation characteristics. Various models based on different parameters (Figure 2.13) can be found in the literature.

2.3.1.1 Angle-only models

The most widely known approach is to model the correlation as a function of the angle θ seen from the receiver to the transmitters. One of the first studies concerning θ was reported in [52]. A piecewise-linear model was extracted from the measurement and given as:

$$\rho(\theta) = \begin{cases} 0.8 - \frac{\theta}{150} & \text{if } \theta \leq 60^\circ \\ 0.4 & \text{if } \theta > 60^\circ \end{cases} \quad (2.84)$$

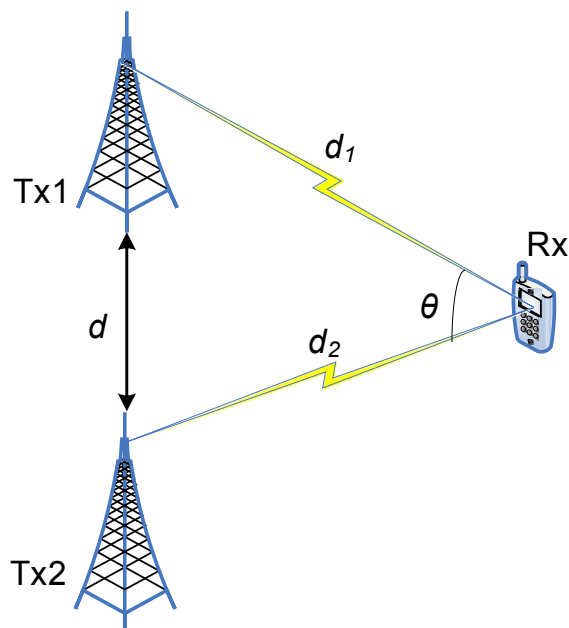


Figure 2.13: Shadow fading correlation parameters

A similar linear model was introduced in [89] as follow:

$$\rho(\theta) = \begin{cases} 0.78 - \frac{7\theta}{1250} & \text{if } 0 \leq \theta < 15^\circ \\ 0.48 - \frac{7\theta}{1250} & \text{if } 15^\circ \leq \theta < 60^\circ \\ 0 & \text{if } 60^\circ \leq \theta \leq 180^\circ \end{cases} \quad (2.85)$$

In [90, 91], a cosine model was proposed as:

$$\rho(\theta) = A \cos(\theta) + B \quad (2.86)$$

with two positive tunable parameters A , B and $A + B \leq 1$. Typical parameter are $A = 0.3$, $B = 0.5$ as in [92] or $A = 0.3$, $B = 0.699$ in [93].

2.3.1.2 Angle-distance models

These models consider the effects of both angle θ and the transmitter separation distance d . An example can be found in [94]. This model is given as:

$$\rho(\theta, d) = \rho(d)\rho(\theta) \quad (2.87)$$

where

$$\rho(d) = e^{-d/d_0} \quad (2.88)$$

and:

$$\rho(\theta) = \begin{cases} 1 & \text{if } \theta \leq 90^\circ \\ 0 & \text{if } \theta > 90^\circ \end{cases} \quad (2.89)$$

In fact, the angle-distance approach is similar to angle-only one because within the same coverage area, the shorter distance between transmitters means the higher probability of small angle θ . However, a contradictory result was presented in [55]. The authors claimed that the correlation should be low even at small angles, if the common propagation path from two transmitters to the receiver is not significant. This observation is taken into account with another variable R expressed in dB which is the distance ratio between two propagation paths.

$$R(\text{dB}) = 10 \left| \log_{10}\left(\frac{d_1}{d_2}\right) \right| \quad (2.90)$$

2.3.1.3 Angle-distance ratio models

These models are based on the angle θ in addition to the ratio R .

An example of this approach is the models proposed in [54]. These models are defined as:

$$\rho(\theta, R) = \begin{cases} f(X, R)\left(0.6 - \frac{\theta}{150}\right) + 0.4 & \text{if } \theta \leq 60^\circ \\ 0.4 & \text{if } \theta > 60^\circ \end{cases} \quad (2.91)$$

or

$$\rho(\theta, R) = \begin{cases} f(X, R)\left(1 - \frac{\theta}{75}\right) + 0.4 & \text{if } \theta \leq 60^\circ \\ 0.4 & \text{if } \theta > 60^\circ \end{cases} \quad (2.92)$$

where

$$f(X, R) = \begin{cases} 1 - \frac{R}{X} & \text{if } R \leq X(\text{dB}) \\ 0 & \text{if } R > X(\text{dB}) \end{cases} \quad (2.93)$$

X denotes the threshold where the distance-dependent correlation reaches its minimum value. X is assumed to be in the range of 6-20 dB.

In reference [53] the authors develop an explicit empirical model which takes into account the effect of θ and R . This model is expressed in the Table 2.6.

Table 2.6: Shadow fading correlation model proposed by Zayana et al. [53]

	$\theta \in [0^\circ, 30^\circ]$	$\theta \in [30^\circ, 60^\circ]$	$\theta \in [60^\circ, 90^\circ]$	$\theta \geq 90^\circ]$
$R(\text{dB}) \in [0, 2]$	$\rho = 0.8$	$\rho = 0.5$	$\rho = 0.4$	$\rho = 0.2$
$R(\text{dB}) \in [2, 4]$	$\rho = 0.6$	$\rho = 0.4$	$\rho = 0.4$	$\rho = 0.2$
$R(\text{dB}) \geq 4$	$\rho = 0.4$	$\rho = 0.2$	$\rho = 0.2$	$\rho = 0.2$

2.3.1.4 Saunders model

In reference [50] Saunders proposed a model which takes into account the impacts of not only θ and R but also the Tx-Rx propagation distance. This model is expressed as:

$$\rho(\theta, R, d_1, d_2) = \begin{cases} \sqrt{R} & \text{for } 0 \leq \theta < \theta_T \\ \left(\frac{\theta_T}{\theta}\right)^\gamma \sqrt{R} & \text{for } \theta_T \leq \theta < \pi \end{cases} \quad (2.94)$$

with

$$\theta_T = \arcsin\left(\frac{d_c}{\min(d_1, d_2)}\right) \quad (2.95)$$

where d_c is the decorrelation distance and d_1, d_2 are distance from the Rx to the Tx1 and Tx2.

This model is the baseline for a number of modified models given in [95–97].

2.3.2 Shadow fading correlation models for relay-based radio mobile network

As analyzed earlier in Introduction section, the shadow fading cross-correlation is even a more crucial issue in a relay-based deployment. However, very little research in the literature studying this problem can be found in the literature. Some work has been recently carried out by the WINNER, the IEEE 802.16j Relay Task Group or the 3GPP in order to predict the shadow fading correlation in a relaying deployment. Unfortunately, as in traditional network, there is not yet a well-agreed model. While the 3GPP assumes a constant correlation coefficient equal to 0.5 for all scenarios, the WINNER specifies zero correlation due to the limited amount of measurement data. Regarding the IEEE 802.16j Task Group, only the model for shadow fading correlation between two BSs which is based on the Saunders work is proposed. The correlation models for the shadow fading between BS-MS and RS-MS links or between two RS-MS links are still for further study.

2.4 Conclusion

This chapter reviewed the basic phenomena of wireless propagation channels necessary to understand the rest of this thesis. A particular focus was put on the path loss and shadow fading characterization and modeling. A number of existing path loss and shadow fading models were investigated. The advantages and disadvantages of each model, especially in terms of the simplicity and the accessibility were provided. As a result, the models which are the most relevant to this thesis objectives were defined.

Chapter 3

Measurement campaign

A measurement campaign is required in order to response to the thesis research objectives given in the previous chapters. This campaign should be able to characterize not only a simple propagation link but multiple links presented in a relaying network. To this end, a multi-link measurement campaign consisting of three nodes i.e. a BS, a RS and a MS was carried out.

3.1 Measurement scenario

The scenario is illustrated in Figure 3.1.

The measurements were performed in two areas called Old Town and Train Station in the city centre of Belfort, France. The measurement environment was a typical medium sized, urban city with 3-5 story buildings and nearly grid-like street layout.

The BS was installed on the roof of a 20-meter high building. It transmitted a narrow band signal toward RS and MS. The BS utilized a sector antenna with a beamwidth of 90° in azimuth and 10° in elevation. The antenna gain in the direction of the main lobe is 12 dBi. The transmitted power was set up at 43 dBm.

The RS was simulated by equipment set placed in a van. An omnidirectional dipole antenna with 2 dBi gain was employed at RS. This antenna is used to receive the signal transmitted from BS as well as to send another narrowband signal to MS. The transmitted power was maintained at 40 dBm. The antenna mast can be raised up so that the antenna height can vary from 4 to 13 meters.

Other equipment set was placed in a car to simulate the MS. It allows simultaneously measuring the signal powers from the BS and the RS. It was

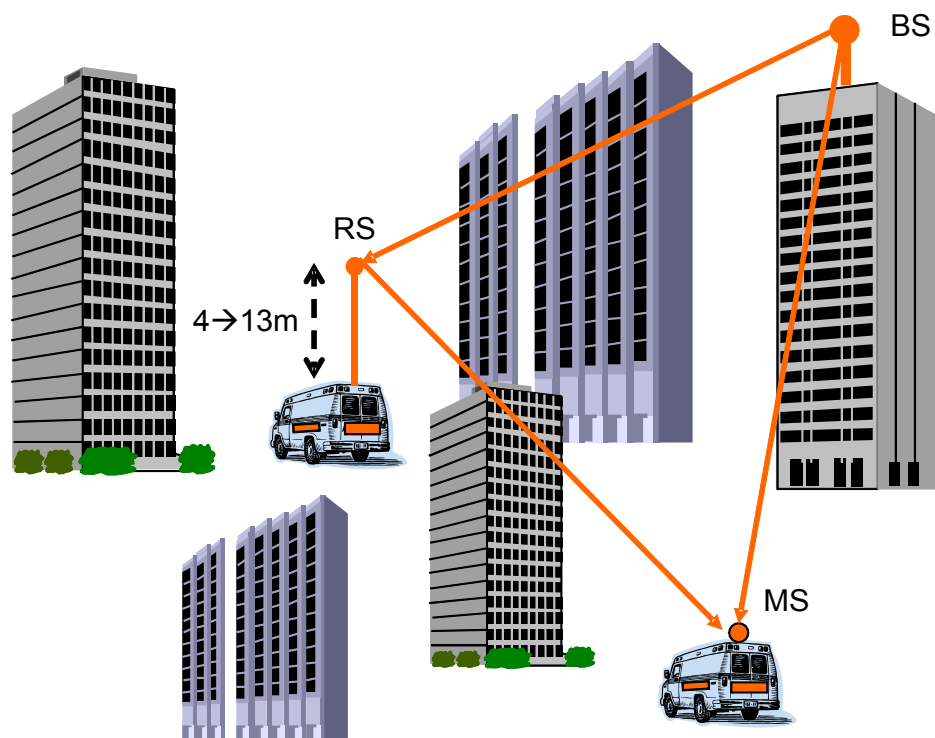


Figure 3.1: Measurement scenario

equipped with a 2 dBi omnidirectional antenna.

The BS, RS and MS equipments are illustrated in Figure 3.2.

All transmitters and receivers were synchronized by a 10 MHz reference source. The frequency band used in this measurement campaign is the UMTS band 2140 - 2155 MHz.

3.2 System construction

All of BS-RS, RS-MS and BS-MS links were expected to be measured in the same condition so that relay contributions could be correctly evaluated. To this end, the three link should ideally use the same frequencies and be simultaneously measured. However, these ideal conditions could not be realized due to several technical problems.

Firstly, the BS-MS and RS-MS signals should be orthogonal in order to be separately measured at MS. Therefore, it was not possible to use the same frequency for all links. Indeed, frequency f_1 was used for BS-RS and BS-MS

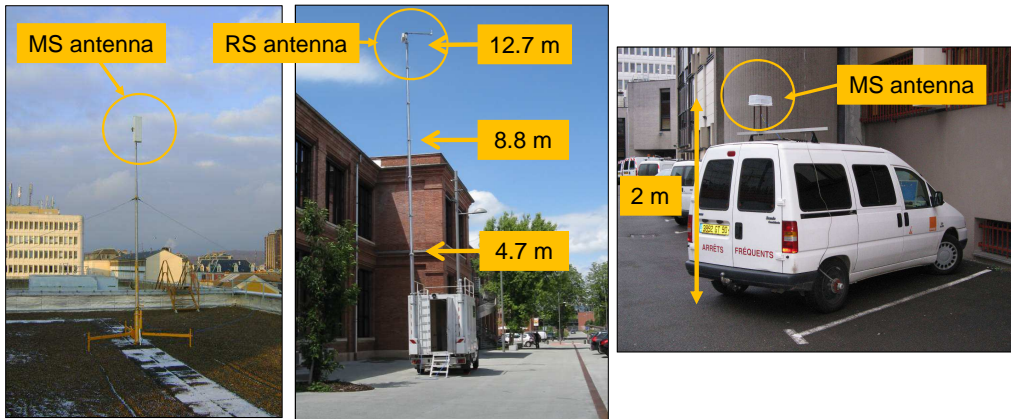


Figure 3.2: BS, RS and MS equipments

links and frequency f_2 was dedicated to RS-MS link. Nevertheless, these frequencies (f_1 and f_2) should be as close as possible in order to assure a fair comparison between different links.

Secondly, the isolation issues made impossible to simultaneously measure BS-RS and RS-MS links. If we considered using a single antenna at the RS for both BS-RS and RS-MS links, the first solution was to use a circulator at the RS to separate two frequencies f_1 and f_2 (Figure 3.3). When the RS was far from the BS, the received power of the signal coming from the BS (at frequency f_1) may fall down at -100 dBm. However, the RS should still maintain the transmitted power (at frequency f_2) as high as about 40 dBm to have an acceptable SNR and coverage area. Taking into account a typical circulator isolation level of 20 dB, the receiver at the RS should be able to measure the f_1 signal power with a level of -100 dBm and rejecting f_2 with a level of 20 dBm. This technical requirement can not be fulfilled with our available receivers. Alternative solutions were using a duplexer or two separate antennas. However, the duplexer requires a high frequency separation while the frequencies f_1 and f_2 need to be as close as possible. On the other hands, using separate antennas required a distance of at least few meters between them. This separation realization was quite cumbersome and made the measurement operation much more complicated. Therefore, this solution was not taken.

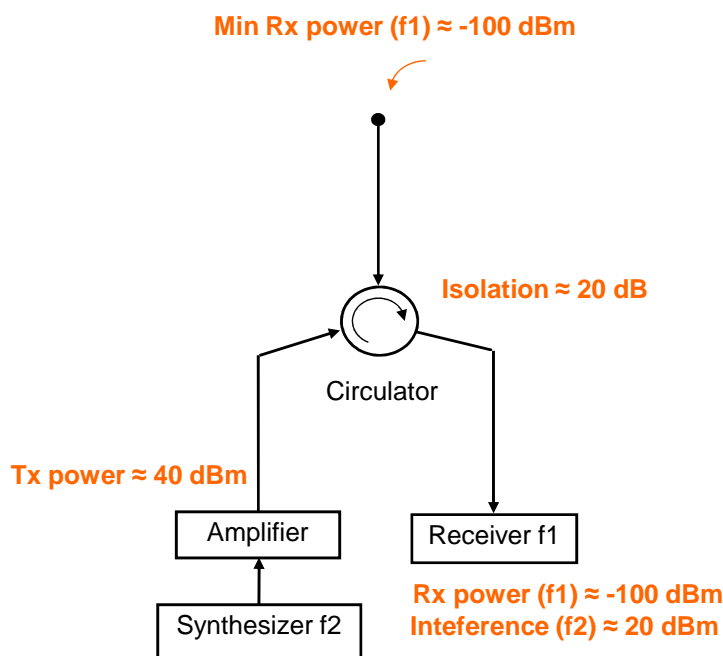


Figure 3.3: Isolation problem at RS

To overcome these technical constraints, we decided to perform the measurement campaign in two phases. The first phase aimed to characterize the BS-RS link. The second one was to simultaneously measure the BS-MS and RS-MS links.

The final radio configuration of the measurement scenario is schematically shown in Figure 3.4.

3.3 Measurement operation

3.3.1 Measurement phase I

This measurement phase was to measure the BS-RS link.

For each RS location, the received power was measured when the RS antenna mast was set at three different heights corresponding to 4.7 m, 8.8 m and 12.7 m (Figure 3.2). These heights were below the roof-top of surrounding buildings. The BS-RS link was then in Non Line-of-sight (NLOS) condition at all RS locations. The RS antenna was mounted at one end of

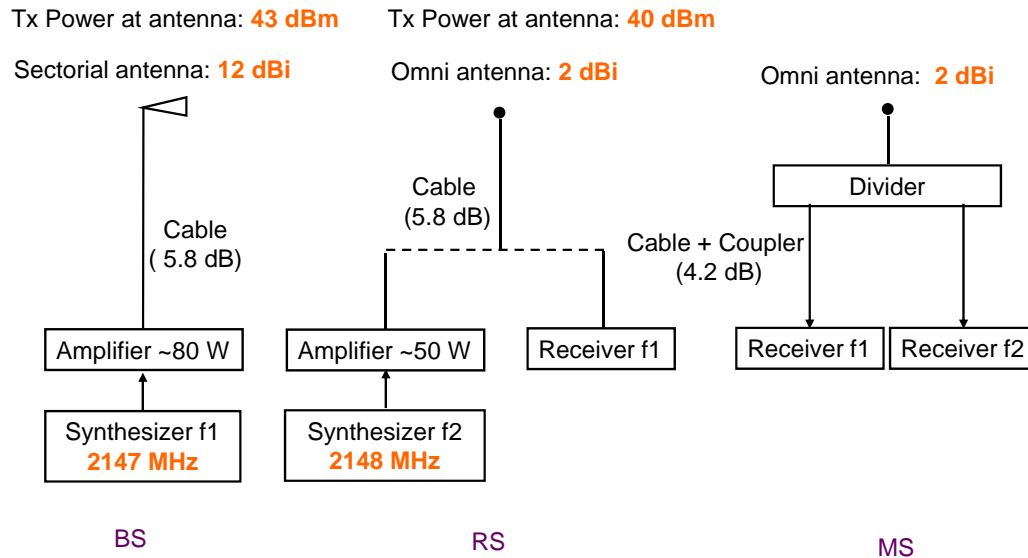


Figure 3.4: Radio configuration at BS, RS and MS

a 1-meter-long pole. The other end of this pole was fixed to the mast. This mast is rotated around its vertical axis during the measurement in order to measure the local variation of RS-MS signal. Two measurements with two rotation directions were performed. The first one was taken when the mast was rotated 360-degrees in clockwise direction and the second one was executed in counter-clockwise direction.

The measurements were performed at a total number of 77 RS locations distributed in two measurement areas i.e. Old Town (Figure 3.5) and Train Station (Figure 3.6). These RS locations were mainly within the BS-RS radius from 200 m to 1000 m.

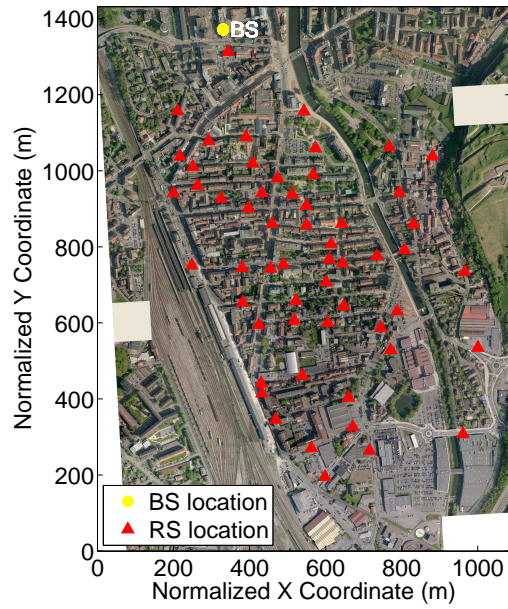


Figure 3.5: RS locations at Train Station area

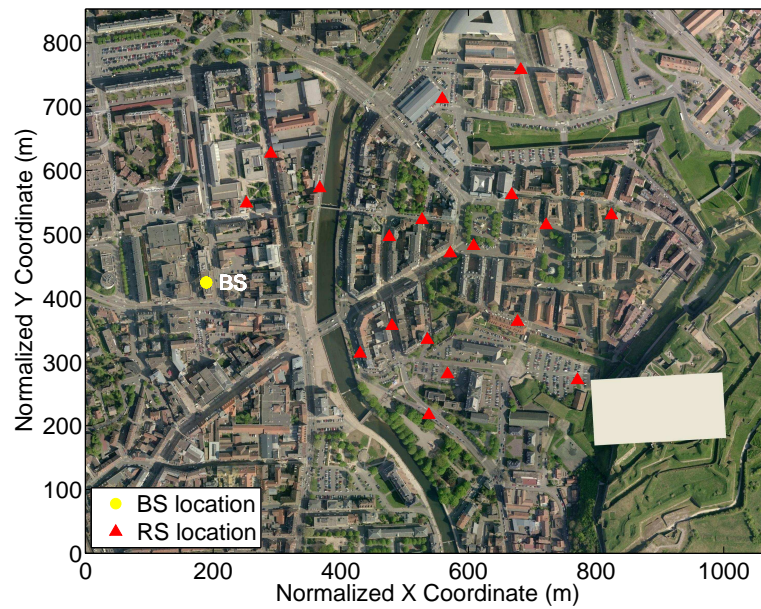


Figure 3.6: RS locations at Old Town area

3.3.2 Measurement phase II

In the second measurement phase, the received powers of signals transmitted from BS and RS were simultaneously measured at MS.

The measurements were consecutively performed with five RS locations in the Train Station area (respectively named RS1, RS2, RS3, RS4, RS5) and then with five RS locations in the Old Town area (named RS6, RS7, RS8, RS9, RS10). These ten RS locations are among the 77 locations taken in the measurement phase I. During the measurement, the received powers of the signal transmitted from the BS and the RS were simultaneously measured while the MS car was moving along a predefined measurement route (Figure 3.7 and Figure 3.8). The measurement routes lengths in the Old Town and Train Station areas are respectively about 9 km and 17 km. The received power measurement was taken every 2 cm (equivalent to $\lambda/7$ where λ is the signal wavelength). A complete measurement route was carried out first when the relay antenna height was set up at 4.7 m. Then the measurement process was repeated with the relay antenna height at 8.8 m and 12.7 m. The mobile positioning was relied on an embedded odometer and geo-referential maps.

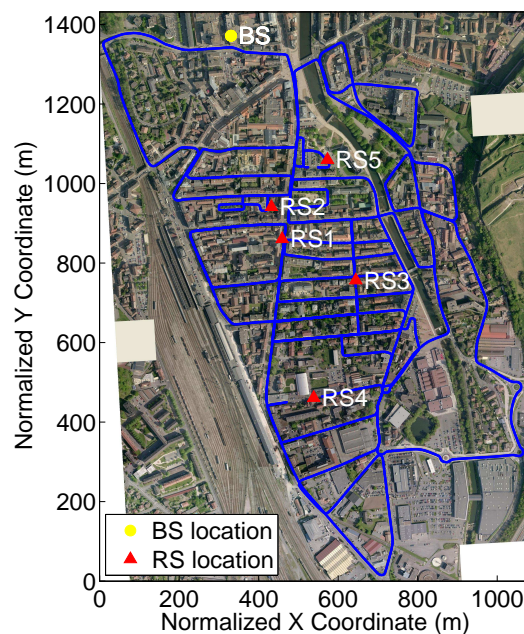


Figure 3.7: RS locations and measurement route at Train Station area

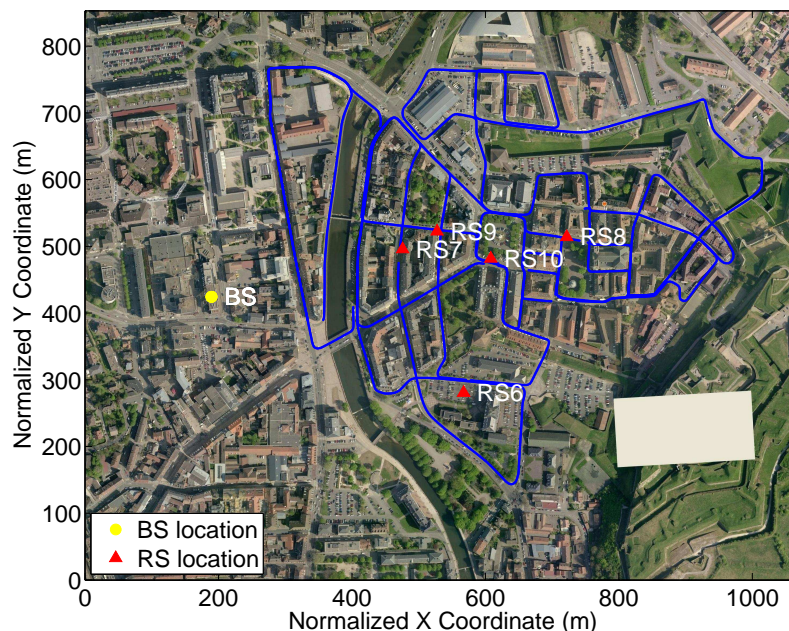


Figure 3.8: RS locations and measurement route at Old Town area

3.4 Data processing

The data obtained with the measurements should be processed before performing any analyses.

For the BS-RS link which was measured in the first measurement phase, the RS locations were firstly defined in a geo-referential map. The mean received power at each RS locations was then obtained by averaging all measurement samples taken when the antenna height was rotated around its vertical axis.

Concerning the data collected with BS-MS/RS-MS measurements, a more sophisticated data processing is required. The data processing steps are illustrated in Figure 3.9. Each step is described in more details in the following sections.

3.4.1 Measurement route localization

The objective of the localization process is to localize the measurement route on a geo-referential map and assign a Lambert coordinate (X , Y) to each measurement point. During the measurement, the total measurement route in each measurement area was divided to several sections. The mea-

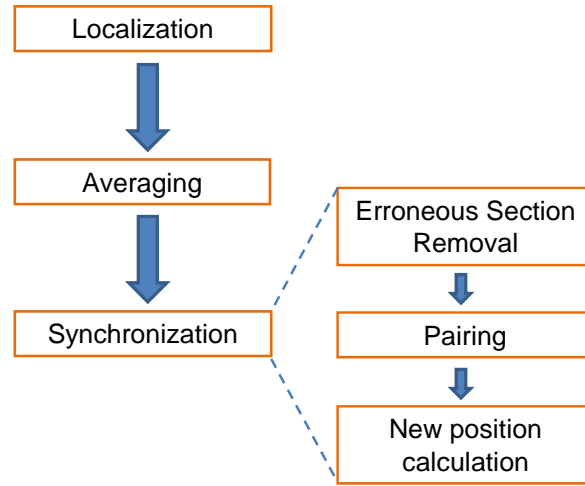


Figure 3.9: Data processing steps for BS-MS/RS-MS measurements

surement was then performed section-by-section. At the end of each section, the measurement vehicle stopped and the temporary data obtained on this section was saved into the computer. The starting and ending points of each section was generally street corners to ease their identification on the geo-referential map.

After the measurement operation, the starting and ending points of each section were located on the map. The measurement route of each section was then manually drawn. The measurement points acquired on each section were then automatically distributed every 2 cm so that they cover the total section length determined by the starting and ending points. The positioning method was validated by comparing the measurement distance, which was defined by the number of measurement points distributed every 2 cm, with the drawn trajectory distance.

As the localization procedure was completed, each measurement point was then associated with a Lambert coordinate. A localization result example is given in Figure 3.10.

3.4.2 Data averaging

The raw signals obtained after the measurement operation consist of fast fading components superimposing on slow fading components. Before being analyzed, the raw signals need to be averaged in order to obtain the local mean power by smoothing out the fast fading part.

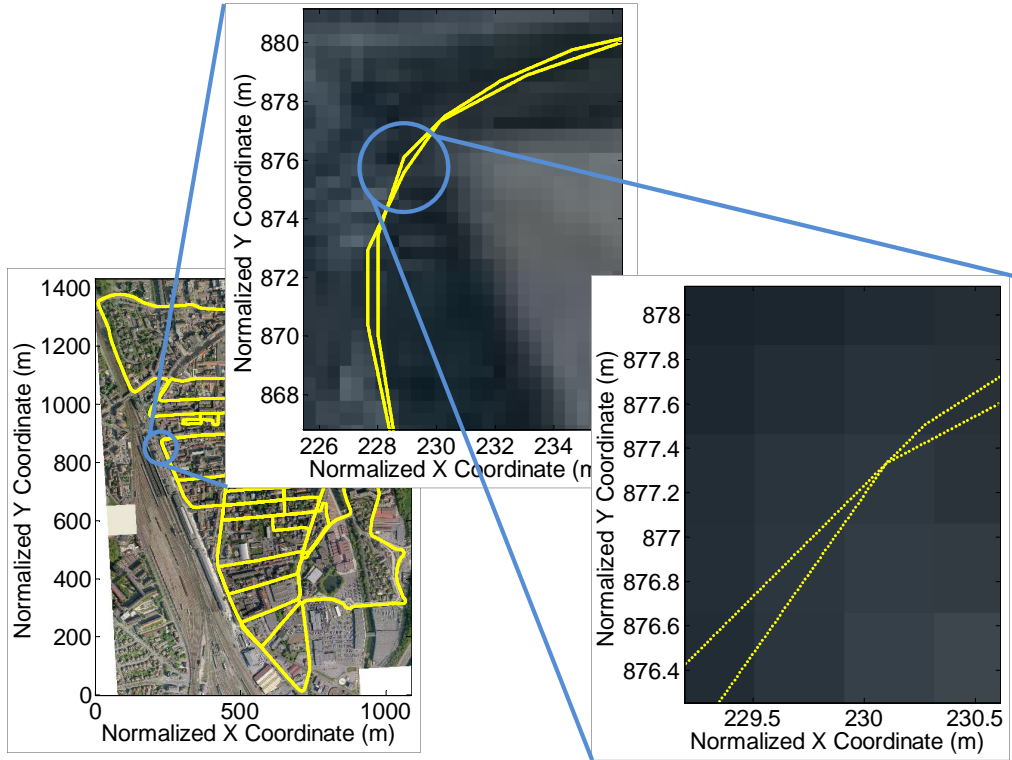


Figure 3.10: A localization procedure example

The raw signals are averaged by performing the shifting window method. This method, which is illustrated in Figure 3.11, is defined by two parameters. The first parameter, W , is the averaging distance expressed in the number of raw measurement points. The second parameter, D , is the shifting distance between two adjacent groups of W measurement points. The proper selection of the W and D values is critical in this averaging method. If W is chosen too short, the fast fading will still present in averaged data. If W is chosen too long, slow fading which should be preserved will be smoothed out.

In the literature, W is determined in the range of $20 \lambda - 40 \lambda$ [98, 99]. We compare the raw data to the averaged data obtained with different values of W and D in order to find the best trade-off values of W and D .

A simulation is performed in order to quantify the errors caused by averaging process taken with different W values. A fading signal is created by interacting 30 rays having identical amplitudes and random phases. The averaged power of these rays is defined as:

$$P_{ray} = \frac{\sum_{i=1}^{30} P(i)}{30} \quad (3.1)$$

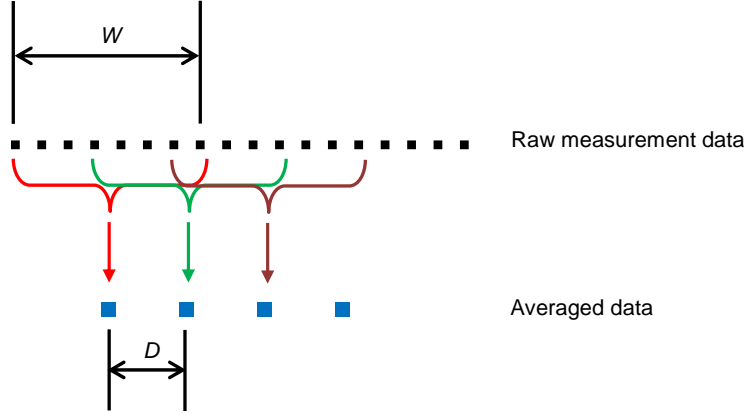


Figure 3.11: Averaging procedure of measurement signal

where $P(i)$ is the power of a ray. $P_{W=20}$ and $P_{W=40}$ are respectively the fading signal powers which are averaged by $W = 20\lambda$ and $W = 40\lambda$ windows. Then we define:

$$PowerDiff_{W=20} = \bigcup_{k=1}^{1000} (P_{ray} - P_{W=20}) \quad (3.2)$$

$$PowerDiff_{W=40} = \bigcup_{k=1}^{1000} (P_{ray} - P_{W=40}) \quad (3.3)$$

where k is the number of simulations.

It is found that $PowerDiff_{W=20}$ and $PowerDiff_{W=40}$ have zero means and standard deviations of 1.3 dB and 1.0 dB, respectively. It means that the results obtained with $W = 20\lambda$ and $W = 40\lambda$ are generally similar. The estimated errors are small and can be negligible. This result is also coherent with our visual inspection analysis.

However, a performance difference is observed with signals averaged with $W = 20\lambda$ and $W = 40\lambda$ when there is a brutal change in propagation condition. An example is given in Figure 3.12. The averaging process taken with $W = 40\lambda$ and $D = 10\lambda$ obviously over-smooth out the raw data when there is a strong change in the received powers. This situation happens when the MS moved from one street to another one which is in better propagation conditions.

Therefore, we conclude that the optimal values of W and D are respectively 20λ , which is equivalent to 2.8 m or 140 measurement points, and 10λ , which is equivalent to 1.4 m or 70 measurement points.

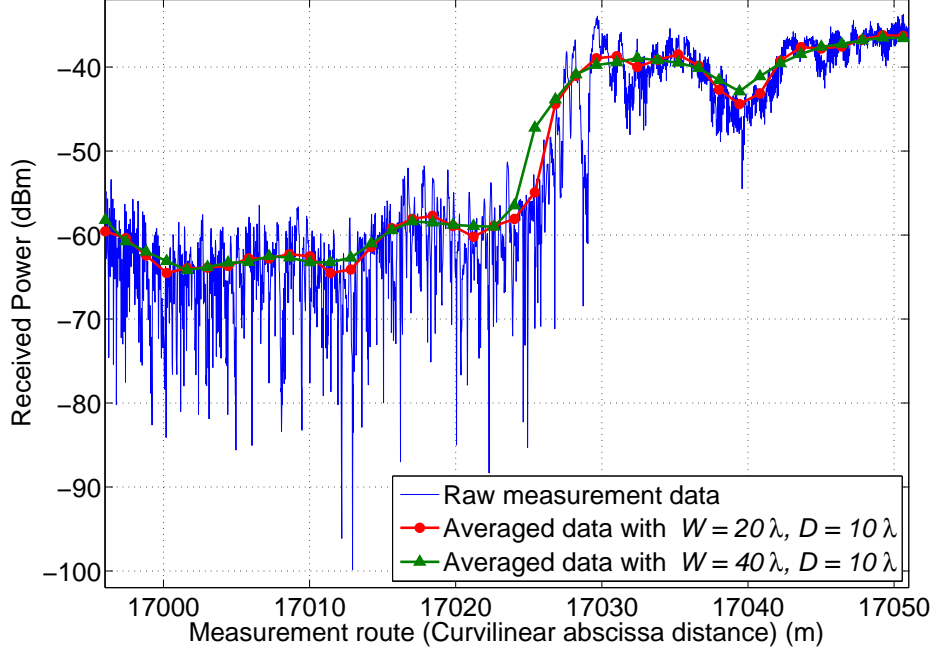


Figure 3.12: Averaged data with different W and D in comparison with raw measurement data

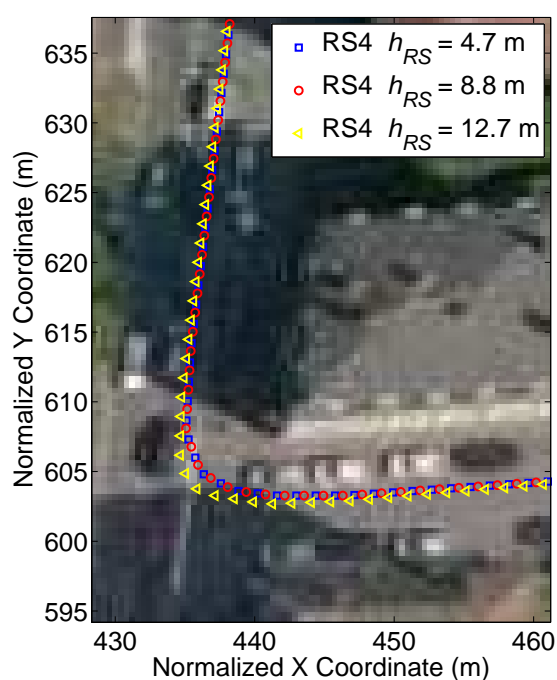
3.4.3 Measurement route synchronization

As described in Section 3.3.2, a predefined measurement route is repeated with 3 antenna heights and 5 relay locations in each measurement area. Thus a total of 15 measurement routes are performed in each measurement area. These routes should be theoretically identical. However, they are very similar but not identical in reality. The first reason is that trajectories taken during the measurement are different due to the traffic or driving mistakes. Secondly, the geographical localization is done independently in a manual manner for each measurement route. Moreover, each measurement route starts and finishes at different positions which are generally close together but not exactly the same. Consequently, the number of measurement points in different measurement routes is different. Figure 3.13 gives an example of this problem showing the measurement routes after the localization performed with RS4 and its 3 different antenna heights. Table 3.1 details the real measurement route lengths and measurement point numbers taken with 3 antenna height.

As a consequent, a straightforward point-to-point comparison is impossi-

Table 3.1: Details of measurement routes with RS4

RS4	Measurement route length (m)	Number of measurement points (after averaging)
$h_{RS} = 4.7$ m	17088	12204
$h_{RS} = 8.8$ m	17070	12191
$h_{RS} = 12.7$ m	17123	12230

**Figure 3.13:** A measurement section performed with RS4 and its 3 antenna heights

ble and the measurement routes should be synchronized.

The synchronization procedures are composed of several steps described below.

1. ***Erroneous section removal:***

The only common sections of all measurement routes are kept. The erroneous sections due to different causes such as driving mistakes are removed. An example of this process is shown in Figure 3.14. The blue section in Figure 3.14a is erroneous due to the driving mistake



Figure 3.14: An example of erroneous section removal

during the measurement. This section is then suppressed as illustrated in Figure 3.14b.

2. ***Pairing:***

After the erroneous removal procedure, the 15 measurement routes on each measurement area have similar trajectories. In order to synchronize them, a route is defined to be the reference. To be simple, the route with the smallest number of measurement points is chosen. The other routes will be synchronized by this reference.

Each point of the reference measurement route is associated with the nearest point of the route needed to be synchronized. This procedure is repeated as many times as measurement routes numbers (15 by area). The pairing procedure is illustrated in Figure 3.15.

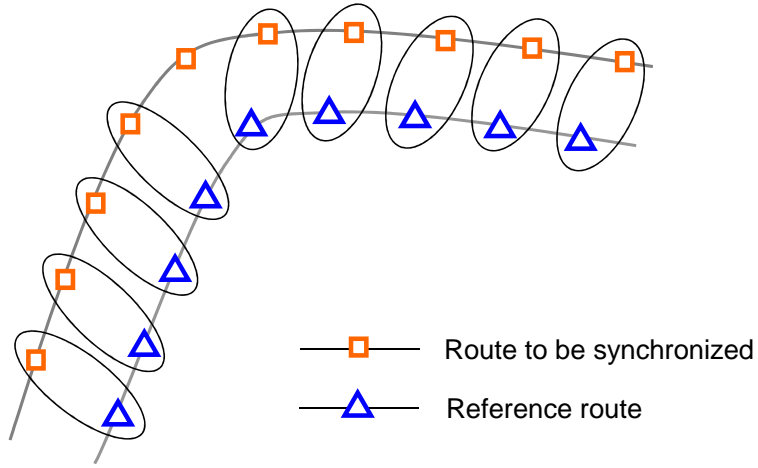


Figure 3.15: Pairing procedure illustration

3. ***New position calculation:***

A new route is created for each measurement area by averaging the coordinates of all 15 measurement routes in a point-by-point manner.

4. ***Results:***

After the localization, averaging and synchronizing process, a set of measurement points is defined for each measurement area. Each point is associated with its Lambert position and the received power from BS and RS for different relay locations as well as different relay antenna heights. The final measurement data for BS-MS link in each measurement area are saved with the format illustrated in Table 3.2.

Table 3.2: BS-MS measurement data

MS Lambert location		RS1			RS2			...	RS5		
X	Y	$h_{RS} = 4.7\text{m}$	$h_{RS} = 8.8\text{m}$	$h_{RS} = 12.7\text{m}$	$h_{RS} = 4.7\text{m}$	$h_{RS} = 8.8\text{m}$	$h_{RS} = 12.7\text{m}$...	$h_{RS} = 4.7\text{m}$	$h_{RS} = 8.8\text{m}$	$h_{RS} = 12.7\text{m}$
X_1	Y_1	$P_{BS-MS}(1,1)$	$P_{BS-MS}(1,2)$	$P_{BS-MS}(1,3)$	$P_{BS-MS}(1,4)$	$P_{BS-MS}(1,5)$	$P_{BS-MS}(1,6)$...	$P_{BS-MS}(1,13)$	$P_{BS-MS}(1,14)$	$P_{BS-MS}(1,15)$
X_2	Y_2	$P_{BS-MS}(2,1)$	$P_{BS-MS}(2,2)$	$P_{BS-MS}(2,3)$	$P_{BS-MS}(2,4)$	$P_{BS-MS}(2,5)$	$P_{BS-MS}(2,6)$...	$P_{BS-MS}(2,13)$	$P_{BS-MS}(2,14)$	$P_{BS-MS}(2,15)$
...
X_m	Y_m	$P_{BS-MS}(m,n)$
...
X_N	Y_N	$P_{BS-MS}(N,1)$	$P_{BS-MS}(N,2)$	$P_{BS-MS}(N,3)$	$P_{BS-MS}(N,4)$	$P_{BS-MS}(N,5)$	$P_{BS-MS}(N,6)$...	$P_{BS-MS}(N,13)$	$P_{BS-MS}(N,14)$	$P_{BS-MS}(N,15)$

Where:

(X_m, Y_m) is the Lambert location at measurement point m ($m \in [1, N]$ with N is the total number of measurement points).

$P_{BS-MS}(m, n)$ is the received power at measurement point m . The abbreviation n ($n \in [1, 15]$) corresponds to the configuration (RS location, RS antenna height)

A similar format is used to store the RS-MS measurement results.

3.5 Measurement validation

As analyzed earlier, potential relay contributions should be evaluated by examining not only a propagation channel but three channels together (BS-RS, RS-MS and BS-MS) in a consistent manner. To this end, a path loss comparison between links is necessary. However, such comparison in any measurement points is impacted by many factors such as the propagation channel non-stationarity, the antenna and the localization.

Concerning the BS-RS link, the measurements taken with three antenna heights are carried out at the same RS locations. Moreover, the utilized antenna is the same for all RS locations. Furthermore, it is observed that the averaged received powers measured with two mast rotation direction i.e. clockwise and counter-clockwise are equal. Therefore, the aforementioned impacts can be neglected in the BS-RS case.

However, these impacts may be more severe with RS-MS/BS-MS links because the 15 measurement routes in each measurement area are measured at different times. Consequently, the propagation channel non-stationarity may lead to the variations in the results obtained with different measurements. Furthermore, the localization and synchronization procedures may also content errors. Besides, the antennas used at RS and MS are different. The potential cumulative errors caused by these factors may lead to false conclusions about the relay contribution.

Therefore, potential errors caused by the aforementioned factors should be quantified in order to guarantee the comparison result validity. The following sections aim to estimate those errors.

3.5.1 Antenna validation

Two different omnidirectional antennas were used at RS and MS. Therefore, it is necessary to verify if this difference has any impacts on the measurement results. To this end, we carried out an additional measurement. The RS and MS antennas were placed together on top of the MS vehicle to measure the signal power transmitted from BS. A complete measurement route was taken in Train Station area. The path losses measured with the two antennas were calculated by Equation 3.4:

$$PL(dB) = P_t - P_r + G_t + G_r - L_{cable} \quad (3.4)$$

where PL is the measured path loss (dB). P_t and P_r are respectively the transmitted and received powers. G_t and G_r are respectively the transmitted and received antenna gain. L_{cable} is the total loss due to the cables used at both transmitted and received ends.

Figure 3.16 shows the path loss measured with MS antenna against that measured with RS antenna. It is obvious that the two measured path losses over the whole measurement route are generally equal. However, if we make a point-to-point comparison, a path loss difference of about 5 dB can occur.

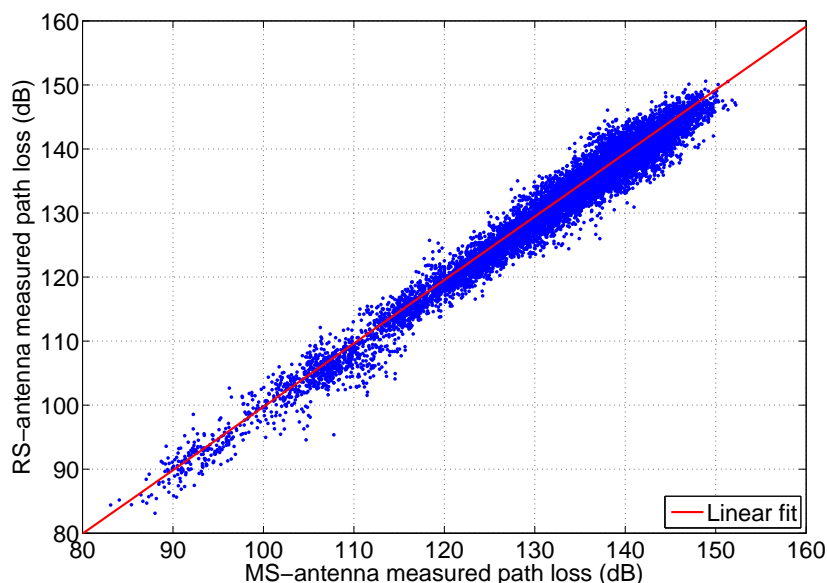


Figure 3.16: MS antenna measured path loss displayed against RS antenna measured one

3.5.2 Localization validation

In the second measurement phase, the BS-MS link was measured with all relay locations and antenna heights. Consequently, the BS-MS link measurement was repeated 15 times with the same measurement route. The received powers of these 15 measurement routes should be theoretically identical after the averaging and synchronization process. The measured data after the averaging and synchronization (from now on called “processed data”) in Train Station and Old Town areas are respectively displayed in Figure 3.17 and Figure 3.18. These 15 measurement data are observed to be generally very similar. The cross-correlation between any two measurement routes is found to be in the range of 0.97-0.98 for both two measurement areas.

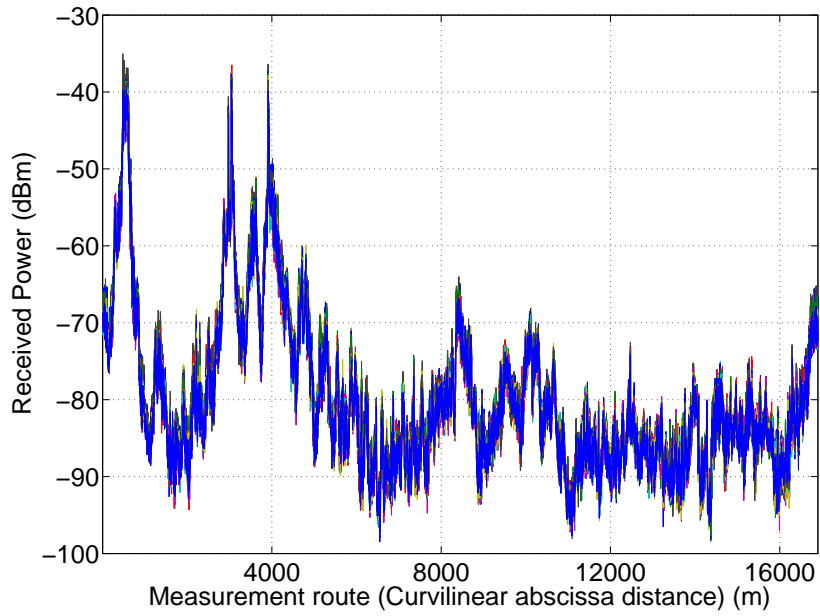


Figure 3.17: 15 processed data of BS-MS links in Train Station area

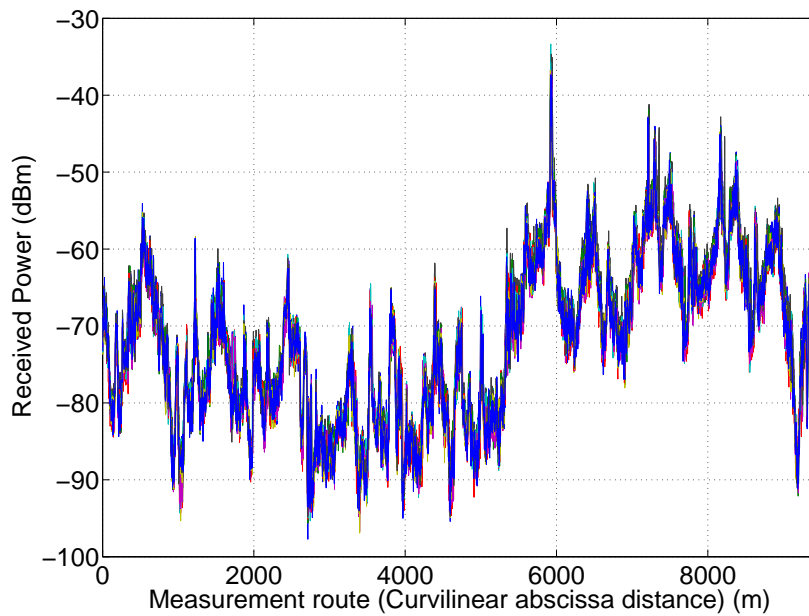


Figure 3.18: 15 processed data of BS-MS links in Old Town area

However, it is found that these measurements are locally shifted from each other. This phenomenon is most clearly seen in segments having “peak” powers. An example taken from Old Town area is given in Figure 3.19. The shifting distance between the first and the last peak is as long as 12 meters. It demonstrates that a potential relay contribution might not be concluded based on a local comparison.

3.5.3 Total measurement validation

The aforementioned observations show certain mismatches among measurement data. Therefore, it is important that these mismatches should be quantified.

If we call $M(n)$ ($n \in [1, 15]$) the average received power of all measurement points in a configuration n , then:

$$M(n) = \frac{\sum_{m=1}^N P_{BS-MS}(m, n)}{N} \quad (3.5)$$

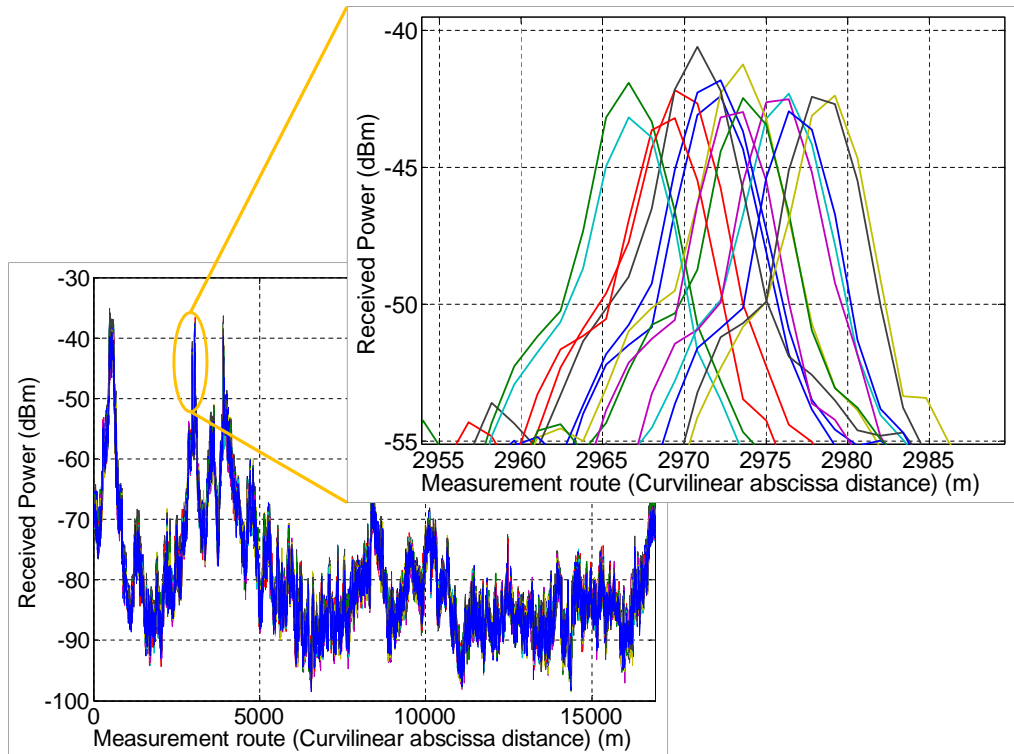


Figure 3.19: An shifting problem example

We defines $diff_all$ as the set of difference between any two values of $M(n)$, then:

$$diff_all = \bigcup_{n_1=1, n_2=2}^{15} |M(n_1) - M(n_2)| \quad (3.6)$$

where \cup is union operation and $(n_1, n_2) \in n, n_1 \neq n_2$. The histogram of $diff_all$ is illustrated in Figure 3.20a. It is found that the 50th and 90th percentile of $diff_all$ are respectively 0.5 dB and 1.0 dB. Therefore, a comparison performed over a complete measurement route between any two links is considered to have sense if the difference is greater than 1.0 dB regardless of the errors caused by the localization, the synchronization or the channel non-stationarity.

Now we consider the received power difference between two any configurations $(n_1, n_2) \in n$, at the same measurement point m . It is defined as:

$$diff(m) = \bigcup_{n_1=1, n_2=2}^{15} |P_{BS-MS}(m, n_1) - P_{BS-MS}(m, n_2)| \quad (3.7)$$

Then the difference at all measurement points is given as:

$$diff_point = \bigcup_{m=1}^N diff(m) \quad (3.8)$$

Figure 3.20b shows the histogram of $diff_point$. The 50th and 90th percentiles of $diff_point$ are respectively 1.4 dB and 3.7 dB. Consequently, if a path loss comparison between any two links at a specific point results in a difference which is smaller than 3.7 dB, a conclusion could not be drawn.

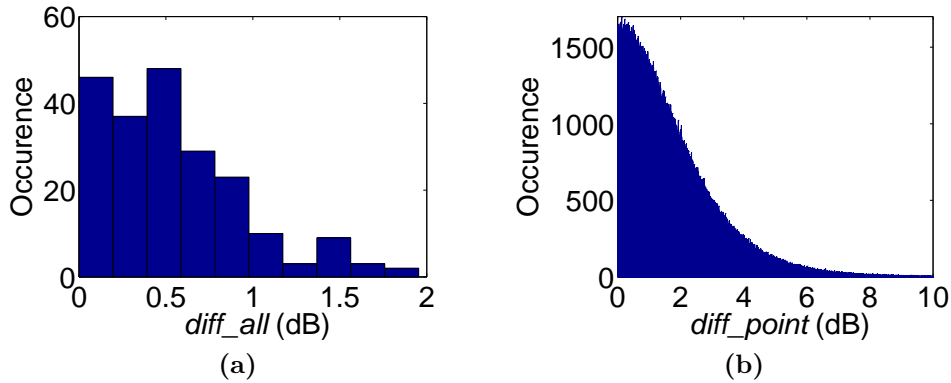


Figure 3.20: Histogram of $diff_all$ and $diff_point$

3.5.4 Discussion

The analysis performed in the previous sections allows establishing an error margin in the “processed data” that we should take into account. This margin is about 1.0 dB, which is considered reasonable, if a comparison between two links is taken over a complete measurement route. However, if a point-to-point comparison is performed, the error margin is increased to 3.7 dB.

3.6 Conclusion

This chapter presented a 2.1 GHz multi-link measurement campaign with relays performed in two outdoor urban areas. This campaign consisted of two phases. The received powers of BS-RS link were measured with 77 RS locations and 3 relay antenna heights in the first phase. The second phase was dedicated to the simultaneous measurement of BS-MS and RS-MS. The measurement data processing procedures including the localization, the averaging and the synchronization were also described. Finally, the potential errors caused by different factors such as the averaging and the localization procedures, the antenna or the channel non-stationary were quantified. Basing on the error quantification results, we concluded that a comparison among path losses measured with different RS locations and relay antenna heights should be done over the whole measurement routes instead of point-to-point manner.

Chapter 4

Multi-link characterization and modeling

Based on the measurement data acquired with the measurement campaign described in Chapter 3, this chapter aims to characterize and model propagation channels in a 3GPP LTE-Advanced relaying system. Multi-link path loss models with focus on BS-RS link will be examined. The analysis results related to relay antenna height impacts on path loss will also be presented. The shadow fading correlations between BS-MS/RS-MS or between RS-MS/RS-MS links will be studied. Finally, the path loss model consistency will be investigated.

4.1 BS-RS link characterization and modeling

4.1.1 Introduction

Propagation channel models integrating reliable path loss models are required in order to design relaying systems. Among three propagation links i.e. BS-RS, RS-MS and BS-MS presented in a relay-based network, the BS-MS and RS-MS links have been more or less studied. The BS-MS link is considered identical to the macro cellular link in a classical mobile network without relays. Path loss models for this link have been the subjects of much research for many years. Consequently, a tremendous model number is proposed. Taking into account the relay antenna height in proposed scenarios [8, 41–43, 64], we can assume the RS-MS link as the micro cellular link in classical networks. Path loss model for this link, especial for LOS scenarios, is also analyzed by many studies although they are less abundant than

BS-MS models. However, very little research can be found in the literature concerning the BS-RS path loss link. Several models are recently suggested by 3GPP [41], WINNER [42] project and IEEE 802.16j [43] task group but their validation in a realistic environment is yet to be fully examined. Therefore, this chapter section will investigate the relaying system path loss models while focusing on the BS-RS link.

As mentioned earlier, a RS consumes radio resource for the backhaul link. Simulation results obtained in 3GPP have shown that the backhaul link is the bottleneck of the relay-enhanced transmission [41]. A potential solution is to favor as much as possible the BS-RS radio link by placing the RS in favorable radio locations. However, in this case the RS is more likely to cause more interference to adjacent cells. Therefore, the relay antenna height is an important parameter which should be taken into account in channel modeling. The challenge is to find the optimal relay antenna height in order to maximize the potential relay contributions. This issue will be examined in the following section.

4.1.2 Relay antenna height impacts on BS-RS link path loss

The BS-RS link path loss is calculated by Equation 3.4.

For each RS location, the calculated path losses with 3 relay antenna heights (h_{RS}) are compared to each other. The comparison results are displayed in Figure 4.1. The Empirical Cumulative Distribution Function (CDF) of path loss calculated with all RS locations and RS antenna heights are presented in Figure 4.2.

These figures clearly show the dependence of path loss on h_{RS} , in which the higher h_{RS} provides the smaller path loss. This dependence is observed in 70 over 77 RS locations.

In order to examine this dependence in lower antenna height (e.g 2m), we calculate also the BS-MS link path loss at MS locations which are the same or close to RS locations. The CDF plot of this path loss is also displayed in Figure 4.2. The path loss measured at the MS level is observed to be slightly greater than that measured at $h_{RS} = 4.7$ m, which confirms the impact of h_{RS} .

The path loss differences between different relay antenna heights are quantified by the histograms in Figure 4.3. This difference between MS level and the slowest RS antenna height is not significant and only about 1 dB (Figure 4.3a). However, the BS-RS link path loss decreases with an average value of 3.5 dB when the RS antenna is raised from 4.7 m to 8.8 m (Figure 4.3b).

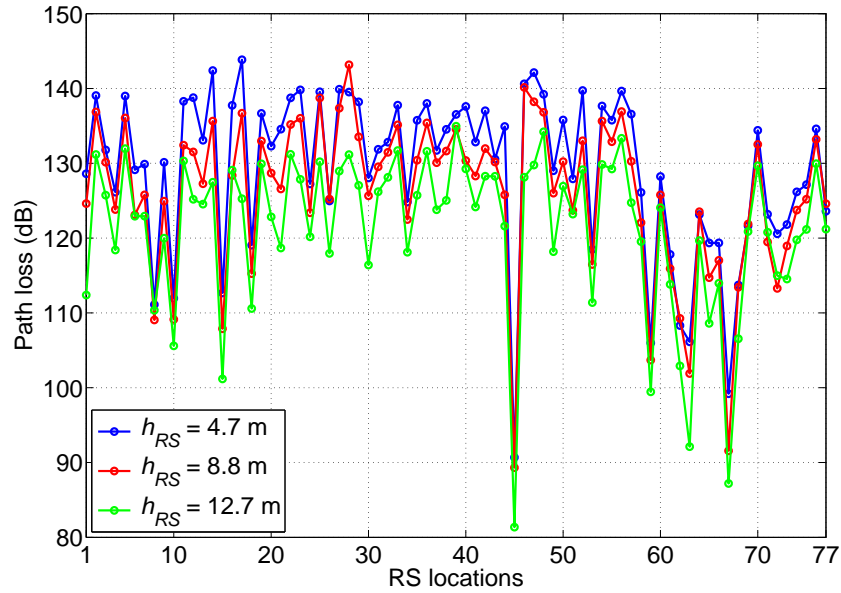


Figure 4.1: Impact of RS antenna height on BS-RS path loss

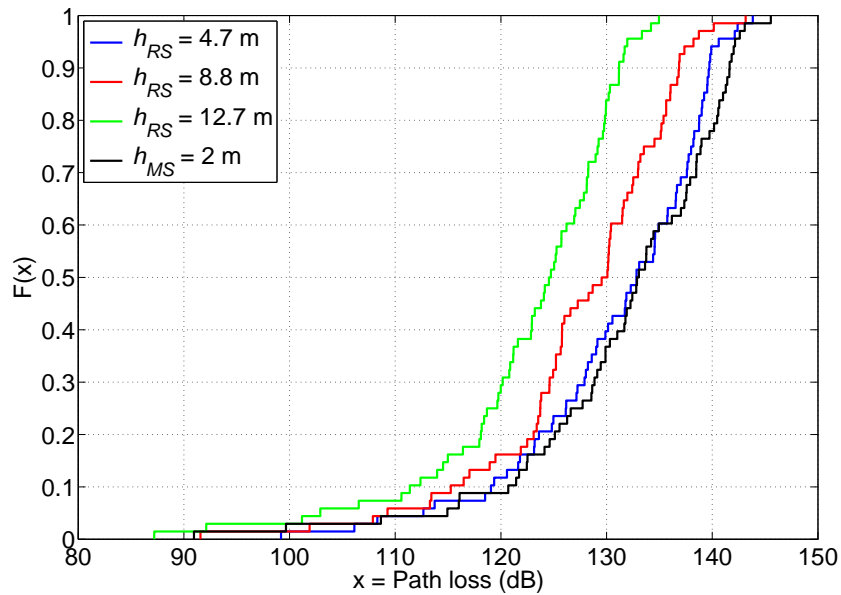


Figure 4.2: Empirical CDF of measured path loss at different RS antenna height

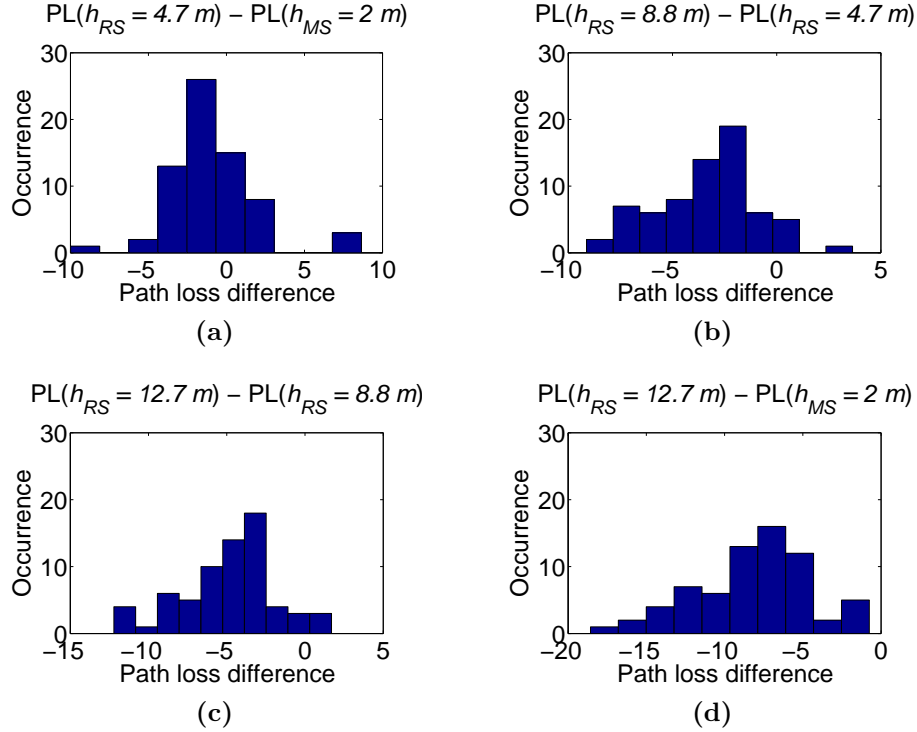


Figure 4.3: Histogram of path loss difference between RS antenna heights

Similarly, an average path loss reduction of 4.6 dB is observed when the h_{RS} is changed from 8.8 m to 12.7 m (Figure 4.3c). Moreover, Figure 4.3d confirms that path loss measured at $h_{RS} = 12.7\text{ m}$ is always smaller in comparison with that measured at MS having the same location. The average reduction is about 8 dB.

To explain the dependence of BS-RS path loss on h_{RS} , it is worth reminding that the BS is installed over the surrounding rooftop and the BS-RS link is in NLOS in most of RS locations. Therefore, the transmitted signal principally propagates over the rooftop. When h_{RS} is high and approaches the roof level i.e. LOS condition, the received signal is less attenuated by the diffraction or reflection caused by surrounding buildings.

4.1.3 Extended research on the impact of relay antenna height

The aforementioned impact of h_{RS} is observed in the outdoor urban area at the frequency of 2.1 GHz. It is of great interest to examine this impact

on other frequencies and environments. To this end, an additional multi-frequency measurement campaign was carried out.

4.1.3.1 Measurement descriptions

Three narrow band signals at frequencies $f_1=900$ MHz, $f_2=2100$ MHz, $f_3=3500$ MHz were transmitted from the roof of a 21-meter high building in an urban environment. The selection of these frequencies was motivated by LTE/LTE-Advanced operating band discussed after the World Radiocommunication Conference 2007 [65]. Although the spectrum allocations for LTE-Advanced have not yet been confirmed, UHF band (698-960 MHz), UMTS (2100 MHz) and C-band (3400-4200 MHz) are among the spectrum bands which were proposed and under consideration to be deployed for future systems [65].

The measurements were performed in different positions on different floors, both inside and outside, of a 5-floor building. The Tx-Rx distance was about 140-160 meters depending on the exact positions of Rx in the reception building. The LOS condition is obtained on the highest floor of reception building.

The measurement environment seen with several aerial angles is illustrated by Figure 4.4.



Figure 4.4: Measurement campaign environment

The transmitted power was set up at 43 dBm for all three frequencies. The mast allowed the transmitter antenna to be few meters above the surrounding buildings (Figure 4.5).

At the reception end, the Rx antenna was installed on a rotating device for the measurement inside the building (Figure 4.5). For the measurement outside the building, the rotating device was replaced by a 2-meter long pole which was hand held. The use of this pole allows reaching through the window to carry out the measurement at about 1 meter outside the building. In both inside and outside cases, the Rx antenna was rotated around its vertical axis during the measurement. This rotation allows avoiding the multi-path effect and measuring the average power as described in Section 3.3.1 of Chapter 3.

The measurements were performed at about 250 different points distributed over 5 floors of the reception building, either indoor or outdoor. The measurement positions on the ground floor are presented in Figure 4.6. Those on other floors were carried out in similar positions.



Figure 4.5: Photos of Tx antenna and Rx set-up with rotating device

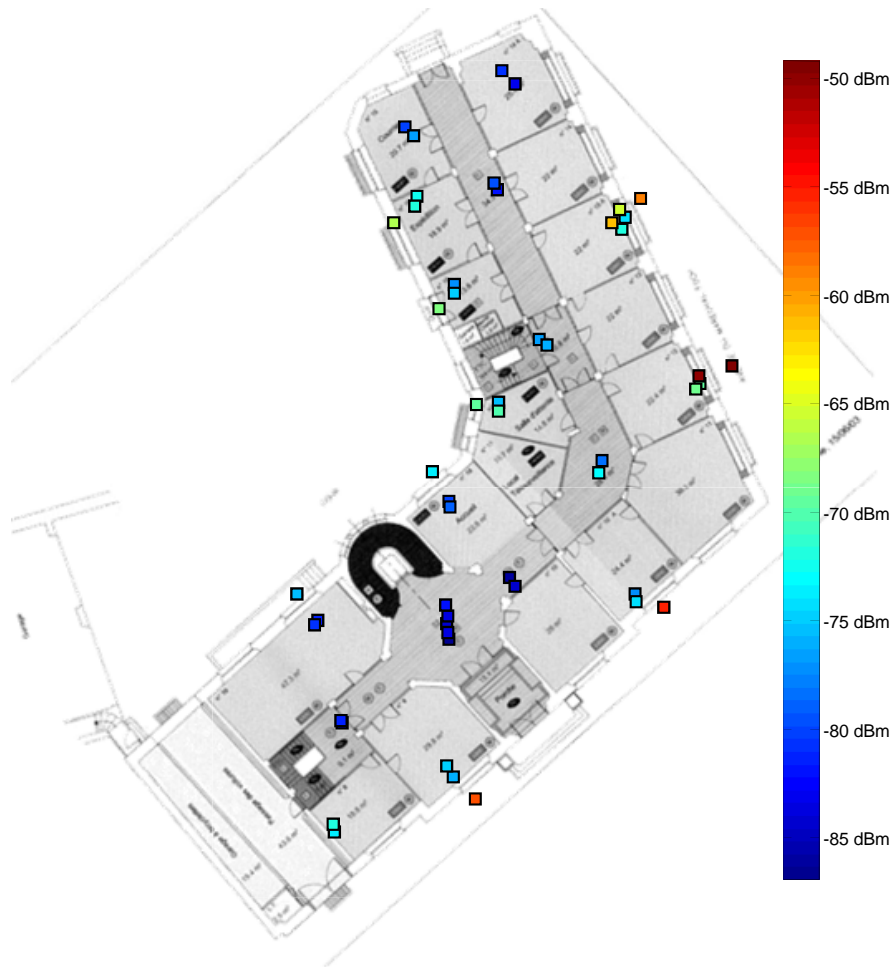


Figure 4.6: Measurement positions at the ground level

4.1.3.2 Received power dependence on floor level

Relay could be deployed in indoor or outdoor environments. Therefore, the total number of measurement points is classified as “indoor” or “outdoor” groups depending on their positions. In order to have a general evaluation of the receive (relay) antenna height impact in an indoor scenario, the mean received power of all indoor reception points on each floor is compared to those on different floors. The result is presented in Figure 4.7b. Despite some small irregularities (e.g. between the second and third floor at 2.1 GHz and 3.5 GHz), the general trend shows the dependence of received power on floor level, in which the higher floor provides better received power. The dependence appears similar at different frequencies.

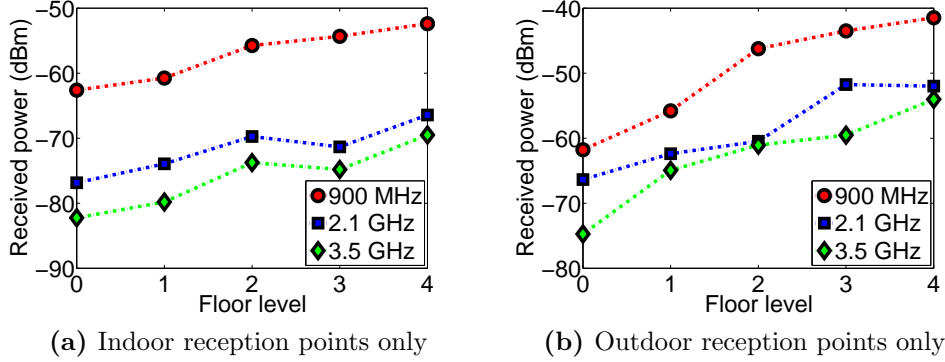


Figure 4.7: Received power dependence on floor level

This trend is also observed in outdoor measurements (Figure 4.7a). The measured floor gain is in the range of 3-8 dB/floor. Each floor height is about 4 meters. Therefore, this floor gain corresponds to the result observed in Section 4.1.2 which is about 3.5-4.6 dB gain for each increasing step of relay antenna height.

The impact of Rx antenna height is examined in more precise conditions by performing the same analyses at outdoor reception points on different facades of the reception building. As illustrated in Figure 4.8, the propagation conditions of these facades are not identical. Facade 2 is at the rear side of the building compared to Tx antenna. All the measurement points carried out on this facade are then completely in NLOS condition. Propagation conditions on facade 1 and 3 are a mixture of LOS and NLOS. The LOS is maintained on the two highest floors of facade 3. However, the lower floors are partially shadowed by trees and a building situated between Tx and Rx. Facade 1 is parallel to the Tx-Rx axis and rather in the LOS condition although it is also slightly obstructed by trees.

The analysis results for these three facades are presented in Figure 4.9. The received power dependence on antenna height observed in previous analyses is clearly confirmed on facade 2 where the NLOS condition is maintained for all measurement positions. Although this dependence is less clear on facade 3, the higher floor levels still generally provide better received power. Furthermore, on these two facades, the dependences are similar at all studied frequencies. However, this trend is no longer observed on facade 1. The received power does not present the dependence on the floor level. This result is explained by the complex propagation condition in this facade. As discussed above, it is a mixed condition between LOS and NLOS with the dominance of LOS. In this condition, link budget and Rx antenna height are



Figure 4.8: Aerial photos showing reception building facades with different propagation conditions.

relatively independent [45, 100].

Similar analyses are also performed with three groups of indoor measurement points which are situated toward three facades of the reception building. The obtained results present the dependence of received power on receiver antenna height and these dependences are similar in all groups of reception points.

4.1.3.3 Conclusion

The above analyses confirm the impact of Rx antenna height on BS-RS link path loss over various frequencies from 900 MHz to 3.5 GHz in both outdoor and indoor environments. This impact is clearly observed when the BS-RS link is completely in NLOS conditions as demonstrated in Section 4.1.2. When the propagation condition becomes a mixture of LOS and NLOS or completely LOS, this impact no longer exists.

4.1.4 Path loss models for BS-RS propagation link

4.1.4.1 Validation of existing path loss models

WINNER, 3GPP and COST-231 WI were shown in Section 2.2.8 as the most relevant models among the existing ones to be applied in relaying systems. In this section, the BS-RS path losses predicted by WINNER B5f,

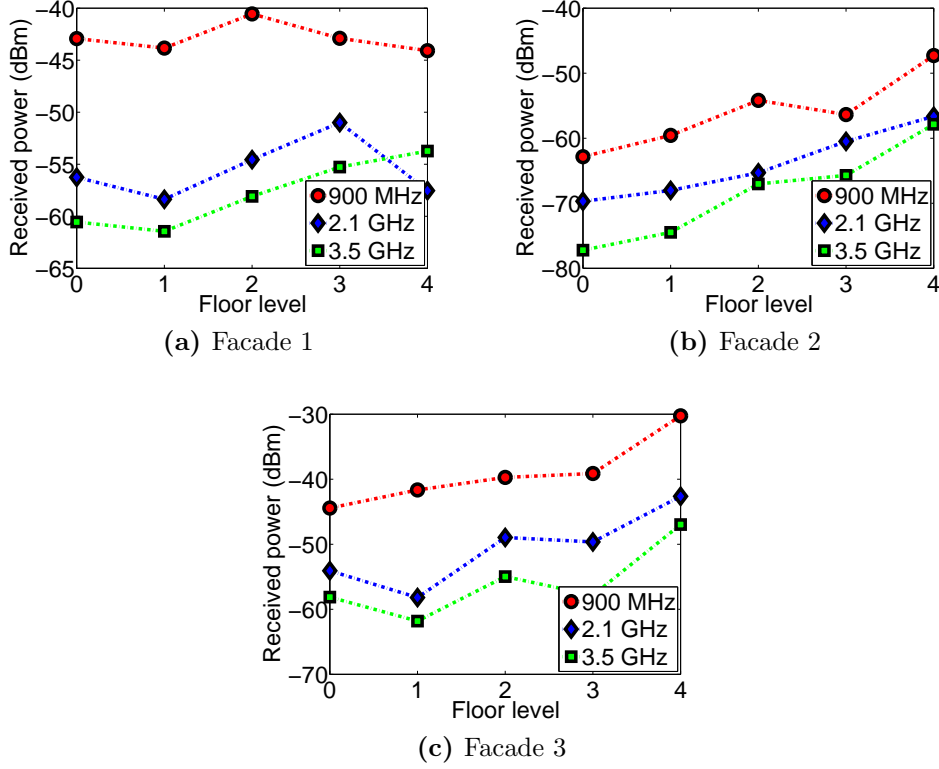


Figure 4.9: Received power dependence on floor level

3GPP Relay and COST-231 WI models are compared to the measurement data. The comparison results are presented in Figure 4.10.

Figure 4.10 demonstrates that 3GPP Relay and WINNER B5f models obviously underestimate the path loss. In the case of WINNER B5f, its non-compatibility is explained by the analytical method used to develop it. Reference [42] shows that it is derived from the model B5a designed for BS-RS link in LOS condition by artificially attenuating the correction factor by 15 dB. However, the distance dependence parameter which should not be identical in LOS and NLOS conditions is unchanged in the two models. Moreover, it is reported from [37] that B5f model is more appropriate to a mixed condition between LOS and NLOS rather than a complete NLOS condition as in the environment of this measurement campaign.

The path loss prediction of COST-231 WI model is given with street width $w = 10$ m, average building height $h_r = 15$ m and average building separation $b = 20$ m. Figure 4.10 shows that the COST-231 WI prediction is the closest to the measurement although this model is neither designed for

relaying systems nor formally specified to use at frequencies beyond 2 GHz. The mean and standard deviation prediction error of this model are provided in Table 4.1.

Table 4.1: Prediction error statistics of COST-231 WI model

	$h_{RS} = 4.7\text{m}$	$h_{RS} = 8.8\text{m}$	$h_{RS} = 12.7\text{m}$
Error mean	5.2 dB	4.1 dB	0.9 dB
Error standard deviation	6.7 dB	7.1 dB	7.1 dB

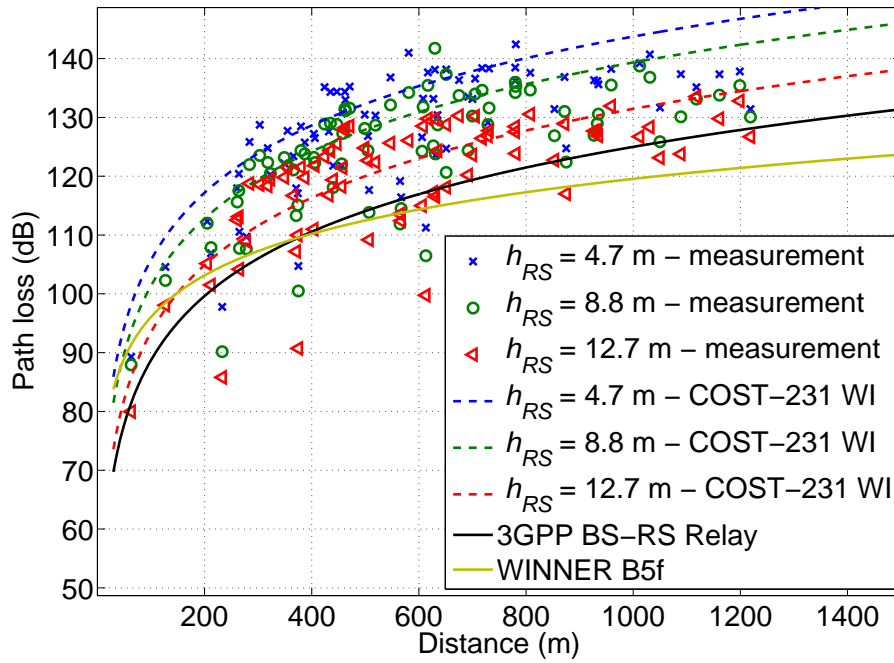


Figure 4.10: Path loss predicted by WINNER B5f, 3GPP Relay and COST-231 WI models in comparison with the measurements

4.1.4.2 Proposed path loss model

As mentioned earlier, the COST-231 WI model performance becomes poor if the terrain is not flat or the land cover is inhomogeneous. Moreover, this model requires detailed knowledge of propagation environment. It defines many parameters and the relation among them. This may make it complex to be applied in certain practical cases, especially for engineering work. Therefore, in order to provide a simple propagation model which is capable of modeling the BS-RS link path loss in 2.1 GHz frequency band while taking into account the impact of relay h_{RS} , we propose a new channel model.

This model is given by:

$$PL(dB) = 34 \log_{10}(d) + 5 + 25.5 \log_{10}(20 - h_{RS}) \quad (4.1)$$

where d [m] is distance between BS and RS, h_{RS} [m] is the RS antenna height. The model is valid for the BS-RS link in NLOS condition and with d in the range from 20 m to 1000 m. The RS antenna height is limited up to 15 m which is suitable for typical relaying deployments.

The model prediction in comparison with the measurement data is illustrated in Figure 4.11. The statistics of the model prediction error are presented in Table 4.2. The standard deviations are from 6 to 7 dB. We observe from Figure 4.11 that there are 4 RS locations in the range of 50-500 meters which are considerably below the model prediction. We suppose that this phenomenon is due to the particular local environment surrounding these RS locations which are observed to be in better propagation conditions than the other ones. At the writing moment of this thesis, a measurement campaign is being planned to confirm this supposition.

It is interesting to investigate the proposed path loss model validation in another propagation environment. To this end, the path loss predicted by the proposed model is compared with measurement data obtained in the additional measurement campaign (Section 4.1.3). The comparison is taken with different measurement points situated at facade 2 and on all levels of reception building. By estimating each level height to be 4 meters, the equivalent received antenna heights are in the range of 2-18 meters. The comparison result is presented in Figure 4.12.

Table 4.2: Prediction error statistics of proposed model

	$h_{RS} = 4.7\text{m}$	$h_{RS} = 8.8\text{m}$	$h_{RS} = 12.7\text{m}$
Error mean	0.26 dB	0.35 dB	0.13 dB
Error standard deviation	6.8 dB	7.0 dB	7.1 dB

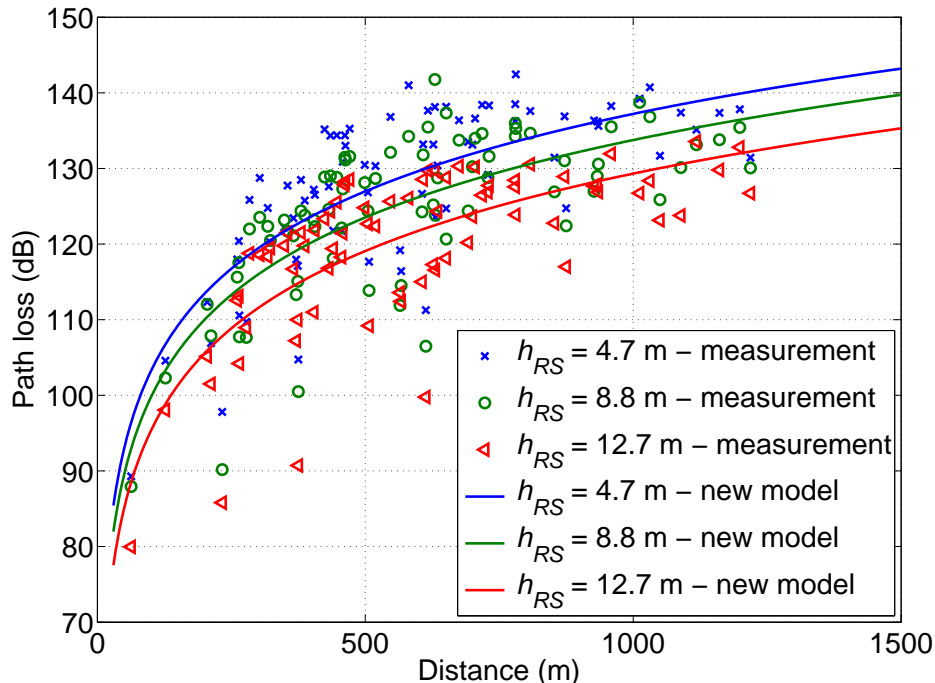


Figure 4.11: Proposed path loss model prediction in comparison with the measurements

Although the measurement points for each level are limited, we observe that the model prediction is generally coherent with the measurements. The mismatches between the measured and predicted path losses are smaller than 5 dB excepting for the 4th level which is outside the model applicability range. These mismatches are acceptable if we consider the difference between the two measurement environments. Indeed, in the first campaign, the RS antenna is installed in a vehicle parked on the street. The surrounding obstacles such as trees, building, etc. are at least several meters away. However, in the additional campaign, the Rx antenna is set on a 2-meter-long pole. Consequently, it is directly shadowed by the reception building.

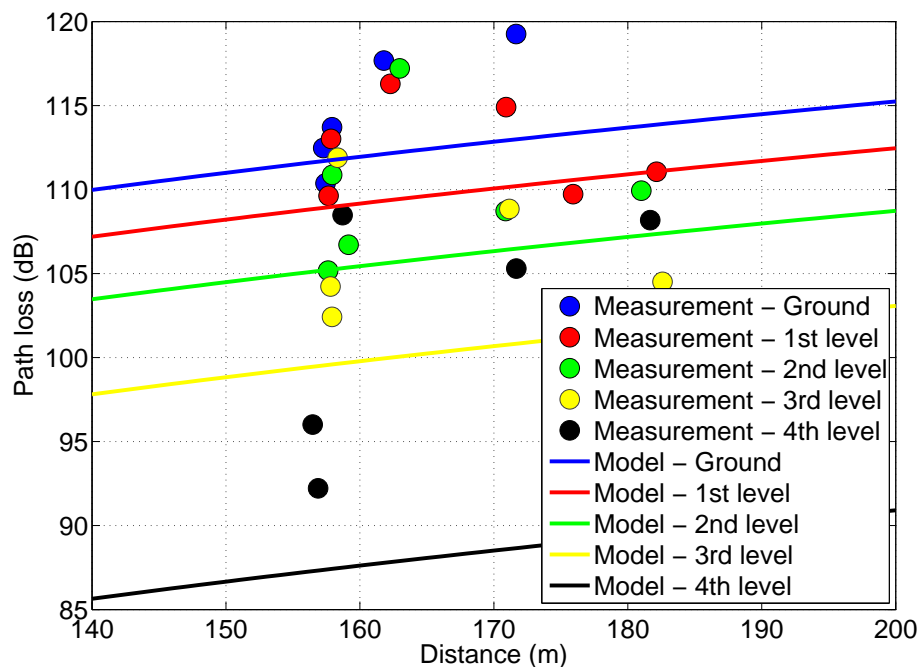


Figure 4.12: Proposed path loss model prediction in comparison with the measurements at facade 2 in the additional measurement campaign

4.2 BS-MS link characterization and modeling

BS-MS link has been studied for many years and available path loss models are abundant in the literature. Path loss models for this link in relaying systems should not have any differences with those in traditional networks. Therefore, BS-MS path loss is not the principal subject of this thesis. Nevertheless, the validation analysis of existing models with measurement data is still necessary in order to evaluate their consistency in relaying systems.

Figure 4.13 and 4.14 presents the path loss predicted by the COST-231 WI, the 3GPP Urban Macro, the 3GPP BS-MS Relay and the WINNER Urban Macro models in comparison with the measurements performed in the Old Town and Train Station areas.

The measured path losses in the two areas demonstrate similar characteristics i.e. similar attenuation power at the same propagation distance. Therefore, the model prediction accuracy related to measurements is the

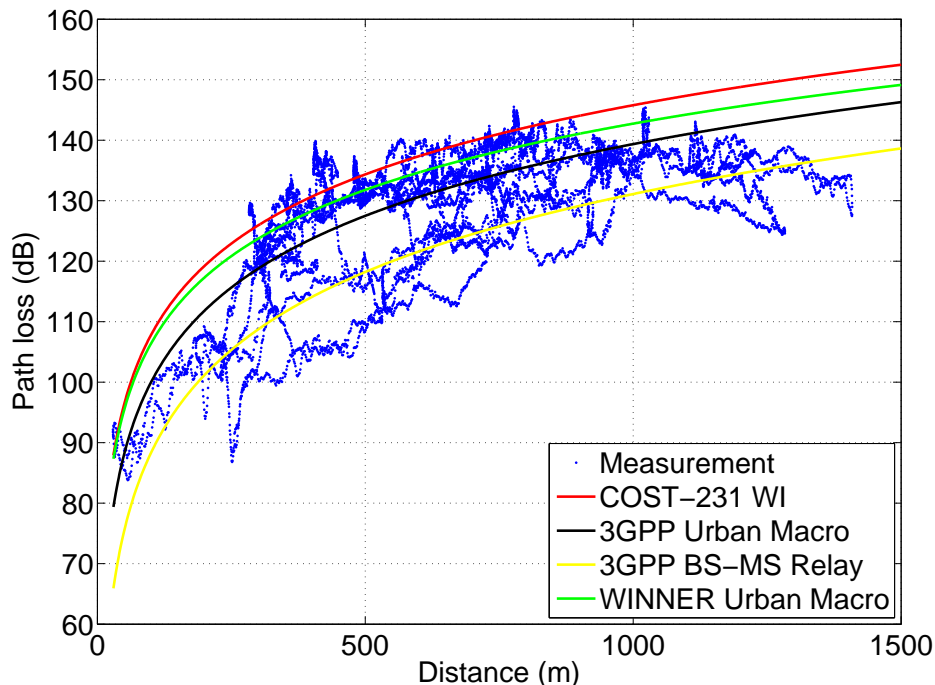


Figure 4.13: Path loss predicted by the COST-231 WI, 3GPP Urban Macro, 3GPP BS-MS Relay and WINNER Urban Macro in comparison with the measurements in Train Station area

same in both areas. These accuracy levels are quite diversified among models. The 3GPP Urban Macro model provides a fairly coherent prediction. While COST-231 WI and the WINNER Urban Macro models overestimate the measured path loss, the 3GPP BS-MS Relay underestimates the latter. A mismatch of about 15 dB can be found between the most optimistic model (i.e. 3GPP BS-MS Relay) and the most pessimistic one (i.e. COST-231 WI).

The measurements at over-1000-meter distance in the Train Station area appear below the global trend of the whole measurement data. This particularity is explained by a special propagation condition favored by a large commercial parking with clear and open space where this measurement section was performed.

The mean and standard deviation of the model prediction errors related to measurements are shown in Table 4.3.

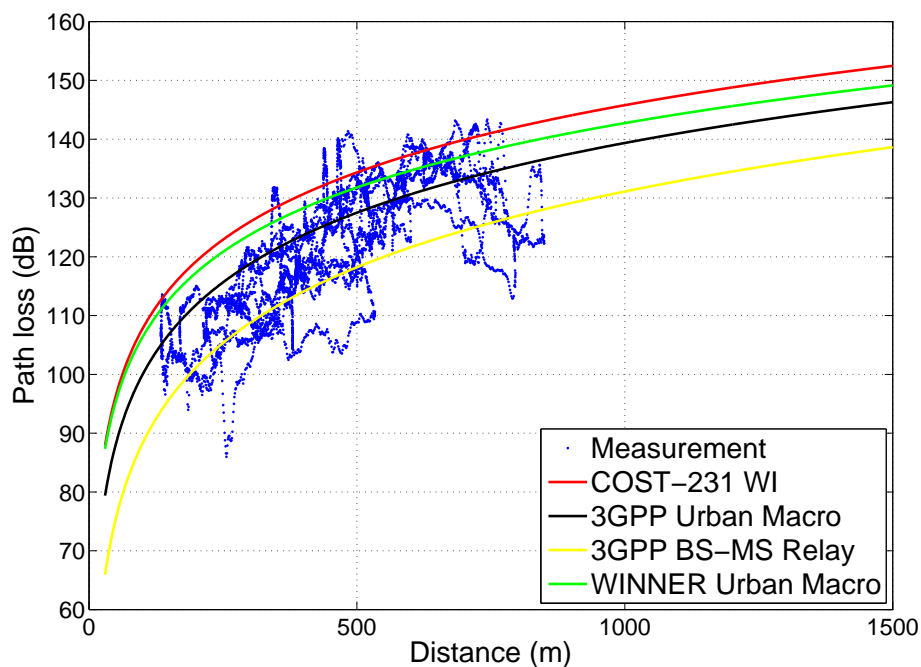


Figure 4.14: Path loss predicted by the COST-231 WI, 3GPP Urban Macro, 3GPP BS-MS Relay and WINNER Urban Macro in comparison with the measurements in Old Town area

Table 4.3: BS-MS model prediction error statistics in comparison with measurements

Path loss models	Error mean (dB)	Error Standard deviation (dB)
COST-231 WI	9.1	7.5
3GPP Urban Macro	2.3	7.5
3GPP BS-MS Relay	-6.9	7.5
WINNER Urban Macro	6.5	7.5

Because of the similarity between the measured path losses in the two areas, it is appropriate to merge these two measurement data sets. A simple path loss model derived from the linear regression taken over these merged data can be given as:

$$PL(dB) = 39 \log_{10}(d) + 20 \quad (4.2)$$

where d is the propagation distance given in meters. The mean and

standard deviation of prediction error of this model are respectively 0 and 7.5 dB.

4.3 RS-MS link characterization and modeling

4.3.1 Propagation condition classification

It is well known from radio propagation theory that LOS radio mobile channel characteristics significantly differs from NLOS ones. Table 4.4 [101] lists some of their most basic phenomenon and the equivalent models employed to model them.

Table 4.4: Typical models for LOS and NLOS radio mobile channels

Propagation phenomenon	Models for LOS conditions	Models for NLOS conditions
Path loss	Dual slope, two-path model	Log-distance model
Shadow fading	Zero-mean lognormal distribution with standard deviation of about 4-6 dB	Zero-mean lognormal distribution with standard deviation of about 8-10 dB
Fast fading	Rice distribution	Rayleigh distribution

From Table 4.4 it is clear that in order to properly model a radio link, its LOS sections should be treated differently to its NLOS ones.

In our measurement campaign, the RS-MS link propagation conditions are not uniform unlike that of BS-RS and BS-MS links which are principally in NLOS. Therefore, RS-MS measurement points should be firstly discriminated before the path loss estimation.

RS-MS measurement points are classified as LOS, OLOS (Obstructed LOS) and NLOS. The classification is manually performed by a visual inspection based on aerial and satellite photos [102, 103] as well as those taken during the measurement campaign. LOS condition is mainly found with measurement points which are close to transmitters i.e. RS. Measurement points are considered in OLOS conditions if they are not really in LOS but in a much better propagation condition in comparison with NLOS points having the same Tx-Rx distance. OLOS conditions are normally found in transition areas between LOS and NLOS. Figure 4.15 shows an example of

LOS/OLOS/NLOS classification carried out with RS3-MS link. The equivalent LOS/OLOS/NLOS measurement points are also displayed in a georeferential map (Figure 4.16). The classification results of other RS locations can be found in Appendix A.

Figure 4.15 shows a fairly clear distinction among propagation conditions, especially between LOS and NLOS ones. The LOS condition is principally found within a range from 10 meters to about 180-200 meter from RS. This distance corresponds to the street length where the RS is situated. The NLOS measurement points are generally found when the propagation distance is longer than 60-70 meters. An approximate 10 dB gap separates the LOS and NLOS point set. The OLOS points are situated in the transition area between LOS and NLOS. Because the number of OLOS points is not significant, our work analyzes only the LOS and NLOS measurement data.

4.3.2 RS-MS link characterization in NLOS conditions

This section characterizes the RS-MS link path loss in NLOS conditions. The RS antenna height impact on this link path loss is also investigated.

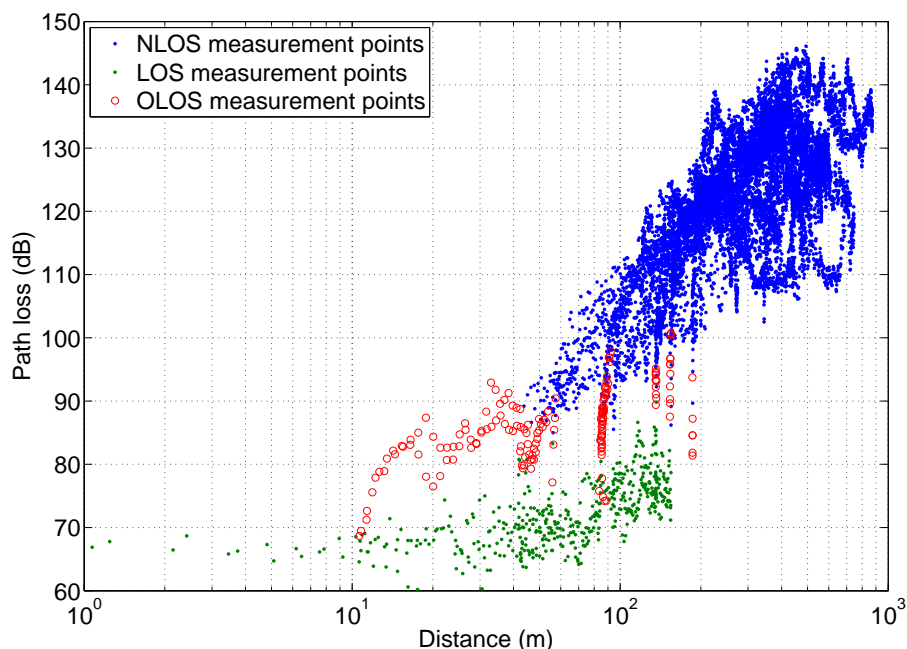


Figure 4.15: An example of LOS/OLOS/NLOS classification

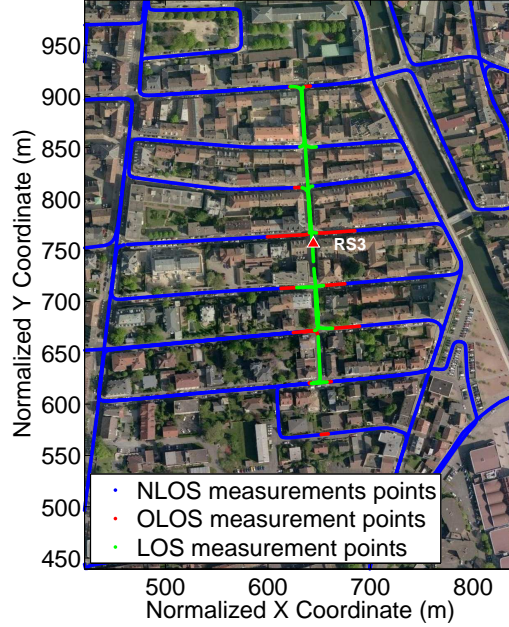


Figure 4.16: An example of LOS/OLOS/NLOS points displayed on the satellite photo

4.3.2.1 RS antenna height impact on RS-MS NLOS link path loss

The impacts of RS antenna height on RS-MS link path loss are different among RS locations. These impacts can be classified into 3 categories.

The first category consists of RS2 and RS4 locations. An example is given in Figure 4.17 which illustrates the RS2-MS NLOS path losses measured with 3 antenna heights. The dependence of RS-MS path loss on h_{RS} is obvious with these RS locations over all propagation distance range. When h_{RS} is raised from 4.7 m to 8.8 m, an average path loss of about 5 dB is reduced. Similarly, the RS-MS link path loss decreases approximately 5 dB when h_{RS} is raised from 8.8 m to 12.7 m.

On the second category, no significant impact of h_{RS} can be observed. This is the case of RS7-MS (Figure 4.18). The path losses measured with three h_{RS} are generally similar over all propagation distance range.

The third category is composed of the other RS locations. An example is presented with RS1-MS link path loss in Figure 4.19. In these cases, the linear regressions performed over path losses measured with 3 RS antenna heights intersect at a propagation distance d_I . This distance varies among RS locations and in the range of 80-120 m. With the propagation distance longer

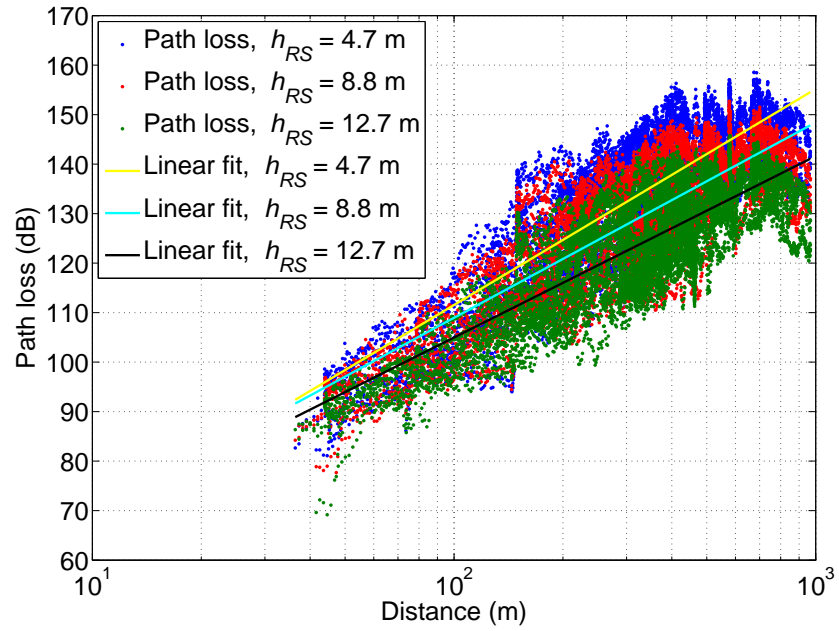


Figure 4.17: RS2-MS NLOS path loss with 3 relay antenna heights

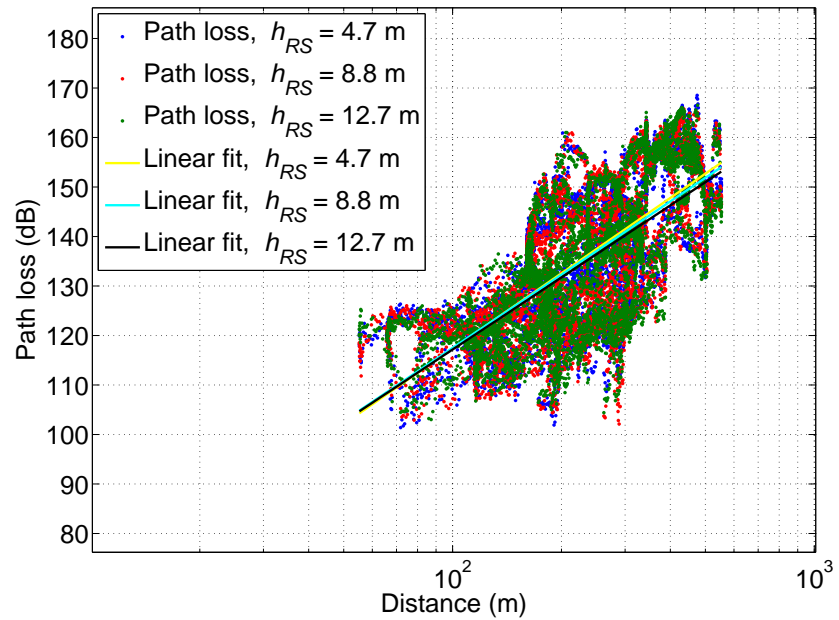


Figure 4.18: RS7-MS NLOS path loss with 3 RS antenna heights

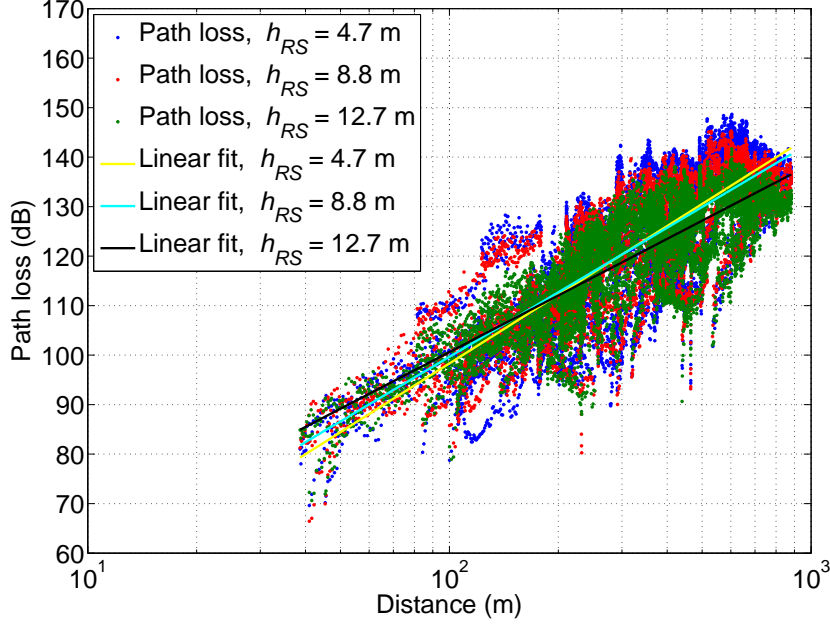


Figure 4.19: RS1-MS NLOS path loss with 3 RS antenna heights

than d_I , the impacts of h_{RS} on path loss are similar to those observed with the first category. On the contrary, with the propagation distance shorter than d_I , the differences among the path losses measured at 3 antenna heights are rather small and can be neglected.

4.3.2.2 RS-MS NLOS link path loss characterization

Unlike BS-MS link path losses which show similar characteristics in the two measurement areas, the measured RS-MS link path losses are strongly different among different RS locations. Large varieties are observed among the measured path losses. In order to quantify these varieties, we merge the measured path losses with all RS locations to create a unique data set and find its linear fit. The linear fits for path losses measured with 3 RS antenna heights are:

With $h_{RS} = 4.7$ m

$$PL(dB) = 42.4 \log_{10}(d) + 23.7 \quad (4.3)$$

With $h_{RS} = 8.8$ m

$$PL(dB) = 36.9 \log_{10}(d) + 35 \quad (4.4)$$

With $h_{RS} = 12.7$ m

$$PL(dB) = 32.2 \log_{10}(d) + 43.6 \quad (4.5)$$

where d is propagation distance in meters.

Table 4.5 shows the measured path loss mean (μ) and standard deviation (σ) errors in comparison with the linear fit.

It is observed from Table 4.5 that the measured path losses greatly vary from each other. Especially, an approximate 20 dB mismatch can be found between the most optimistic (e.g RS1-MS (Figure 4.19)) and the most pessimistic cases (e.g RS7-MS (Figure 4.18)). These differences may be due to the particular characteristics of local environment surrounding each RS locations such as the street orientation, the presence of unobstructed space close to RS, etc.

4.3.2.3 Discussions

The RS-MS link characterization is rather challenging due to the large measured path loss variability among RS locations. Furthermore, the impacts of relay antenna height are also diversified. These path loss and impact differences may be related to the local environment which surrounds each RS locations. Further research should be carried out in order to investigate more thoroughly this issue.

Due to the considerable difference observed among RS-MS links, a global model which is applicable for all RS locations may not be suitable. It may be

Table 4.5: Measured path loss error mean (μ) and standard deviation (σ) in comparison with the linear fit

RS locations	$h_{RS} = 4.7\text{m}$		$h_{RS} = 8.8\text{m}$		$h_{RS} = 12.7\text{m}$	
	μ (dB)	σ (dB)	μ (dB)	σ (dB)	μ (dB)	σ (dB)
RS1	-8.3	8.6	-6.0	7.6	-4.5	6.6
RS2	3.6	7.9	1.3	7.6	-0.8	7.0
RS3	-1.7	9.2	-0.5	8.8	-0.5	7.9
RS4	-2.5	7.8	-5.3	6.5	-6.2	5.9
RS5	-4.4	9.9	-3.7	8.9	-2.8	7.9
RS6	6.7	9.0	7.9	9.2	6.4	7.6
RS7	11.7	10.8	12.9	11.1	14.9	11.3
RS8	-4.9	8.4	-3.4	7.8	-2.5	7.8
RS9	4.7	8.5	6.1	9.7	5.5	7.9
RS10	5.1	8.9	2.1	9.1	2.7	9.0

more appropriate to characterize the RS-MS link by several models. Each of these models is dedicated to a particular microcellular propagation condition.

4.3.3 RS-MS link characterization in LOS conditions

4.3.3.1 RS antenna height impact on RS-MS LOS link path loss

The h_{RS} impact on RS-MS link path loss is observed to be distinct over two propagation distance range. Figure 4.20 gives an example illustrating this impact. The measured path loss taken with other RS locations can be seen in Appendix B.

If the propagation distance is longer than about 50-60 meters, no clear dependence of path loss on h_{RS} can be seen. This observation is coherent with the results found in the literature [44, 45, 100] which conclude that path loss and antenna height are independent in LOS conditions.

When the propagation distance is within the range of up to 50-60 meters, the measured path loss is slightly greater when h_{RS} increases from 4.7 m to 12.7 m. This phenomenon is due to the effects of the antenna radiation pattern and the differences between the ground distance and the real antenna separation. These effects are illustrated in Figure 4.21 where d and D are respectively the ground and real distance between the two antennas; h_{RS} is

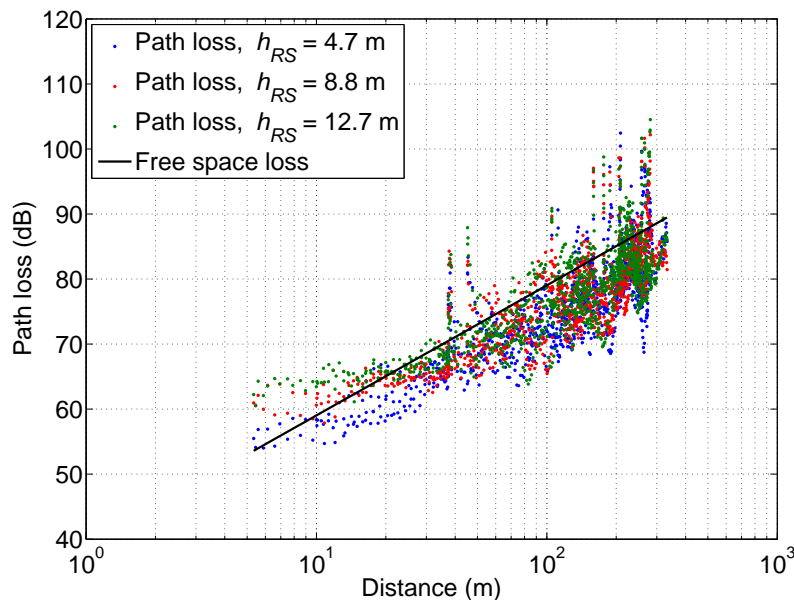


Figure 4.20: RS1-MS LOS path loss with 3 RS antenna heights

the RS antenna height; G is the maximum gain of the dipole antennas used at both RS and MS; α is the angle between the horizontal line and the actual RS-MS link; $G(\alpha)$ is the antenna gain at the angle α .

The path losses displayed in Figure 4.20 are calculated as:

$$PL = P_t - P_r + 2G - L_{cable} \quad (4.6)$$

In reality, the signal arriving at the MS propagates over the distance $D = d/\cos(\alpha)$ and with the antenna gain $G(\alpha) = G + 20 \log_{10}(\cos(\alpha))$. If we assume the log-distance power attenuation, the received power is then given as:

$$P_r = P_t - (20 \log_{10}(D) + K) + 2G(\alpha) - L_{cable} \quad (4.7)$$

$$P_r = P_t - 20 \log_{10}(D) + 2(G + 20 \log_{10}(\cos(\alpha))) + K - L_{cable} \quad (4.8)$$

where K is a parameter which depends on frequency. To be simple, we can assume $K = 0$ without losing the generality.

Therefore

$$\begin{aligned} PL &= P_t - (P_t - 20 \log_{10}(D) + 2G(\alpha) - L_{cable}) + 2G - L_{cable} \\ &= 20 \log_{10}(D) - 2G(\alpha) \\ &= 20 \log_{10}(D) - 40 \log_{10}(\cos(\alpha)) \\ &= 20 \log_{10}(d) - 60 \log_{10}(\cos(\alpha)) \\ &= 20 \log_{10}(d) - 60 \log_{10}\left(\frac{d}{\sqrt{h_{RS}^2 + d^2}}\right) \end{aligned} \quad (4.9)$$

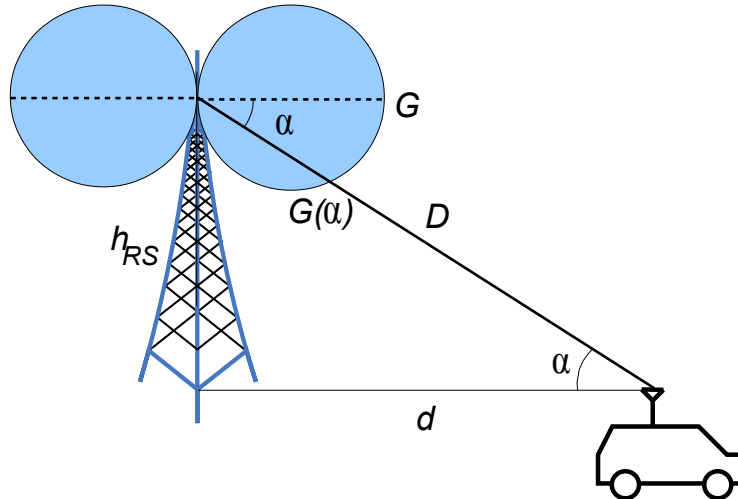


Figure 4.21: Antenna radiation pattern effects on path loss

PL plots given by the Equation 4.9 at three antenna heights are shown in Figure 4.22. The log-distance path loss is also display for comparison.

Two conclusions can be extracted from Figure 4.22.

- Firstly, when the propagation distance is up to about 50-60 meters, the higher antenna heights provide the stronger path losses. Beyond this distance, h_{RS} becomes much smaller than d ($h_{RS} \ll d$) and $\cos(\alpha) \rightarrow 1$, $d \approx D$ and $G \approx G(\alpha)$. Therefore, the aforementioned effects are no longer observed.

- Secondly, the log-distance path loss model based on the Tx-Rx ground distance can only be applied when the propagation distance is longer than a certain value. This value in our measurement is equivalent to about 50-60 meters. Below this distance, another model should be used. This conclusion is important because only ground distances are generally taken in system simulations. The implementation of 3D data which could provide the real separation distance between antennas is not always possible.

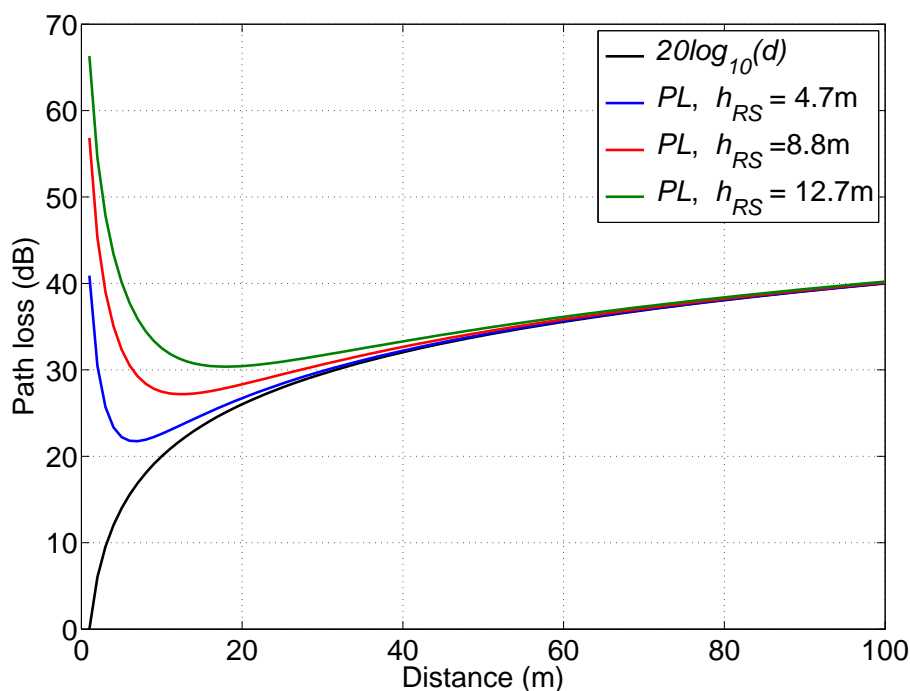


Figure 4.22: Simulation of Antenna radiation pattern and propagation distance effects on path loss

4.3.3.2 RS-MS LOS link path loss characterization

Similar to the measured RS-MS path losses in NLOS conditions, those in LOS conditions demonstrate also a strong variability depending on RS locations. For instance, the path losses observed with RS6-MS (Figure C.5), RS7-MS (Figure 4.23), RS9-MS (Figure C.7) and RS10-MS (Figure C.8) links are about 10 dB greater than those measured with the other RS locations (e.g. (Figure 4.20)). We are aware that this 10 dB gap is significant, especially in LOS conditions. This result might be due to local environments surrounding each RS locations. However, this mismatch might also be related to a manipulation error possibly happened during the measurement operation. Therefore, further investigation will be taken in order to examine this problem.

The measured path loss is seen to be smaller than free space loss in several cases (e.g Figure 4.20). This phenomenon may be caused by the street where the RS is placed in. As described in Section 4.3.1, LOS measurement points are normally found within the street length where the RS is situated. This street surrounding by building blocks may act as a waveguide resulting the path losses better than free space loss.

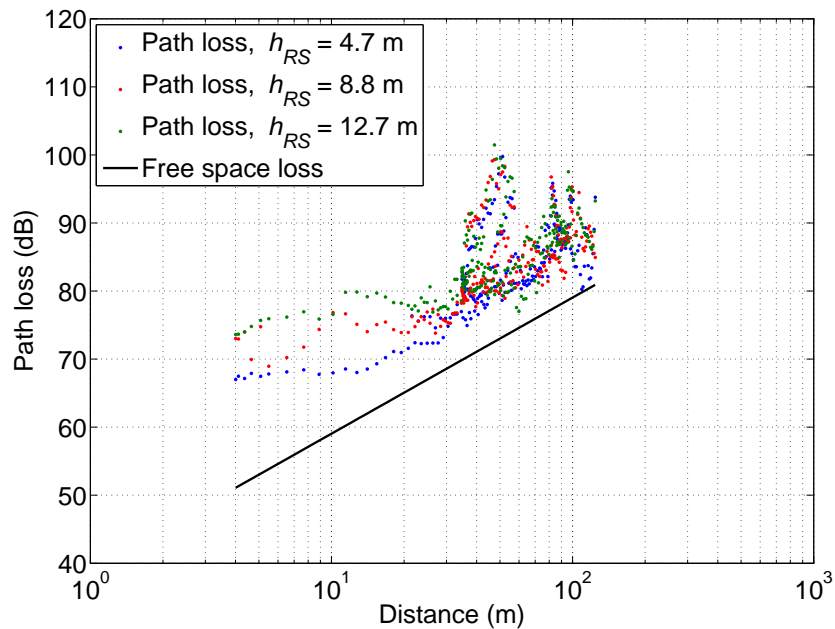


Figure 4.23: RS7-MS LOS path loss with 3 RS antenna heights

4.4 Shadow fading correlation characterization and modeling

The shadow fading correlation of different links can significantly affect the system performance [50]. This issue in relaying systems is even more important due to the presence of multiple-links i.e. BS-MS, BS-RS and RS-MS. Therefore, the understanding of the shadow fading correlation between links in relaying systems is an indispensable requirement.

Some work has been recently carried out by the WINNER project [42], the IEEE 802.16j Relay Task Group [43] or the 3GPP [41] in order to tackle this matter. Unfortunately, there is currently no well-agreed model for shadow fading correlation prediction. While the 3GPP assumes a constant correlation coefficient equal to 0.5 for all scenarios, the WINNER specifies zero correlation due to the limited amount of measurement data. Regarding the IEEE 802.16j Task Group, only the model for shadowing correlation between two BSs which is based on the Saunders work [50] is proposed. However, this model is not feasible in every case as proved in [51]. The correlation models for the shadowing between BS-MS and RS-MS links or between two RS-MS links are still for further study.

In this context, this section aims to characterize the shadow fading of BS-MS and RS-MS links. The shadow fading correlations between BS-MS and RS-MS links or between two any RS-MS links are also investigated.

4.4.1 Shadow fading characterization

As described earlier in Section 2.1.2, the propagation loss is the sum of three distinct components:

$$\textit{Propagation Loss} = \textit{Path Loss} + \textit{Shadow Fading} + \textit{Fast Fading}$$

The effects of path loss and fast fading have to be removed in order to characterize the shadow fading (SF). Firstly, the fast fading part is removed by using a sliding window with a window size of 20λ and a sliding distance of 10λ as described in Section 3.4.2. Then, the path loss effect is removed by applying a linear regression to the data in the logarithm domain. The measurements in NLOS and LOS conditions are separated before applying the linear fit in order to obtain the optimal estimation of shadow fading. Only the measurement samples in NLOS conditions with respect to both transmitters are concerned in this thesis.

The aforementioned method is applied for each BS-MS and RS-MS link to extract its own SF . The SFs of all BS-MS and RS-MS links are found

to be log-normal distributed with zero mean. Figure 4.24 presents an example where the SF distributions of BS-MS and RS1-MS links are illustrated in comparison with the normal fit. The measured shadow fading standard deviations (σ_{SF}) are around 7 dB for BS-MS links and in the range of 7-11 dB for RS-MS links. σ_{SF} for each link is summarized in Table 4.6. It can be seen that the σ_{SF} of RS-MS links are similar at different RS antenna heights.

Model parameters from the 3GPP, the WINNER and the IEEE 802.16j are also displayed for comparison. It is observed that all of the values described by 3GPP, WINNER and 802.16j for BS-MS link match to the measured data. However, in the case of RS-MS link, only the values provided by 3GPP agree with measured ones. WINNER and 802.16j model propose σ_{SF} in the range of 3-4 dB which are strongly below the measured σ_{SF} . Reference [43] shows that 802.16j model for RS-MS link is derived from the corresponding RS-MS WINNER model. This latter was developed by assuming an urban area with Manhattan-like street lay-out which is not the case of the environment presented in this paper. This explains the mismatch between the measured σ_{SF} and those described by WINNER and IEEE 802.16j.

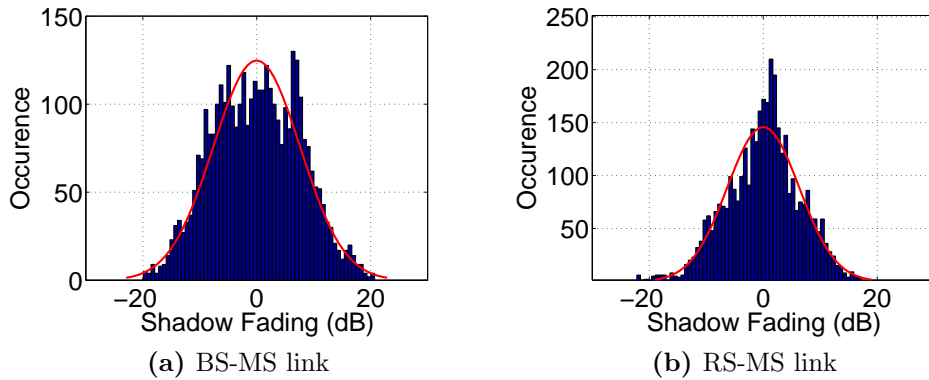


Figure 4.24: Measured SF distribution

Table 4.6: Measured σ_{SF} in comparison with model-proposed ones

	Shadow fading Standard deviation (dB)					
	Measurement			3GPP	WINNER	802.16j
	4.7m	8.8m	12.7m			
BS-MS Train Station	6.8			6	8	8
BS-MS Old Town	7.2					
RS1-MS	8.5	7.5	6.5	10	4	3.1
RS2-MS	7.9	7.4	6.9			
RS3-MS	9.1	8.8	7.9			
RS4-MS	8.0	6.7	5.8			
RS5-MS	10	8.6	7.5			
RS6-MS	8.9	9.0	7.5			
RS7-MS	10.6	10.8	10.8			
RS8-MS	8.5	8.5	9.0			
RS9-MS	7.8	9.2	7.2			
RS10-MS	8.4	8.9	8.7			

4.4.2 Shadow fading correlation characterization

4.4.2.1 General characterization

The correlation coefficient between the SF of two transmission links is calculated by Equation 2.83. In the following parts of this work, $\rho_{(BS-MS,RS-MS)}$ and $\rho_{(RS-MS,RS-MS)}$ are used to respectively denote the shadow fading correlation coefficient between BS-MS/RS-MS links and between two RS-MS links.

Firstly, the impact of RS antenna height on the shadow fading correlation is examined. For each RS location, the shadow fading correlation between the same RS-MS link and with different antenna height (4.7 m, 8.8 m and 12.7 m) is calculated. The calculation results show that the SFs of the same RS-MS link when RS antenna is at different heights are highly correlated. High coefficients from 0.75 to 0.96 are observed at all RS locations. Figure 4.25 illustrates an example where the shadow fading components of the RS1-MS link obtained with 3 antenna heights are presented. This strong correlation is explained by the fact that even when the RS antenna mast is at the highest position, it is still below the roof-top level of the surrounding

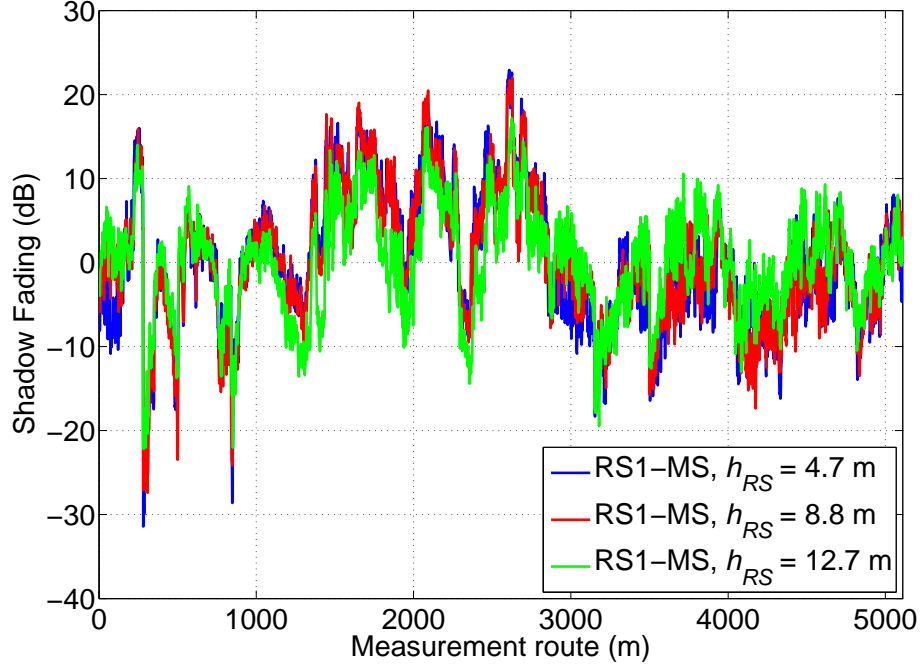


Figure 4.25: SF of RS1-MS link measured with 3 antenna heights

buildings. Hence, the RS-MS link is always under the NLOS condition and the obstacles presented in the propagation path which cause the shadow fading remain the same with three RS antenna heights. Thus, the RS antenna height does not significantly affect the shadowing correlation.

Secondly, $\rho_{(BS-MS,RS-MS)}$ and $\rho_{(RS-MS,RS-MS)}$ in each measurement area are calculated over the entire measurement route. The results for the Train Station and the Old Town areas are respectively presented in Table 4.7 and 4.8. Because the SF components obtained with different RS are strongly correlated, only the results when RS antenna is set up at 12.7 m are displayed. The correlation coefficients are found to be widely varied from -0.04 to 0.57. Moreover, it is noted that the coefficients are positive in most cases excepting for $\rho_{(RS_1-MS,RS_4-MS)} = -0.04$ and $\rho_{(RS_2-MS,RS_3-MS)} = -0.01$ which can be considered as zero. Meanwhile, several papers [104–106] show quite strong negative values. However, these papers were based on either indoor environment or outdoor with relatively short measurement routes. In these cases, the MS moving direction related to transmitters could make negative coefficients.

Moreover, the values in the Old Town area are slightly greater than those in the Train Station. This difference may be due to the presence of several open and flat spaces in the south of the Train Station causing a less

Table 4.7: Shadow fading correlation between different links in Tran Station area

	RS1-MS	RS2-MS	RS3-MS	RS4-MS	RS5-MS
BS-MS	0.23	0.36	0.12	0.29	0.42
RS1-MS	-	0.49	0.14	-0.04	0.15
RS2-MS		-	-0.01	0.23	0.24
RS3-MS			-	0.11	0.10
RS4-MS				-	0.25

Table 4.8: Shadow fading correlation between different links in Old Town area

	RS6-MS	RS7-MS	RS8-MS	RS9-MS	RS10-MS
BS-MS	0.27	0.57	0.06	0.32	0.15
RS6-MS	-	0.50	0.30	0.14	0.42
RS7-MS		-	0.17	0.53	0.39
RS8-MS			-	0.28	0.25
RS9-MS				-	0.38

homogenous environment.

The results presented in Table 4.7 and 4.8 also exhibit the dependence of $\rho_{(BS-MS,RS-MS)}$ and $\rho_{(RS-MS,RS-MS)}$ on the transmitter separation. This dependence is illustrated in Figure 4.26. It is observed that the correlations decrease when the distances between transmitters increase. Moreover, the highest coefficients which are around 0.5 are observed between transmitter pairs having a small separation such as between RS1-RS2, RS7-RS9 or between BS-RS7, etc. These values are remarkable considering the length of the measurement routes.

4.4.2.2 Dependence of shadow fading correlation on the angle (θ)

The angle seen from the MS to the transmitters (θ) is recognized as an important parameter having a significant impact on the shadow fading correlation [50–55]. It was reported a strong correlation on the order of 0.6 to 0.8 with small θ . This correlation was observed to decrease toward zero when θ becomes greater. Although this angular property has been discussed in many papers for traditional radio mobiles network i.e. without the presence of RS, this issue has not yet been adequately studied in relaying deployments. In this work, the dependence of shadow fading correlation on the angle θ is investigated by dividing the entire measurement data into groups according to

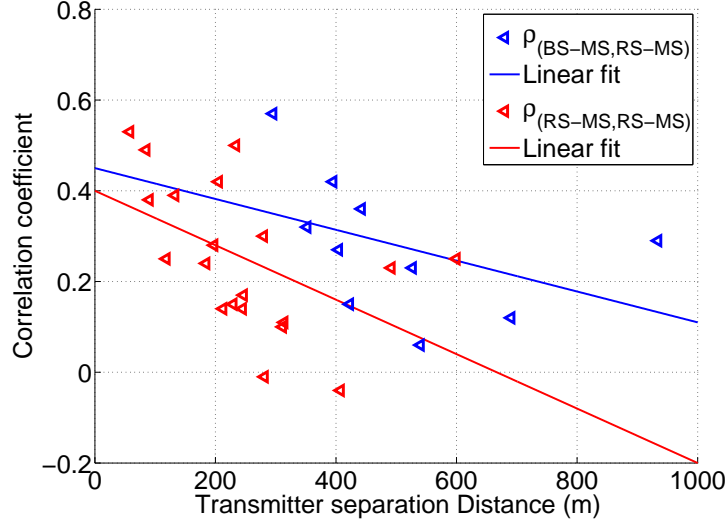


Figure 4.26: Dependence of SF correlation on the transmitter separation distance

their associated angle θ . The number of measurement samples in each angular group should be statistically significant in order to ensure the reliability of the results. In addition, the correlation coefficient comparison between groups is only valid if the SF characteristics of every group are similar to each other and similar to all data characteristics i.e. log-normal distribution with zero mean. To satisfy these conditions, the data were dynamically divided into groups which encompass five, ten or twenty degrees of the 180° range. The angular groups as well as the number of measurement samples in each group are shown in the Figure 4.27.

The $\rho_{(BS-MS,RS-MS)}$ and $\rho_{(RS-MS,RS-MS)}$ calculated over each angular group are displayed as a function of θ in Figure 4.28. It appears that the highest correlations which are from 0.4 to 0.6 are observed when angle θ is smaller than ten degrees. When the angle θ increases up to about 60-80 degrees, the correlation coefficients rapidly decrease toward zero. This trend is observed in both $\rho_{(BS-MS,RS-MS)}$ and $\rho_{(RS-MS,RS-MS)}$ cases and generally corresponds to the result found in the literature for the traditional wireless network [50, 54, 107, 108]. This result is explained by the MS position related to transmitters. Indeed, when the angle θ is small, the common propagation path between two links increases. Thus, the two links are affected in a similar way by the obstacles. This results in a strongly correlated shadow fading. Otherwise, the increasing angle θ means the reduction of common propagation path leading to a minor or no correlation.

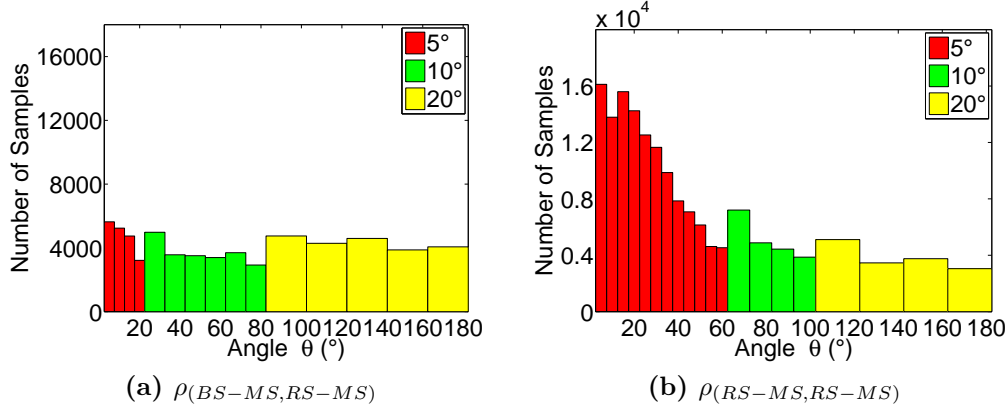


Figure 4.27: Angular groups for SF correlation calculation

Based on the aforementioned argument, the SF s from different links are expected to be totally uncorrelated when the angle θ is as high as 180 degrees. This is also a common result which has been expressed in many papers [53, 54]. However, a contradictory result is observed with our measurements, especially in the case of $\rho_{(BS-MS, RS-MS)}$. As presented in the Figure 4.28, the correlations of about 0.2-0.3 appeared when the angle θ is in the angular range of 140 - 180 degrees. This phenomenon is noticeable because a large number of data samples are used for the calculation. This result may be due to the specific measurement conditions. From Figure 3.5 and Figure 3.6, it can be seen that the BS and RS locations are generally lined up. Moreover, the principal areas of the measurement environment are composed of building blocks whose structures and heights are relatively similar. These building blocks are parallel to each other and perpendicular to the transmitter axis. When angle θ increases towards 180 degrees, the MS moved to the zone between two transmitters. In this case, the signals coming from these transmitters are obstructed similarly by the parallel building blocks which are on two sides of MS. These facts, in addition to the building structural similarities, lead to certain correlations although the signals arrive at MS from two different directions.

In summary, although SF correlations observed with angle θ higher than 10 degrees present different angular dependences, their coefficients are minor and considered as negligible. This result indicates that a simple uncorrelated SF model for signals from different transmitters can be used in system level simulation when the angle seen from MS to these transmitters is higher than 10 degrees. However, a correlation coefficient of 0.5 should be taken into account in the case where this angle is smaller than 10 degrees.

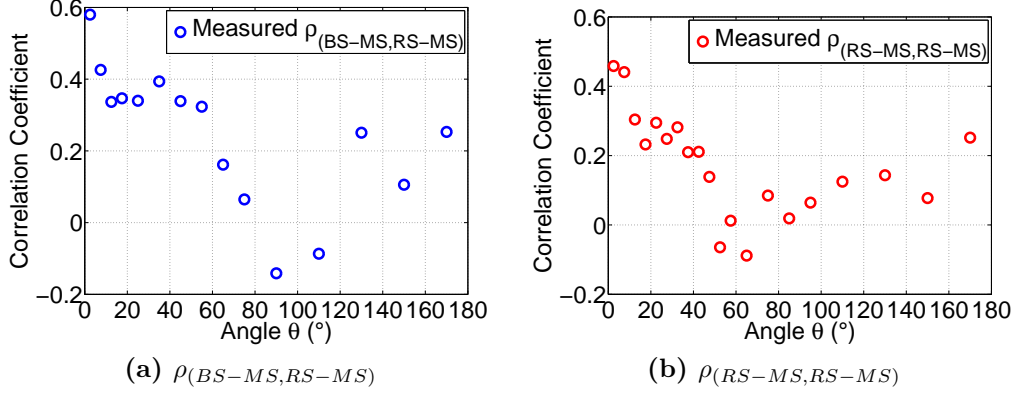


Figure 4.28: Measured SF correlation vs. angle θ

4.5 Path loss consistency

The real contribution of relays should be evaluated by system simulations. Unlike for classical radio mobile networks, the simulation for relaying deployment should be able to simulate not only a particular propagation link but all links (BS-MS, BS-RS and RS-MS) by a consistent manner. However, our preliminary analyses reveal the inconsistency in the existing path loss models. An example is given with WINNER models.

Section 4.1.4 demonstrates that BS-RS WINNER model underestimates the measurement. The mismatch is about 10 dB. Moreover, the prediction of BS-MS WINNER model is about 6 dB over the measurement. Consequently, if a simulation is based on WINNER model, the relay contribution in term of link budget provided by this simulation is artificially increased by 16 dB.

The aforementioned observations emphasize the importance of path loss model consistency in system simulations. Further analyses are then required in order to study more thoroughly this issue.

4.6 Conclusion

This last chapter focused on multi-link channel characterization and modeling based on the data collected from the measurement campaign presented in Chapter 3.

Firstly, the impact of relay antenna height on link path loss was analyzed. A path loss reduction of about 8 dB was observed with BS-RS link when h_{RS} was raised from 4.7 meters to 12.7 meters. Moreover, this impact was confirmed with additional measurements taken with other frequencies and in

other environment. However, this impact was only seen with NLOS conditions. When propagation conditions became LOS or LOS-NLOS-mixture, measured path loss no longer depended on h_{RS} .

Relay antenna height impact on RS-MS link path loss was shown to be more sophisticated than that observed in BS-RS links. When RS-MS links were in NLOS conditions, this impact was divided into 3 categories depending on RS locations. When RS-MS links were in LOS conditions, no dependence between path loss and h_{RS} was found. The dependence observed with small propagation distance was related to the effects of the antenna radiation pattern and the differences between the ground distance and the real antenna separation. A simulation was performed and confirmed this phenomena.

Secondly, the path loss of BS-MS, BS-RS and RS-MS links was characterized and modeled. Various existing path loss models were evaluated with the measurement data. A simple path loss model taking into account the relay antenna height impact was proposed for BS-RS link in relaying systems.

A particular problem was observed with RS-MS link of which the measured path loss exhibited large variability among different RS locations. Further studied should be carried out in order to more thoroughly investigate this problem.

Another subject tackled in this chapter was the shadow fading correlation among propagation links presented in relaying scenarios. The shadow fadings of different links were characterized and compared to those provided by existing models. The correlation between shadow fadings of a BS-MS and a RS-MS link or between two RS-MS links was analyzed. The relation between this correlation with the relay antenna height, the transmitter separation distance and the angle seen from MS to transmitters was also examined. Especially, dynamic angular groups were used to model the shadow fading correlation. We suggested that a correlation coefficient of 0.5 should be taken into account for 0-10 degree angular sample groups. Otherwise, a simple uncorrelated shadow fading model can be used.

Finally, the preliminary analyses concerning the path loss model consistency were carried out. For instance, our analyses reveal a false path loss gain of about 16 dB given by WINNER model due to the inconsistency of this model.

Conclusion and Perspective

Conclusion

Radio mobile communication systems have been constantly evolving to meet the users' growing demands in term of data rate, quality of service, coverage and mobility. In this context, 3GPP has developed LTE-Advanced and submitted it to ITU as a candidate for IMT-Advanced (4G) systems. LTE-Advanced aims to meet and even go beyond the ITU requirements for a system belonging to IMT-Advanced. To this end, many technical components have been included to LTE-Advanced. Among these, relays have been emerged as a low-cost solution to solve the cell-edge problem, reduce the gap between the peak and cell-edge data rate, extend the coverage and improve the overall cell performance.

As a hot research topic with great application potential, relay technologies have been actively studied for the last few years. However, suitable propagation models which could be integrated in system simulations to provide the reliable estimation of relay contribution have not thoroughly considered yet.

In this context, this thesis has been carried out in order to evaluate the existing propagation model and provide new ones which are dedicated to relaying scenarios. To this end, an extensive multi-link measurement campaign with a BS and 10 RS locations has been performed in outdoor urban areas. The contributions of this thesis can be summarized as below:

- **RS antenna height impact on BS-RS link path loss:**

Our analyses showed the dependence of the BS-RS link path loss on the RS antenna height. An average path loss reduction of about 8 dB was observed when the RS antenna height has raised from 4.7 m to 12.7 m. This dependence was explained by the NLOS propagation conditions between BS and RS. In fact, BS was installed over the surrounding rooftop and the transmitted signal principally propagates over the rooftop. When the h_{RS} was high and approaches the roof level i.e. LOS condition, the received signal was less attenuated by the diffraction or reflection caused by surrounding buildings.

In order to examine this dependence on other environments, an additional measurement campaign was carried out. The analyses taken with this measurement data confirmed the RS antenna height impact on NLOS conditions, even when the Rx was placed indoor. This impact was also observed in different frequencies i.e. 900 MHz or 3.5 GHz. However, when the propagation condition became LOS or mixture of NLOS and LOS, this impact was no longer observed.

– **RS antenna height impact on RS-MS link path loss:**

The impact of the RS antenna height on RS-MS link was rather diversified depending on propagation conditions (NLOS or LOS) and RS locations.

When RS-MS link was in NLOS, this impact was different with 3 RS location groups.

In the first group, the dependence of RS-MS path loss on h_{RS} was obvious over all propagation distance range and similar to that observed with BS-RS link. An average reduction of about 10 dB was observed when h_{RS} changed from 4.7 m to 12.7 m.

In the second group, no significant impact of h_{RS} could be observed. The path losses measured with 3 h_{RS} were generally similar over all propagation distance range.

In the third group, the linear regressions performed with 3 RS antenna heights intersected at a propagation distance d_I which was in the range of 80-120 m. With the propagation distance longer than d_I , the impacts of h_{RS} on path loss were similar to those observed with the first group. On the contrary, with the propagation distance shorter than d_I , no impact could be found.

The h_{RS} impacts on RS-MS link path loss in LOS were observed to be distinct over two propagation distance range. If the propagation distance was longer than about 50-60 meters, no clear dependence of path loss on h_{RS} could be seen. On the other case, the measured path loss was slightly greater when h_{RS} increased from 4.7 m to 12.7 m. This phenomenon was due to the effects of the antenna radiation pattern and the differences between the ground distance and the real antenna separation.

– **BS-RS link path loss characterization and modeling:**

The measured BS-RS link path loss was compared against those predicted by WINNER, 3GPP and COST-231 WI models. The comparison results demonstrated that 3GPP Relay and WINNER B5f models strongly underestimated the path loss. The COST-231 WI model provided the closest prediction in comparison to the measurement although this model was neither designed for relaying systems nor for-

mally specified to be used at frequencies beyond 2 GHz. However, COST-231 WI model presented some disadvantages. For instance, it required detailed knowledge of propagation environment. Moreover, COST-231 WI model defined many parameters and the relation among them. This may make it complex to be applied in certain practical cases, especially for engineering work or simulation tools. Therefore, a new channel model was proposed in order to provide a simple propagation model which is capable of modeling the BS-RS link path loss in 2.1 GHz frequency band while taking into account the impact of h_{RS} . This model was validated with measurement data gathered from two different measurement campaigns.

– **BS-MS and RS-MS link path losses characterization:**

BS-MS link has been the subject of tremendous studies for many years and was not focused in this thesis. However, preliminary analyses were performed with RS-MS links path loss. Unlike BS-MS link path losses which showed the similar characteristics in the two measurement areas, the RS-MS link path losses in both LOS and NLOs conditions were strongly different among different RS locations. Large varieties which could be up to 20 dB were observed among the measured path losses. These differences might be due to the particular characteristics of local environments surrounding each RS locations. Besides, an manipulation error unawarably happened during the measurement campaign might be another cause. Further research should be carried out in order to investigate more thoroughly this issue.

– **Path loss consistency:**

Some initial observations related to the path loss consistency were performed as part of this thesis. For instance, BS-RS WINNER model prediction was about 10 dB under the measurement. However, the BS-MS WINNER model prediction was about 6 dB over the measurement. Consequently, if a simulation is based on WINNER models, the relay contribution in term of link budget provided by this simulation was artificially increased by 16 dB.

– **Shadow fading correlation characterization and modeling:**

The shadow fading cross-correlations between a BS-MS link and a RS-MS link or between two RS-MS links were experimentally characterized. The correlation coefficients were found to vary from 0 to 0.6. Furthermore, the shadow fading angular properties were examined. It was observed that the correlation of 0.5 was found when the angle θ seen from MS to the transmitters is smaller than 10 degrees. Although correlations observed with angle θ higher than 10 degrees present different angular dependences, their coefficients are minor and considered as

negligible. Consequently, a correlation coefficient of 0.5 should be taken into account in analysis tools for 0-10 degree angular sample groups. A simple uncorrelated shadow fading model for signals from different transmitters can be used for the other cases.

Perspectives

Considering current progress in relaying technologies and results achieved with this thesis, we suggest several directions for future work.

- **Finalize the multi-link channel modeling and path loss consistency:**

The analyses executed in this thesis show the strong variability among the RS-MS link path loss measured with different RS locations. This issue should be analyzed more thoroughly by investigating the measurement environment surrounding each RS. A hypothesis of potential measurement errors should also be examined.

The channel inconsistency observed in this thesis should be pursued by more complete studies.

The LOS/NLOS probability in RS-MS link should also be investigated. The final objective is to develop a reliable propagation channel model set for outdoor urban environments. These models should be simple to be easily applicable in practical cases. On the other hand, they should be capable of modeling multi-link channels in a consistent manner.

- **Measurement and modeling of arrival directions at the relay:**

The power gain observed in the BS-RS link by increasing the antenna height increases not only to the useful signal but also interferent one. This interference could be limited by using a directional antenna pointing to the BS. A measurement campaign dedicated to the characterization of the direction of arrival at RS should be organized. The analysis results are expected to show whether a directional antenna help improving the SNR at the RS.

Appendix A

**LOS/OLOS/NLOS
classification for all RS-MS
links**

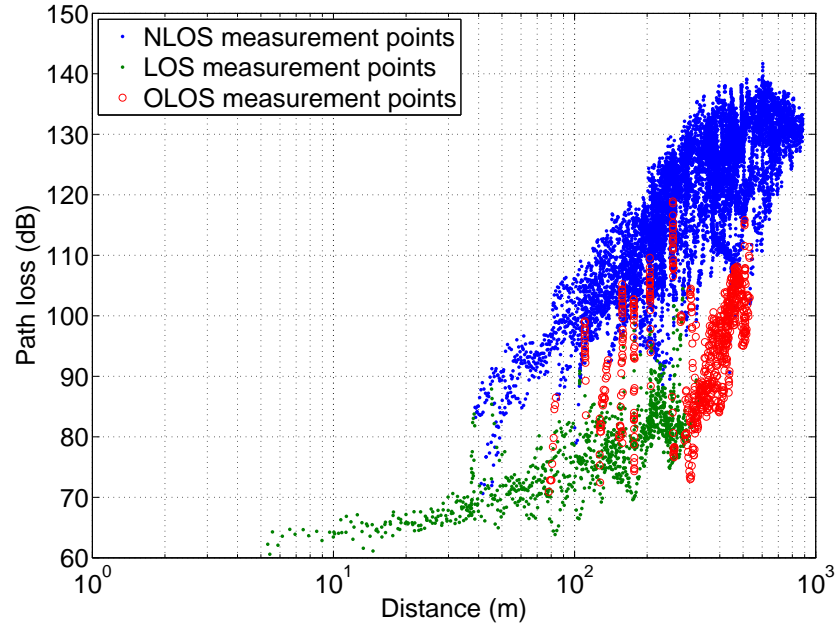


Figure A.1: LOS/OLOS/NLOS classification for RS1-MS link

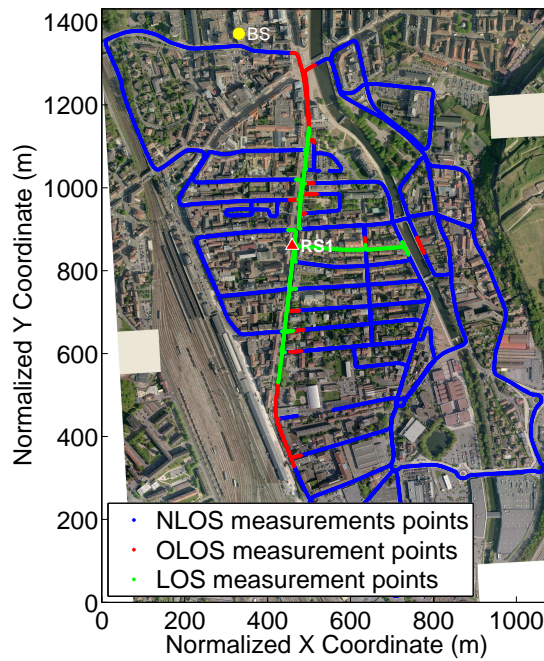


Figure A.2: RS1-MS LOS/OLOS/NLOS measurement points

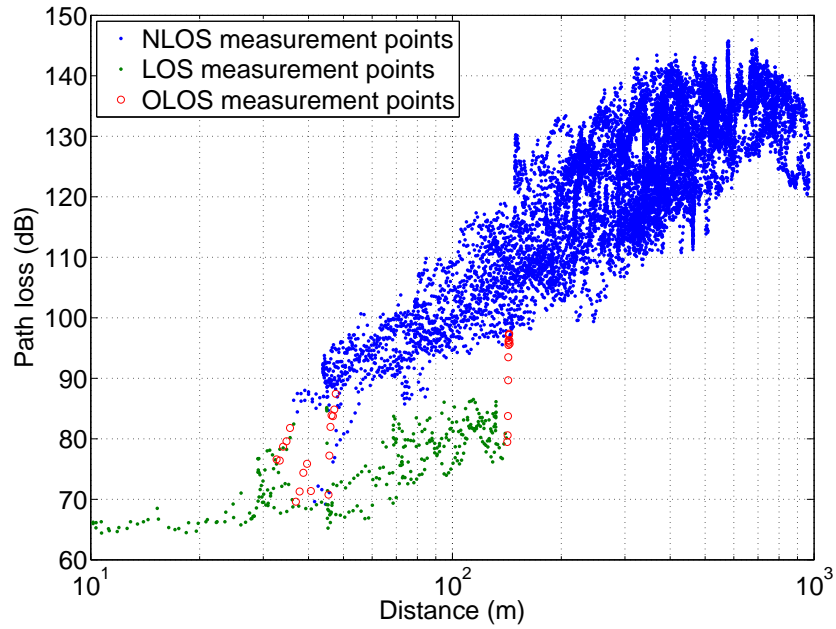


Figure A.3: LOS/OLOS/NLOS classification for RS2-MS link

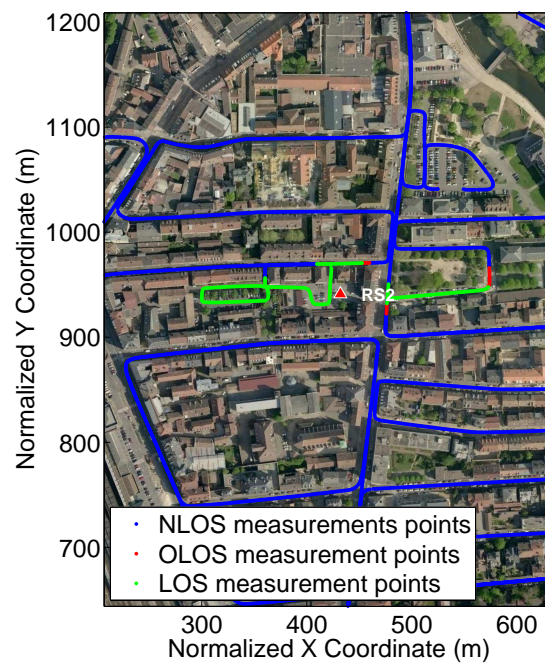


Figure A.4: RS2-MS LOS/OLOS/NLOS measurement points

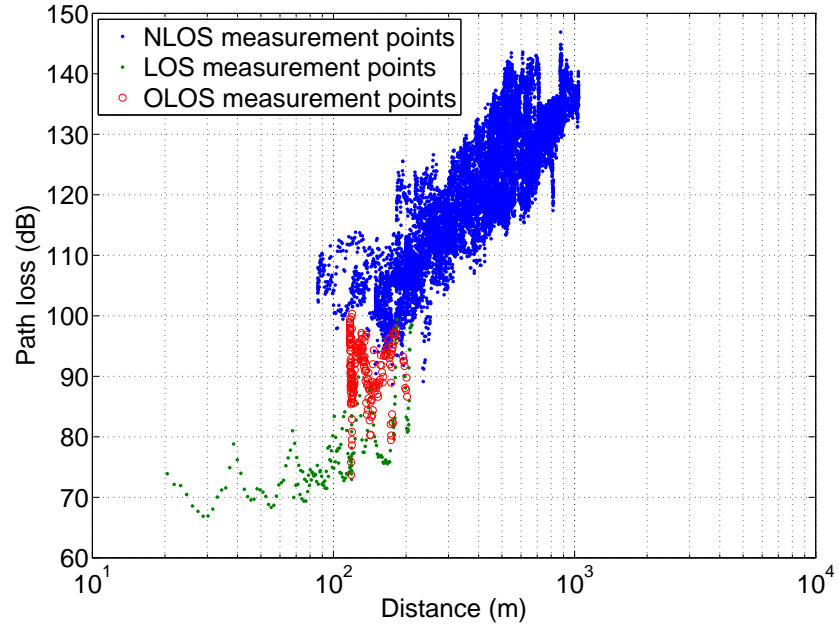


Figure A.5: LOS/OLOS/NLOS classification for RS4-MS link

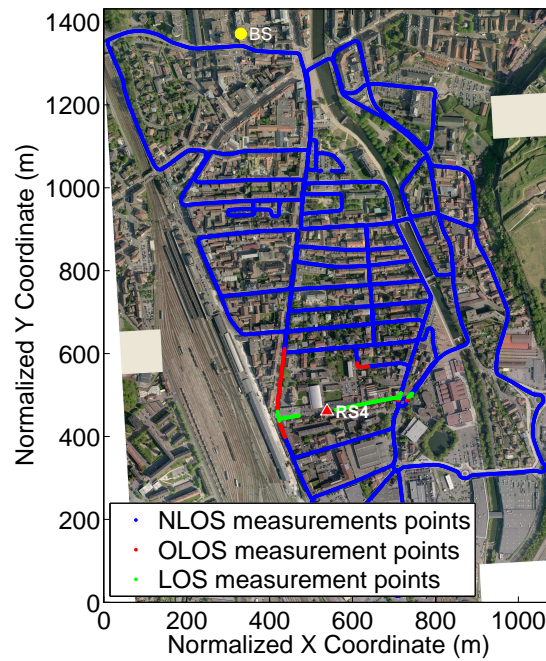


Figure A.6: RS4-MS LOS/OLOS/NLOS measurement points

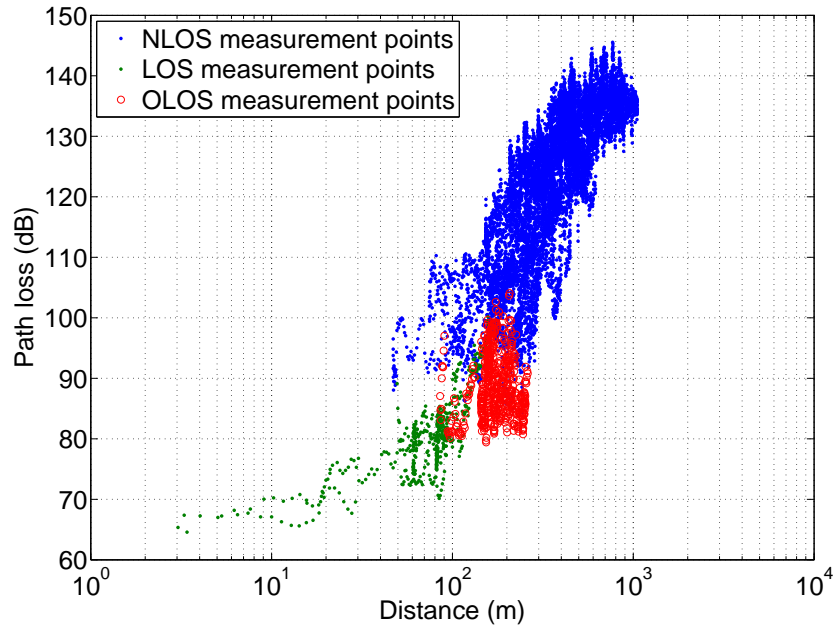


Figure A.7: LOS/OLOS/NLOS classification for RS5-MS link

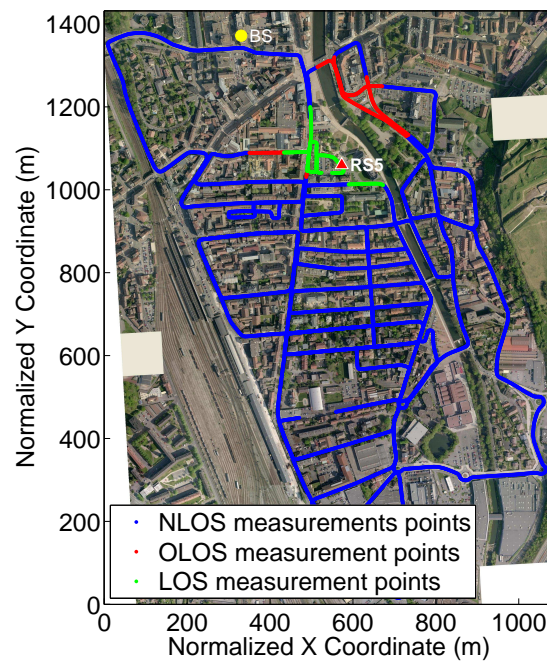


Figure A.8: RS5-MS LOS/OLOS/NLOS measurement points

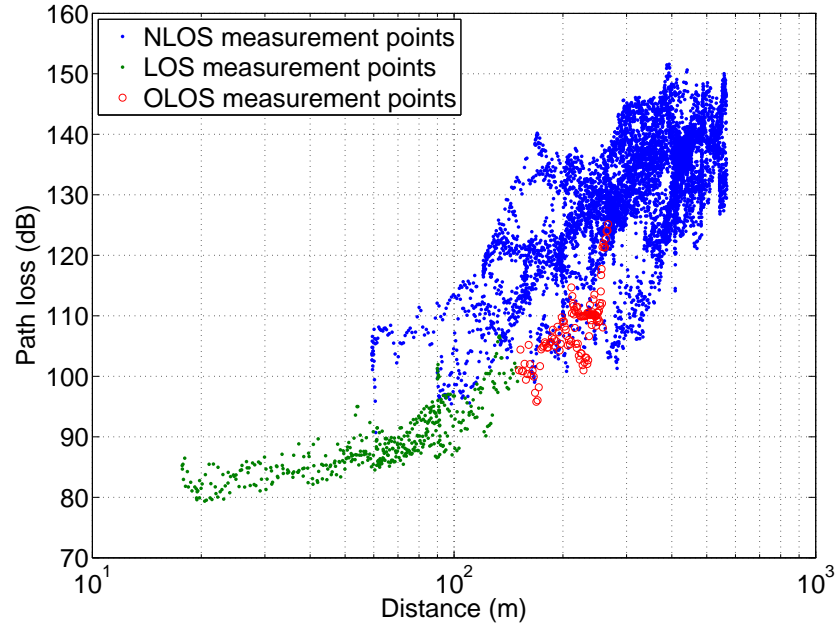


Figure A.9: LOS/OLOS/NLOS classification for RS6-MS link

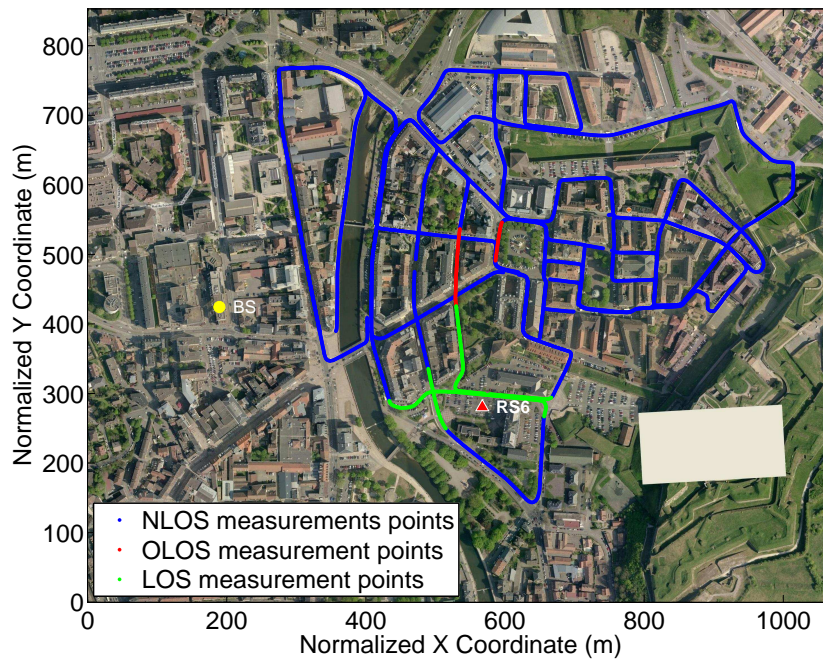


Figure A.10: RS6-MS LOS/OLOS/NLOS measurement points

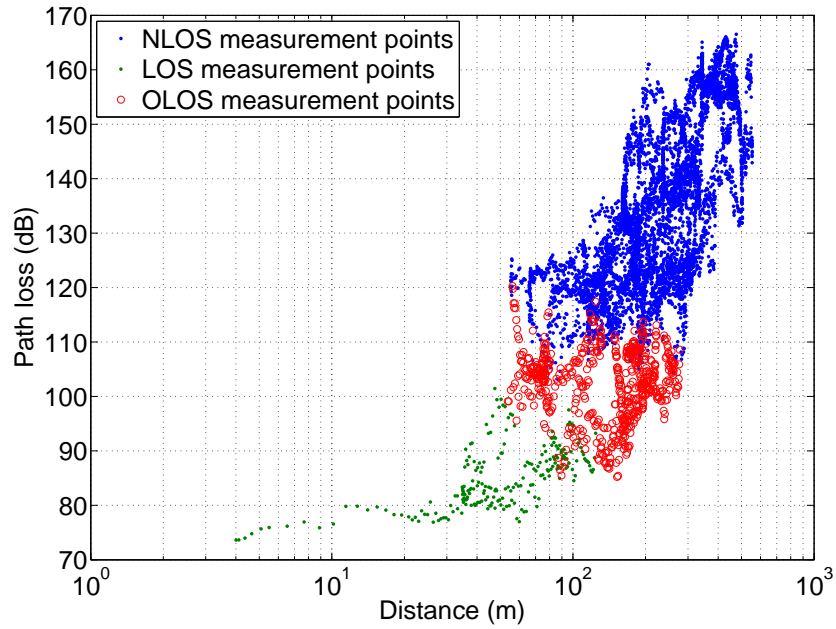


Figure A.11: LOS/OLOS/NLOS classification for RS7-MS link

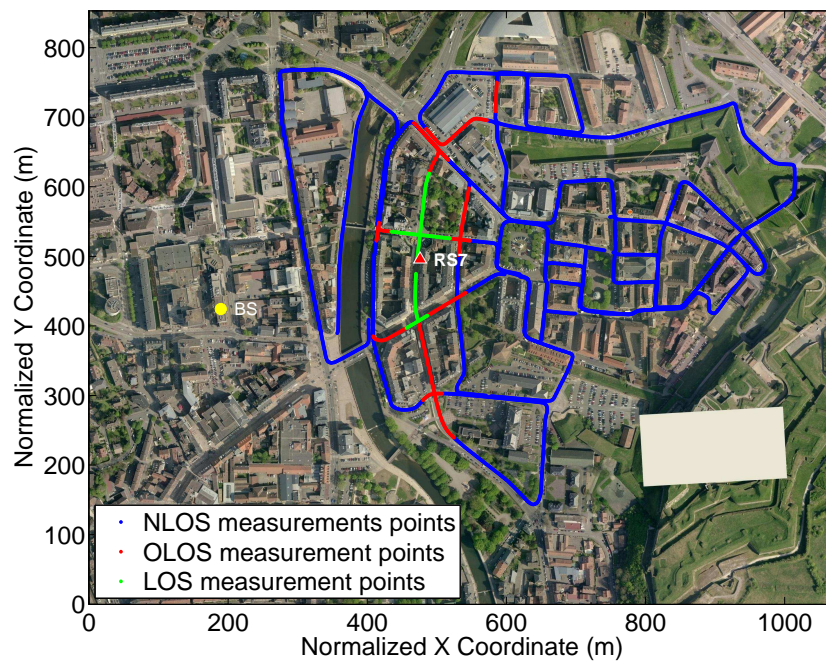


Figure A.12: RS7-MS LOS/OLOS/NLOS measurement points

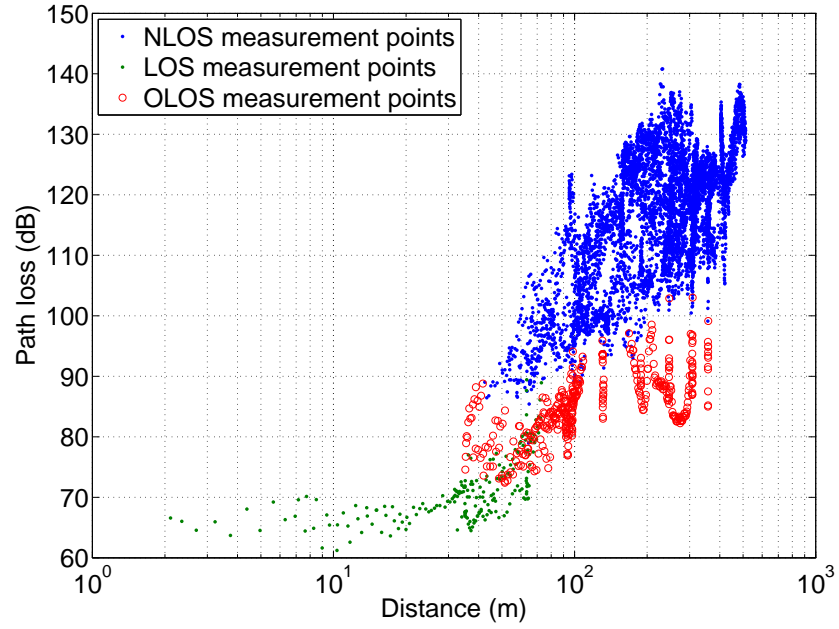


Figure A.13: LOS/OLOS/NLOS classification for RS8-MS link

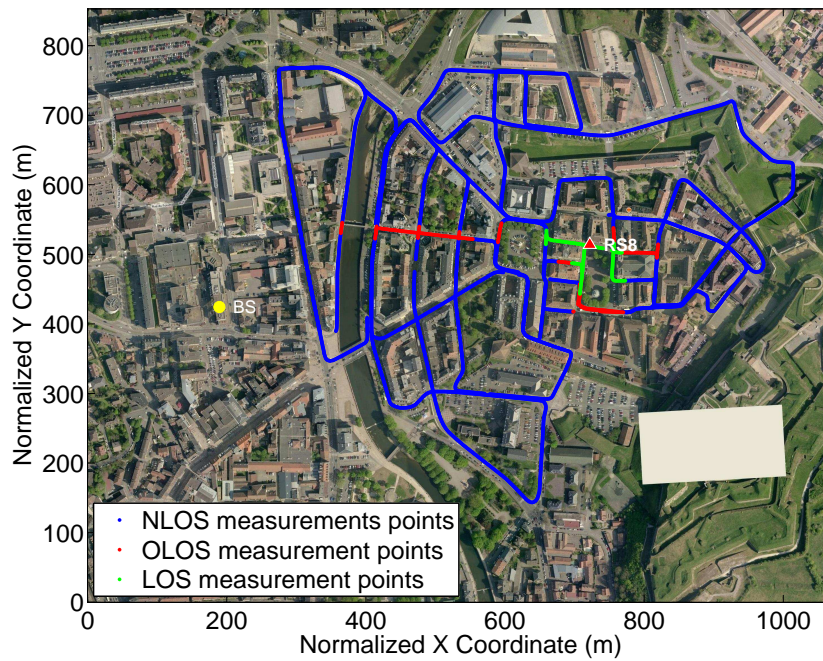


Figure A.14: RS8-MS LOS/OLOS/NLOS measurement points

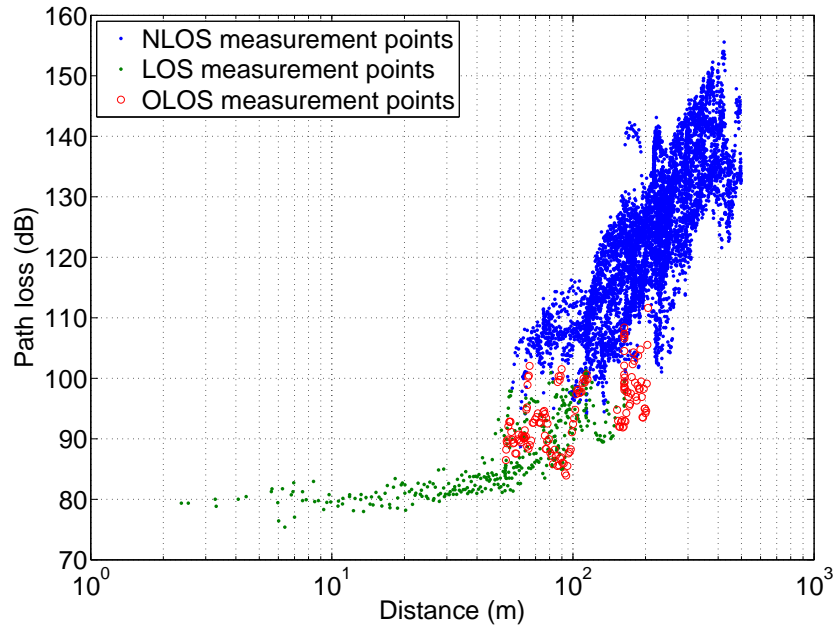


Figure A.15: LOS/OLOS/NLOS classification for RS9-MS link

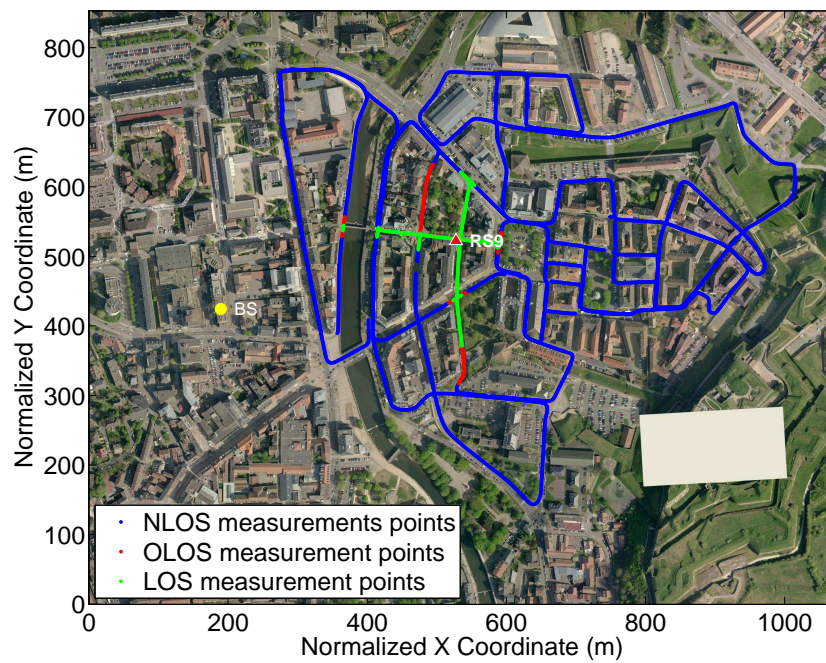


Figure A.16: RS9-MS LOS/OLOS/NLOS measurement points

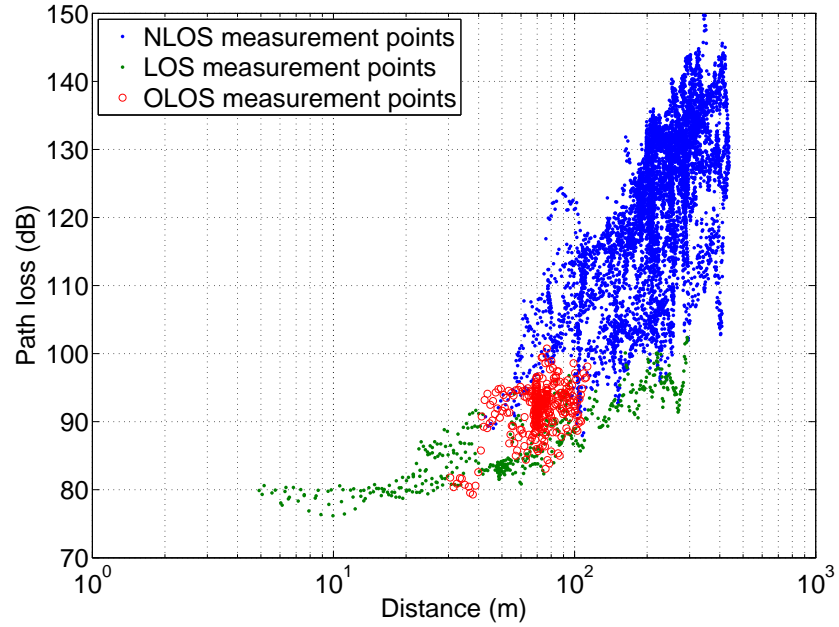


Figure A.17: LOS/OLOS/NLOS classification for RS10-MS link

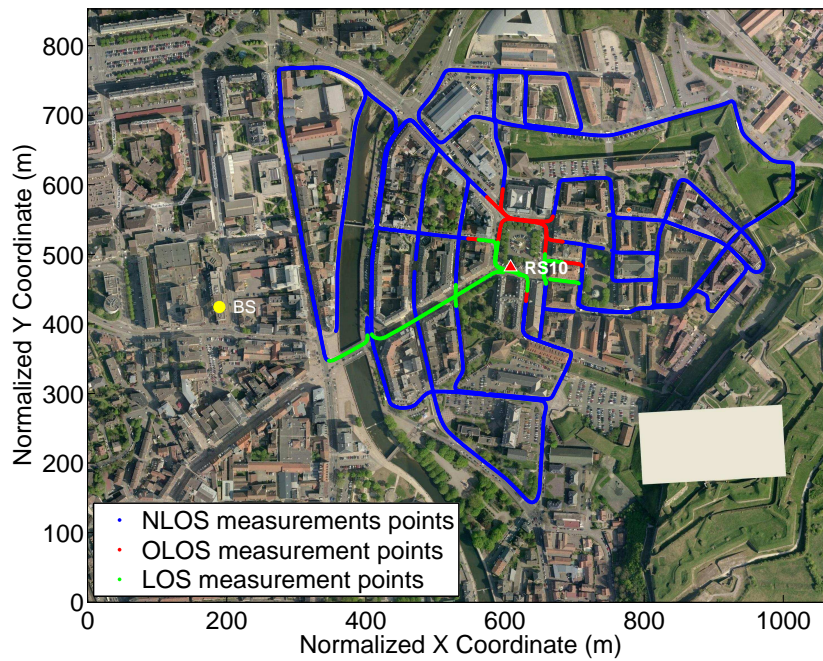


Figure A.18: RS10-MS LOS/OLOS/NLOS measurement points

Appendix B

RS-MS link path loss in NLOS conditions

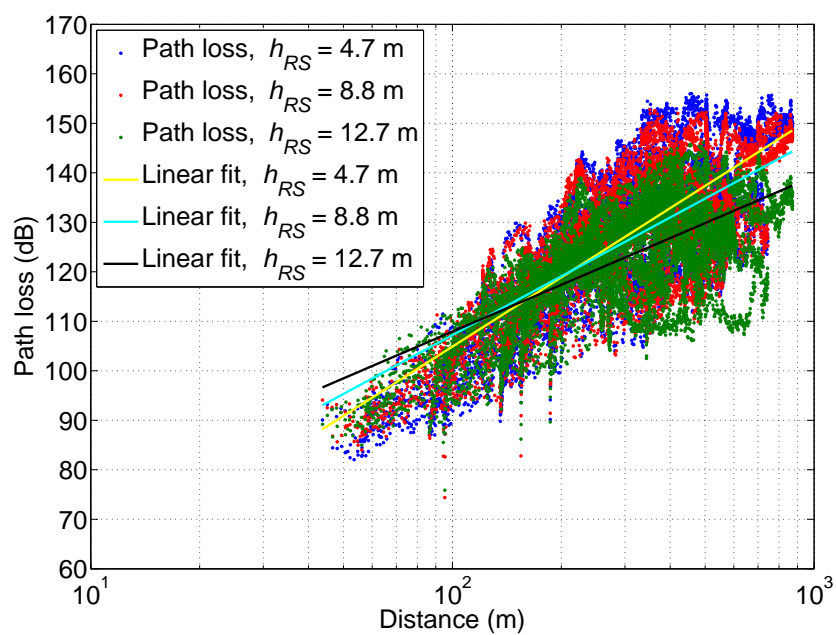


Figure B.1: RS3-MS NLOS path loss with 3 RS antenna heights

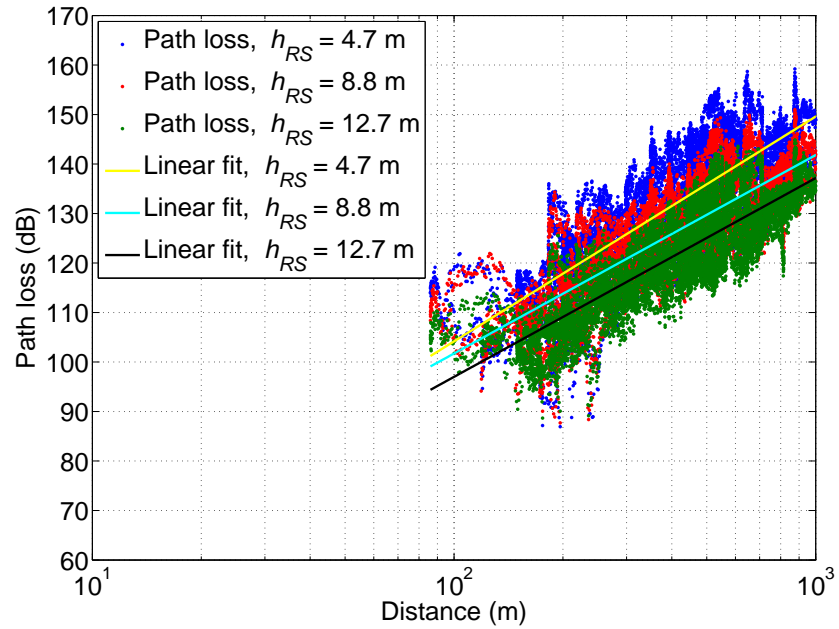


Figure B.2: RS4-MS NLOS path loss with 3 RS antenna heights

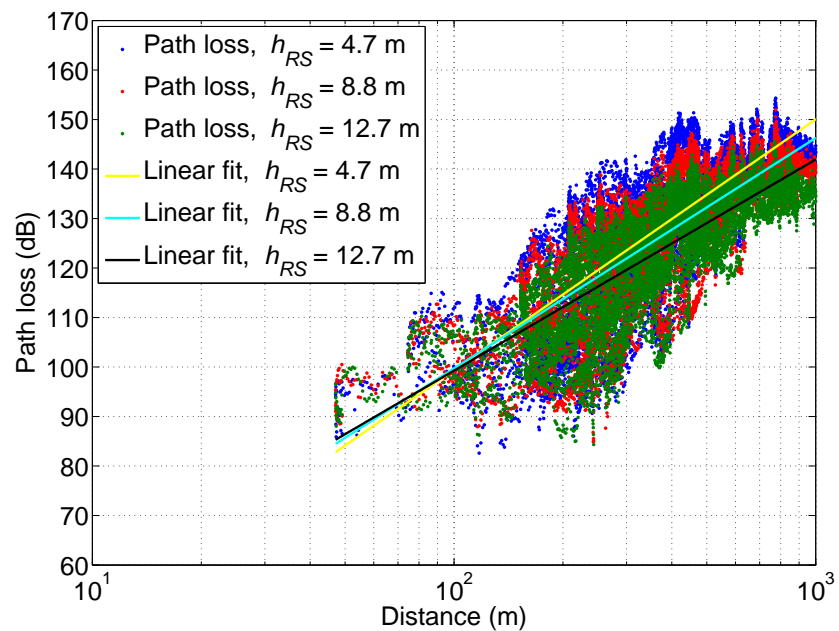


Figure B.3: RS5-MS NLOS path loss with 3 RS antenna heights

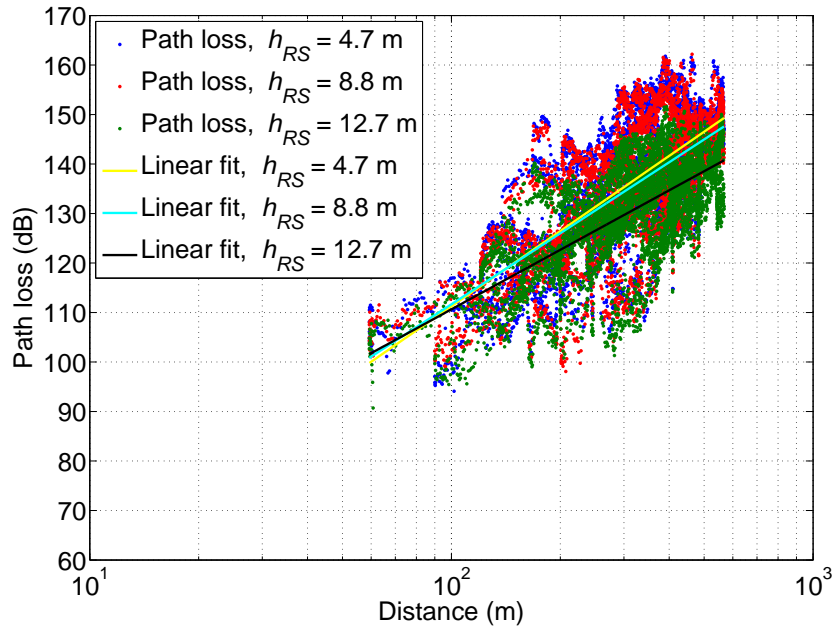


Figure B.4: RS6-MS NLOS path loss with 3 RS antenna heights

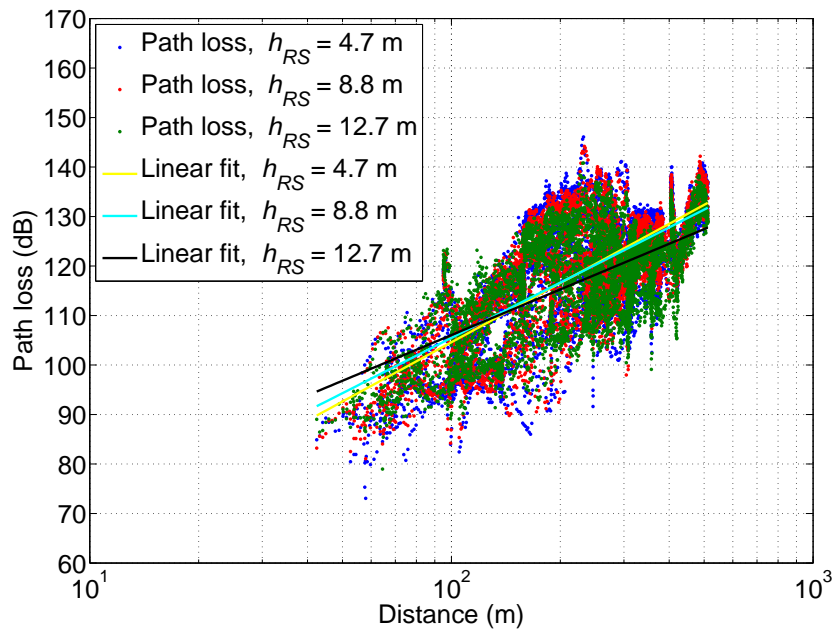


Figure B.5: RS8-MS NLOS path loss with 3 RS antenna heights

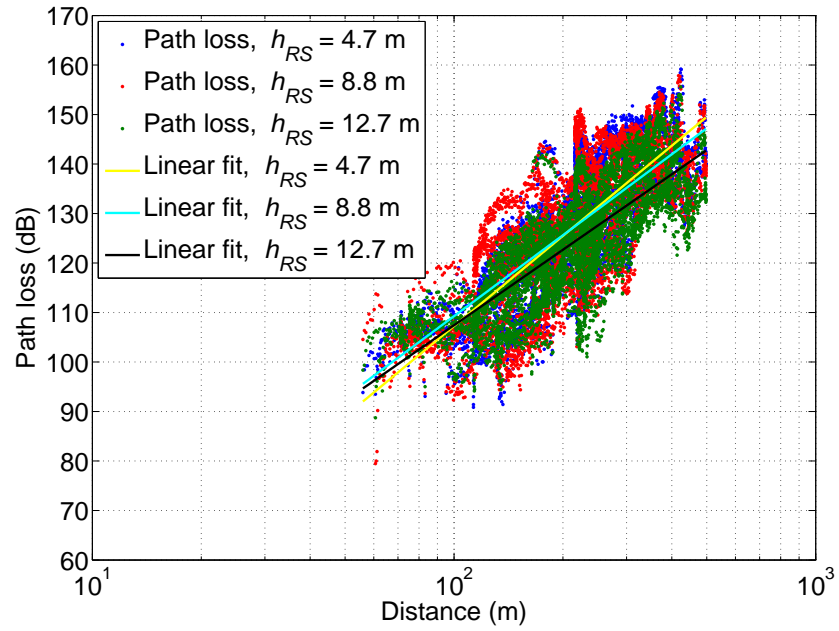


Figure B.6: RS9-MS NLOS path loss with 3 RS antenna heights

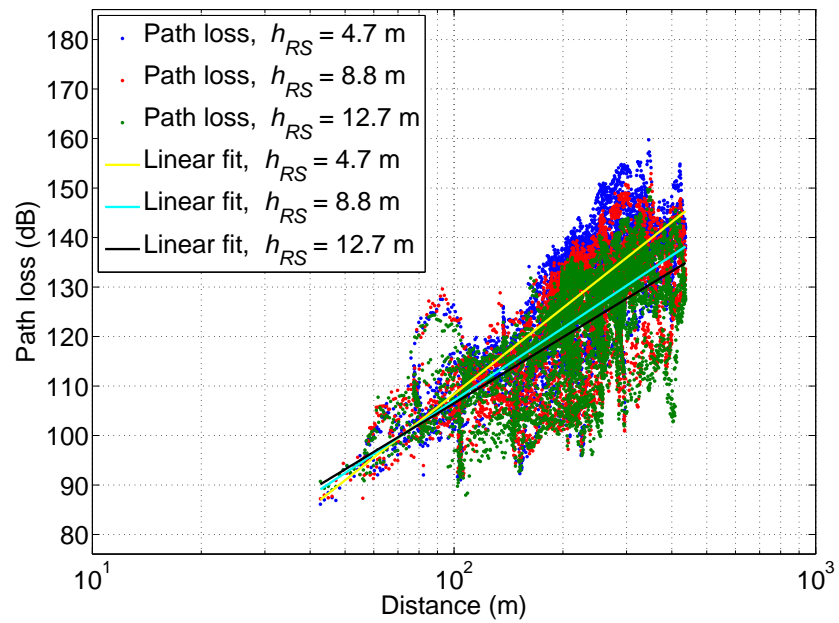


Figure B.7: RS10-MS NLOS path loss with 3 RS antenna heights

Appendix C

RS-MS link path loss in LOS conditions

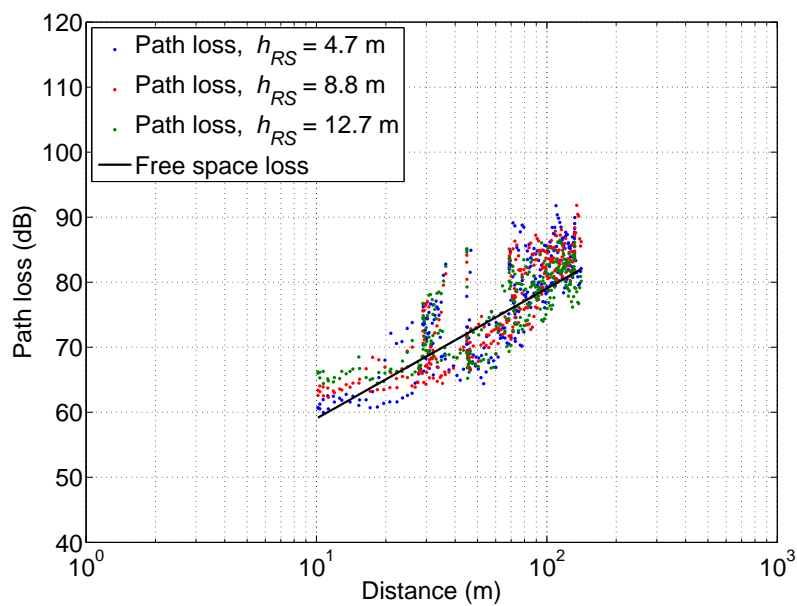


Figure C.1: RS2-MS LOS path loss with 3 RS antenna heights

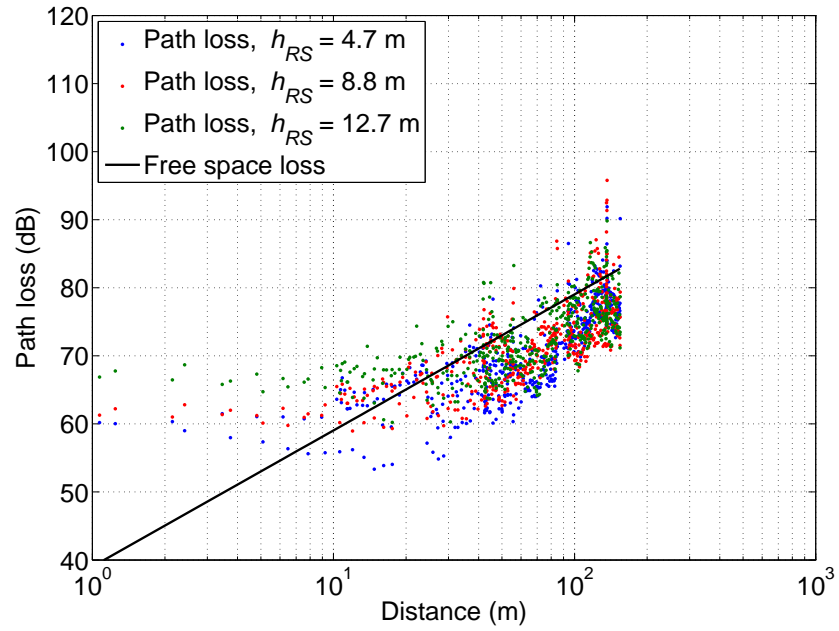


Figure C.2: RS3-MS LOS path loss with 3 RS antenna heights

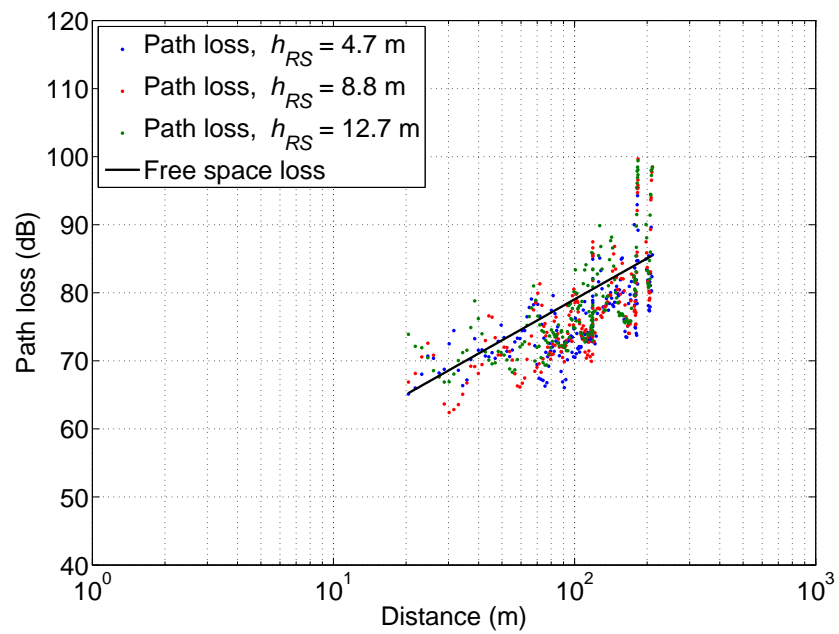


Figure C.3: RS4-MS LOS path loss with 3 RS antenna heights

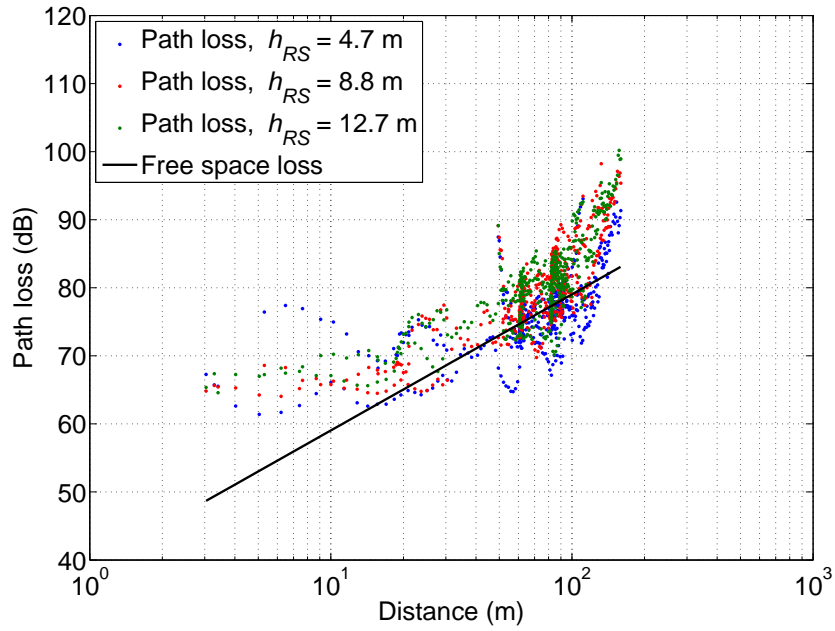


Figure C.4: RS5-MS LOS path loss with 3 RS antenna heights

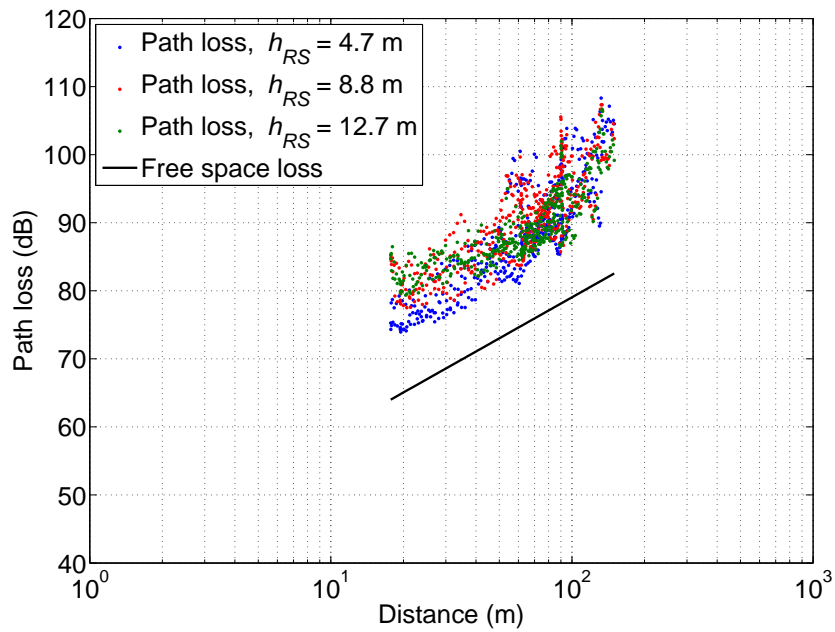


Figure C.5: RS6-MS LOS path loss with 3 RS antenna heights

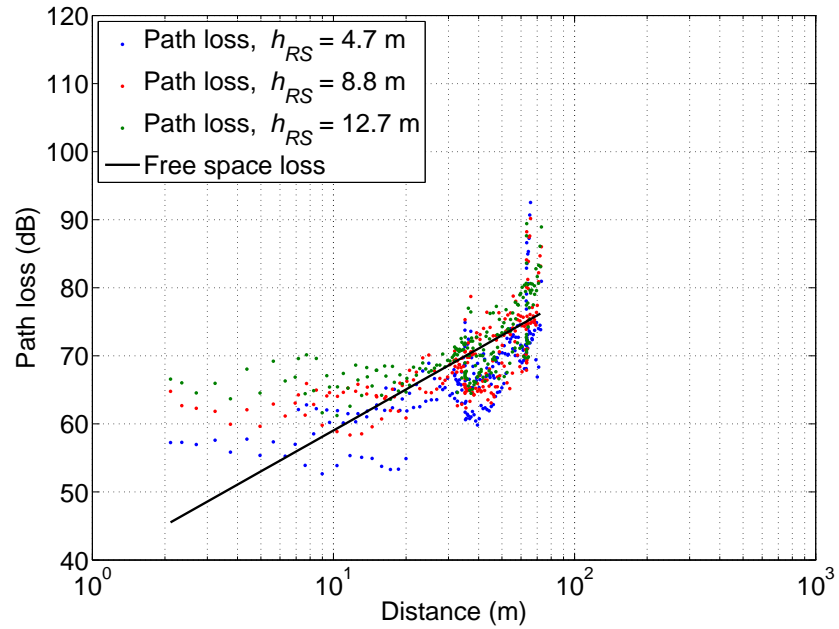


Figure C.6: RS8-MS LOS path loss with 3 RS antenna heights

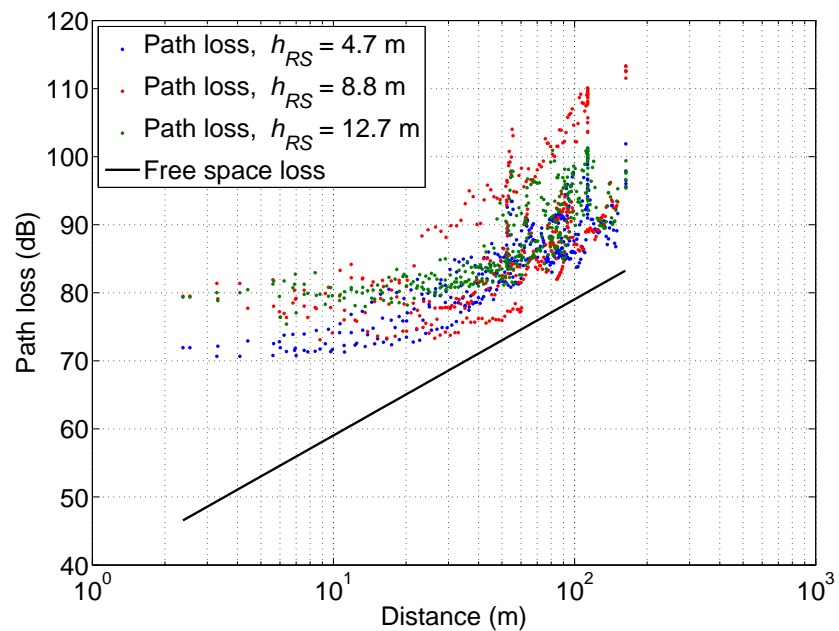


Figure C.7: RS9-MS LOS path loss with 3 RS antenna heights

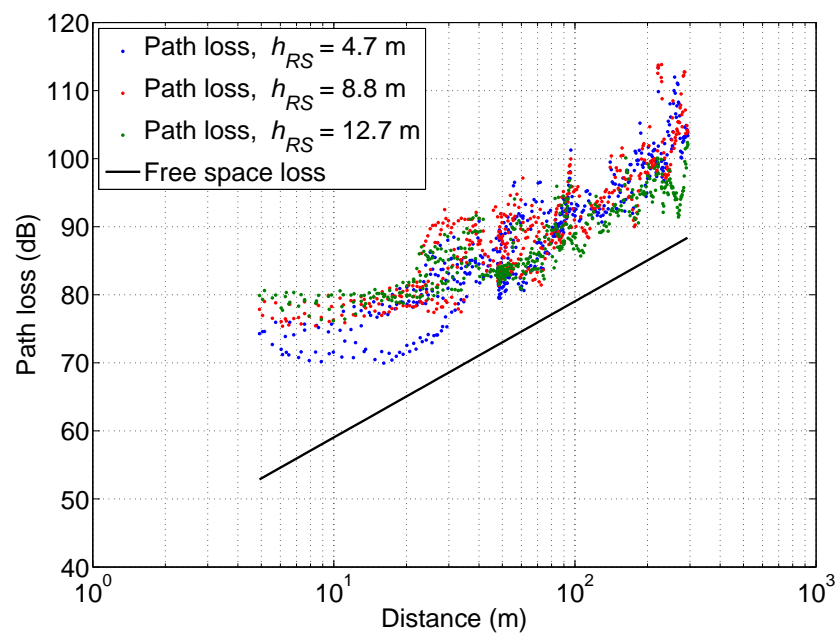


Figure C.8: RS10-MS LOS path loss with 3 RS antenna heights

Personal publications

Quang Hien Chu, Jean-Marc Conrat, Jean-Christophe Cousin, *Experimental Characterization and Modeling of Shadow Fading Correlation for Relaying Systems*, presented at 2011 IEEE 74th Vehicular Technology Conference (VTC2011-Fall), 5-8 September 2011, San Francisco, United States.
(**VTC2011-Fall San Francisco Best Student Paper Award**)

Quang Hien Chu, Jean-Marc Conrat, Jean-Christophe Cousin, *Propagation path loss models for LTE-Advanced urban relaying systems*, presented at 2011 IEEE International Symposium on Antennas and Propagation (APS/URSI), 3-8 July 2011, Spokane, Washington, United States.

Quang Hien Chu, Jean-Marc Conrat, Jean-Christophe Cousin, *On the Characterization of Multi-Link Shadow Fading Correlation for Urban Relaying Systems*, accepted to be presented at 2011 IEEE 22nd International Symposium on Personal, Indoor and Mobile Radio Communications (PIMRC), 11-14 September 2011, Toronto, Canada.

Quang Hien Chu, Jean-Marc Conrat, Jean-Christophe Cousin, *On the impact of receive antenna height in a LTE-Advanced relaying scenario*, presented at 2010 European Wireless Technology Conference (EuWIT), 27-28 September 2010, Paris, France.

Quang Hien Chu, Jean-Marc Conrat, Jean-Christophe Cousin, *Path loss Characterization for LTE-Advanced relaying propagation channel*, presented at COST 2100 Management Committee Meeting, 23-25 November 2010, Bologna, Italy.

Bibliography

- [1] Alexandre Gouraud and Thomas Salzer. Réseaux mobiles de 4e génération : Les opérateurs peuvent-ils s'en remettre aux industriels. Technical report, Orange Labs, 2005.
- [2] Xiaohu You, Dongming Wang, Pengcheng Zhu, and Bin Sheng. Cell edge performance of cellular mobile systems. *Selected Areas in Communications, IEEE Journal on*, 29(6):1139 –1150, june 2011. ISSN 0733-8716. doi: 10.1109/JSAC.2011.110603.
- [3] V. Sreng, H. Yanikomeroglu, and D. Falconer. Coverage enhancement through two-hop relaying in cellular radio systems. In *Wireless Communications and Networking Conference, 2002. WCNC2002. 2002 IEEE*, volume 2, pages 881 – 885 vol.2, mar 2002. doi: 10.1109/WCNC.2002.993387.
- [4] Jaeweon Cho and Z.J. Haas. Throughput enhancement by multi-hop relaying in cellular radio networks with non-uniform traffic distribution. In *Vehicular Technology Conference, 2003. VTC 2003-Fall. 2003 IEEE 58th*, volume 5, pages 3065 – 3069 Vol.5, oct. 2003. doi: 10.1109/VETEFCF.2003.1286187.
- [5] A.K. Dinnis and J.S. Thompson. Increasing high data rate coverage in cellular systems using relaying. In *Vehicular Technology Conference, 2004. VTC2004-Fall. 2004 IEEE 60th*, volume 5, pages 3424 – 3428 Vol. 5, sept. 2004. doi: 10.1109/VETEFCF.2004.1404699.
- [6] N. Esseling, B.H. Walke, and R. Pabst. Performance evaluation of a fixed relay concept for next generation wireless systems. In *Personal, Indoor and Mobile Radio Communications, 2004. PIMRC 2004. 15th IEEE International Symposium on*, volume 2, pages 744 – 751 Vol.2, sept. 2004. doi: 10.1109/PIMRC.2004.1373800.
- [7] Huining Hu, H. Yanikomeroglu, D.D. Falconer, and S. Periyalwar. Range extension without capacity penalty in cellular networks with

- digital fixed relays. In *Global Telecommunications Conference, 2004. GLOBECOM '04. IEEE*, volume 5, pages 3053 – 3057 Vol.5, nov.-3 dec. 2004. doi: 10.1109/GLOCOM.2004.1378913.
- [8] R. Pabst, B.H. Walke, D.C. Schultz, P. Herhold, H. Yanikomeroglu, S. Mukherjee, H. Viswanathan, M. Lott, W. Zirwas, M. Dohler, H. Aghvami, D.D. Falconer, and G.P. Fettweis. Relay-based deployment concepts for wireless and mobile broadband radio. *Communications Magazine, IEEE*, 42(9):80 – 89, sept. 2004. ISSN 0163-6804. doi: 10.1109/MCOM.2004.1336724.
- [9] S. Mukherjee and H. Viswanathan. Analysis of throughput gains from relays in cellular networks. In *Global Telecommunications Conference, 2005. GLOBECOM '05. IEEE*, volume 6, pages 6 pp. –3476, dec. 2005. doi: 10.1109/GLOCOM.2005.1578418.
- [10] Z. Dawy and S. Arayssi. Advanced Fixed Relaying in Multihop Based Cellular Networks. In *Communications, 2006. ICC '06. IEEE International Conference on*, volume 10, pages 4526 –4531, june 2006. doi: 10.1109/ICC.2006.255352.
- [11] H. Nourizadeh, S. Nourizadeh, and R. Tafazolli. Performance Evaluation of Cellular Networks with Mobile and Fixed Relay Station. In *Vehicular Technology Conference, 2006. VTC-2006 Fall. 2006 IEEE 64th*, pages 1 –5, sept. 2006. doi: 10.1109/VTCF.2006.501.
- [12] M. Rahman and H. Yanikomeroglu. WLC15-5: QoS Provisioning in the Absence of ARQ in Cellular Fixed Relay Networks through Inter-Cell Coordination. In *Global Telecommunications Conference, 2006. GLOBECOM '06. IEEE*, pages 1 –5, 27 2006-dec. 1 2006. doi: 10.1109/GLOCOM.2006.702.
- [13] B. Timus. A Coverage Analysis of Amplify-and-Forward Relaying Schemes in Outdoor Urban Environment. In *Wireless and Mobile Communications, 2006. ICWMC '06. International Conference on*, page 56, july 2006. doi: 10.1109/ICWMC.2006.1.
- [14] Ping Li, Mengtian Rong, Yisheng Xue, Lan Wang, and E. Schulz. Performance Analysis of Cellular System Enhanced with Two-Hop Fixed Relay Nodes. In *Vehicular Technology Conference, 2007. VTC2007-Spring. IEEE 65th*, pages 929 –933, april 2007. doi: 10.1109/VETECS.2007.200.

-
- [15] Tao Liu, Mengtian Rong, Yisheng Xue, and E. Schulz. Joint Routing and Resource Partitioning in Relay Enhanced Cellular Network. In *Wireless Communications and Networking Conference, 2007.WCNC 2007. IEEE*, pages 4133 –4138, march 2007. doi: 10.1109/WCNC.2007.755.
- [16] K. Balachandran, J. Kang, K. Karakayali, and J. Singh. Capacity Benefits of Relays with In-Band Backhauling in Cellular Networks. In *Communications, 2008. ICC '08. IEEE International Conference on*, pages 3736 –3742, may 2008. doi: 10.1109/ICC.2008.702.
- [17] G. Farhadi and N.C. Beaulieu. Amplify-and-Forward Cooperative Systems with Fixed Gain Relays. In *Communications, 2008. ICC '08. IEEE International Conference on*, pages 4300 –4305, may 2008. doi: 10.1109/ICC.2008.807.
- [18] R. Irmer and F. Diehm. On coverage and capacity of relaying in LTE-advanced in example deployments. In *Personal, Indoor and Mobile Radio Communications, 2008. PIMRC 2008. IEEE 19th International Symposium on*, pages 1 –5, sept. 2008. doi: 10.1109/PIMRC.2008.4699896.
- [19] S. Parkvall, E. Dahlman, A. Furuskar, Y. Jading, M. Olsson, S. Wanstedt, and K. Zangi. LTE-Advanced - Evolving LTE towards IMT-Advanced. In *Vehicular Technology Conference, 2008. VTC 2008-Fall. IEEE 68th*, pages 1 –5, sept. 2008. doi: 10.1109/VETEFCF.2008.313.
- [20] R. Schoenen, R. Halfmann, and B.H. Walke. MAC Performance of a 3GPP-LTE Multihop Cellular Network. In *Communications, 2008. ICC '08. IEEE International Conference on*, pages 4819 –4824, may 2008. doi: 10.1109/ICC.2008.903.
- [21] R. Schoenen, W. Zirwas, and B.H. Walke. Raising coverage and capacity using fixed relays in a realistic scenario. In *Wireless Conference, 2008. EW 2008. 14th European*, pages 1 –6, june 2008. doi: 10.1109/EW.2008.4623913.
- [22] D. Soldani and S. Dixit. Wireless relays for broadband access [radio communications series]. *Communications Magazine, IEEE*, 46(3):58 –66, march 2008. ISSN 0163-6804. doi: 10.1109/MCOM.2008.4463772.
- [23] T. Beniero, S. Redana, J. Hamalainen, and B. Raaf. Effect of Relaying on Coverage in 3GPP LTE-Advanced. In *Vehicular Technology Con-*

- ference, 2009. *VTC Spring 2009. IEEE 69th*, pages 1 –5, april 2009. doi: 10.1109/VETECS.2009.5073520.
- [24] A. Bou Saleh, S. Redana, B. Raaf, T. Riihonen, J. Hamalainen, and R. Wichman. Performance of Amplify-and-Forward and Decode-and-Forward Relays in LTE-Advanced. In *Vehicular Technology Conference Fall (VTC 2009-Fall), 2009 IEEE 70th*, pages 1 –5, sept. 2009. doi: 10.1109/VETECEF.2009.5378824.
- [25] Di Dong, Jianhua Zhang, Yu Zhang, and Xin Nie. Large Scale Characteristics and Capacity Evaluation of Outdoor Relay Channels at 2.35 GHz. In *Vehicular Technology Conference Fall (VTC 2009-Fall), 2009 IEEE 70th*, pages 1 –5, sept. 2009. doi: 10.1109/VETECEF.2009.5379072.
- [26] Min Liang, Fang Liu, Zhe Chen, Ya Feng Wang, and Da Cheng Yang. A Novel Frequency Reuse Scheme for OFDMA Based Relay Enhanced Cellular Networks. In *Vehicular Technology Conference, 2009. VTC Spring 2009. IEEE 69th*, pages 1 –5, april 2009. doi: 10.1109/VETECS.2009.5073319.
- [27] Huang Lin, Daqing Gu, Wenbo Wang, and Hongwen Yang. Capacity analysis of dedicated fixed and mobile relay in LTE-Advanced cellular networks. In *Communications Technology and Applications, 2009. ICCTA '09. IEEE International Conference on*, pages 354 –359, oct. 2009. doi: 10.1109/ICCOMTA.2009.5349178.
- [28] P.E. Mogensen, T. Koivisto, K.I. Pedersen, I.Z. Kovacs, B. Raaf, K. Pajukoski, and M.J. Rinne. LTE-Advanced: The path towards gigabit/s in wireless mobile communications. In *Wireless Communication, Vehicular Technology, Information Theory and Aerospace Electronic Systems Technology, 2009. Wireless VITAE 2009. 1st International Conference on*, pages 147 –151, may 2009. doi: 10.1109/WIRELESSVITAE.2009.5172440.
- [29] Jongrok Park, Hyukmin Son, and Sanghoon Lee. Throughput and QoS improvement via fixed relay station cooperated beam-forming. *Wireless Communications, IEEE Transactions on*, 8(5):2400 –2409, may 2009. ISSN 1536-1276. doi: 10.1109/TWC.2009.071079.
- [30] Steven W. Peters, Ali Y. Panah, Kien T. Truong, and Robert W. Heath. Relay Architectures for 3GPP LTE-Advanced. *EURASIP Journal on*

- Wireless Communications and Networking*, 2009, 2009. doi: 10.1155/2009/618787.
- [31] J. Sydir and R. Taori. An evolved cellular system architecture incorporating relay stations. *Communications Magazine, IEEE*, 47(6):115–121, june 2009. ISSN 0163-6804. doi: 10.1109/MCOM.2009.5116808.
- [32] Hui Tian, Fan Jiang, Xijun Wang, Xiaoying Tang, and Jietao Zhang. An Inter-Cell Interference Coordination Scheme for Relay Based Cellular Networks. In *Wireless Communications, Networking and Mobile Computing, 2009. WiCom '09. 5th International Conference on*, pages 1–4, sept. 2009. doi: 10.1109/WICOM.2009.5304579.
- [33] T. Wirth, V. Venkatkumar, T. Haustein, E. Schulz, and R. Halfmann. LTE-Advanced Relaying for Outdoor Range Extension. In *Vehicular Technology Conference Fall (VTC 2009-Fall), 2009 IEEE 70th*, pages 1–4, sept. 2009. doi: 10.1109/VETECEF.2009.5378969.
- [34] Yang Yang, Honglin Hu, Jing Xu, and Guoqiang Mao. Relay technologies for WiMax and LTE-advanced mobile systems. *Communications Magazine, IEEE*, 47(10):100–105, october 2009. ISSN 0163-6804. doi: 10.1109/MCOM.2009.5273815.
- [35] E. Yilmaz, R. Knopp, and D. Gesbert. On the gains of fixed relays in cellular networks with intercell interference. In *Signal Processing Advances in Wireless Communications, 2009. SPAWC '09. IEEE 10th Workshop on*, pages 603–607, june 2009. doi: 10.1109/SPAWC.2009.5161856.
- [36] Hongbing Cheng and Yu-Dong Yao. Cognitive-Relay-Based Intercell Interference Cancellation in Cellular Systems. *Vehicular Technology, IEEE Transactions on*, 59(4):1901–1909, may 2010. ISSN 0018-9545. doi: 10.1109/TVT.2010.2040399.
- [37] Quang Hien Chu, J.-M. Conrat, and J.-C. Cousin. On the impact of receive antenna height in a LTE-Advanced relaying scenario. In *Wireless Technology Conference (EuWIT), 2010 European*, pages 129–132, sept. 2010.
- [38] R. Schoenen, W. Zirwas, and B.H. Walke. Capacity and Coverage Analysis of a 3GPP-LTE Multihop Deployment Scenario. In *Communications Workshops, 2008. ICC Workshops '08. IEEE International Conference on*, pages 31–36, may 2008. doi: 10.1109/ICCW.2008.11.

- [39] Woonsik Lee, Minh-Viet Nguyen, and Hwang Soo Lee. A resource allocation algorithm and system architecture to extend the cell coverage and alleviate the inter-cell interference. In *Computers and Communications, 2008. ISCC 2008. IEEE Symposium on*, pages 222 –227, july 2008. doi: 10.1109/ISCC.2008.4625677.
- [40] M. Rahman, H. Yanikomeroglu, and W. Wong. Interference Avoidance with Dynamic Inter-Cell Coordination for Downlink LTE System. In *Wireless Communications and Networking Conference, 2009. WCNC 2009. IEEE*, pages 1 –6, april 2009. doi: 10.1109/WCNC.2009.4917761.
- [41] 3rd Generation Partnership Project. TR 36.814 v.9.0.0: Further Advancements for E-UTRA, Physical Layer Aspects. Technical report, 2010.
- [42] WINNER project. IST-4-027756 WINNER II D 1.1.2 v1.2, WINNER II Channel Models. Technical report, 2006.
- [43] IEEE 802.16 Working Group. Multi-hop Relay System Evaluation Methodology (Channel Model and Performance Metric). Technical report, 2007.
- [44] J.D. Parsons, A.M.D. Turkmani, and Feng Ju. The effect of base station antenna height on 900 MHz microcellular mobile radio systems. In *Microcellular Mobile Radio, IEE Colloquium on*, pages 7/1 –7/6, feb 1989.
- [45] K. Sakawa, H. Masui, M. Ishii, H. Shimizu, and T. Kobayashi. Microwave path-loss characteristics in an urban area with base station antenna on top of a tall building. In *Broadband Communications, 2002. Access, Transmission, Networking. 2002 International Zurich Seminar on*, pages 31–1 –31–4, 2002. doi: 10.1109/IZSBC.2002.991774.
- [46] Matthew Webb, Gavin Watkins, Chris Williams, Tim Harrold, Roger Feng, and Mark Beach. Mobile Multihop: Measurements vs. Models. *European Cooperation in the Field of Scientific and Technical Research, COST 2100*, 2007.
- [47] V.S. Abhayawardhana, I.J. Wassell, D. Crosby, M.P. Sellars, and M.G. Brown. Comparison of empirical propagation path loss models for fixed wireless access systems. In *Vehicular Technology Conference, 2005. VTC 2005-Spring. 2005 IEEE 61st*, volume 1, pages 73 – 77 Vol. 1, may-1 june 2005. doi: 10.1109/VETECS.2005.1543252.

- [48] K.G. Tan and T.A. Rahman. Receiving antenna height dependence of radio propagation path loss in fixed wireless access environment. In *Microwave Conference, 1999 Asia Pacific*, volume 3, pages 797–800 vol.3, 1999. doi: 10.1109/APMC.1999.833713.
- [49] J. Medbo, J. Furuskog, M. Riback, and J.-E. Berg. Multi-frequency path loss in an outdoor to indoor macrocellular scenario. In *Antennas and Propagation, 2009. EuCAP 2009. 3rd European Conference on*, pages 3601–3605, march 2009.
- [50] Simon R. Saunders and Zavala Alejandro Aragon. *Antennas and Propagation for Wireless Communication Systems*. John Wiley & Sons, 2007.
- [51] S.S. Szyszkowicz, H. Yanikomeroglu, and J.S. Thompson. On the Feasibility of Wireless Shadowing Correlation Models. *Vehicular Technology, IEEE Transactions on*, 59(9):4222–4236, 2010. ISSN 0018-9545. doi: 10.1109/TVT.2010.2082006.
- [52] V. Graziano. Propagation correlations at 900 MHz. *Vehicular Technology, IEEE Transactions on*, 27(4):182–189, November 1978. ISSN 0018-9545. doi: 10.1109/T-VT.1978.23747.
- [53] K. Zayana and B. Guisnet. Measurements and modelisation of shadowing cross-correlations between two base-stations. In *Universal Personal Communications, 1998. ICUPC '98. IEEE 1998 International Conference on*, volume 1, pages 101–105 vol.1, October 1998. doi: 10.1109/ICUPC.1998.732812.
- [54] T. Klingenbrunn and P. Mogensen. Modelling cross-correlated shadowing in network simulations. In *Vehicular Technology Conference, 1999. VTC 1999 - Fall. IEEE VTS 50th*, volume 3, pages 1407–1411 vol.3, 1999. doi: 10.1109/VETEFCF.1999.801494.
- [55] J. Weitzen and T.J. Lowe. Measurement of angular and distance correlation properties of log-normal shadowing at 1900 MHz and its application to design of PCS systems. *Vehicular Technology, IEEE Transactions on*, 51(2):265–273, March 2002. ISSN 0018-9545. doi: 10.1109/25.994804.
- [56] Juha Korhonen. *Introduction to 3G Mobile Communication*. Artech House Publishers, 2003.

-
- [57] 3rd Generation Partnership Project. [Online] Available: <http://www/3gpp.org>.
- [58] 3rd Generation Partnership Project. TR36.913: Require for further advancements for E-UTRA (LTE-Advanced). Technical report, 2008.
- [59] K. Etemad. Overview of mobile WiMAX technology and evolution. *Communications Magazine, IEEE*, 46(10):31–40, october 2008. ISSN 0163-6804. doi: 10.1109/MCOM.2008.4644117.
- [60] IEEE. IEEE Standard for Local and Metropolitan Area Networks - Part 16: Air Interface for Fixed Broadband Wireless Systems (IEEE Std 802.16-2004), 2004.
- [61] IEEE. Amendments to IEEE Standard for Local and Metropolitan Area Networks - Part 16: Air Interface for Fixed Broadband Wireless Access Systems (IEEE Std 802-16 2005), 2005.
- [62] IEEE. Draft Standard for Local and Metropolitan Area Networks - Part 16: Air Interface for Fixed and Mobile Broadband Wireless Access Systems, Multihop Relay Specifications (IEEE 802-16 Relay Task Group), .
- [63] IEEE. Draft Standard for Local and Metropolitan Area Networks - Part 16: Air Interface for Fixed and Mobile Broadband Wireless Access Systems, Advanced Air Interface (IEEE 802.16m), .
- [64] Eric Hardouin, Thomas Derham, Lin Huang, and Alexandre Gouraud. 3GPP LTE-Advanced Overview. Technical report, Orange Labs, 2010.
- [65] Takaharu Nakamura. LTE-Advanced (3GPP Release 10 and Beyond) - RF aspects, 2009. URL http://www.3gpp.org/ftp/workshop/2009-12-17_ITU-R_IMT-Adv_eval/docs/pdf/REV-090006.pdf.
- [66] Theodore S. Rappaport. *Wireless Communication, Principle and Practice*. Prentice Hall, 1996.
- [67] J.B. Andersen, T.S. Rappaport, and S. Yoshida. Propagation measurements and models for wireless communications channels. *Communications Magazine, IEEE*, 33(1):42–49, jan 1995. ISSN 0163-6804. doi: 10.1109/35.339880.
- [68] T. Okumura, E. Ohmori, and K. Fukuda. Field Strength and its Variability in VHF and UHF Land Mobile Service. *Review Electrical Communication Laboratory*, 16:825–873, 1968.

-
- [69] M. Hata. Empirical formula for propagation loss in land mobile radio services. *Vehicular Technology, IEEE Transactions on*, 29(3):317 – 325, aug 1980. ISSN 0018-9545. doi: 10.1109/T-VT.1980.23859.
- [70] COST 231. Digital Mobile Radio Towards Future Generation Systems, Final Report. Technical report, 1999.
- [71] ITU-R. Recommendation P.1411-5: Propagation data and prediction methods for the planning of short-range outdoor radiocommunication systems and radio local area networks in the frequency range 300 MHz to 100 GHz, 2009.
- [72] IEEE 802.16 Working Group. Technical report: Channel Models for Fixed Wireless Applications. Technical report, 2003.
- [73] J.H. Whitteker. Measurements of path loss at 910 mhz for proposed microcell urban mobile systems. *Vehicular Technology, IEEE Transactions on*, 37(3):125 –129, aug 1988. ISSN 0018-9545. doi: 10.1109/25.16538.
- [74] E. Green and M. Hata. Microcellular propagation measurements in an urban environment. In *Personal, Indoor and Mobile Radio Communications., IEEE International Symposium on*, pages 324 –328, sep 1991. doi: 10.1109/PIMRC.1991.571510.
- [75] R.J.C. Bultitude and D.A. Hughes. Propagation loss at 1.8 ghz on microcellular mobile radio channels. In *Personal, Indoor and Mobile Radio Communications, 1996. PIMRC'96., Seventh IEEE International Symposium on*, volume 3, pages 786 –790 vol.3, oct 1996. doi: 10.1109/PIMRC.1996.568388.
- [76] K. Taira, S. Sekizawa, Gang Wu, H. Harada, and Y. Hase. Propagation loss characteristics for microcellular mobile communications in microwave band. In *Universal Personal Communications, 1996. Record., 1996 5th IEEE International Conference on*, volume 2, pages 842 –846 vol.2, sep-2 oct 1996. doi: 10.1109/ICUPC.1996.562695.
- [77] W.C.Y. Lee and D.J.Y. Lee. Microcell prediction in dense urban area. *Vehicular Technology, IEEE Transactions on*, 47(1):246 –253, feb 1998. ISSN 0018-9545. doi: 10.1109/25.661051.
- [78] Y. Oda, K. Tsunekawa, and M. Hata. Advanced los path-loss model in microcellular mobile communications. *Vehicular Technology, IEEE*

- Transactions on*, 49(6):2121 –2125, nov 2000. ISSN 0018-9545. doi: 10.1109/25.901884.
- [79] J. Walfisch and H.L. Bertoni. A theoretical model of UHF propagation in urban environments. *Antennas and Propagation, IEEE Transactions on*, 36(12):1788 –1796, dec 1988. ISSN 0018-926X. doi: 10.1109/8.14401.
- [80] F. Ikegami, S. Yoshida, T. Takeuchi, and M. Umehira. Propagation factors controlling mean field strength on urban streets. *Antennas and Propagation, IEEE Transactions on*, 32(8):822 – 829, aug 1984. ISSN 0018-926X. doi: 10.1109/TAP.1984.1143419.
- [81] W. Mohr. The WINNER (wireless world initiative new radio) project-development of a radio interface for systems beyond 3G. In *Personal, Indoor and Mobile Radio Communications, 2005. PIMRC 2005. IEEE 16th International Symposium on*, volume 2, pages 857 –862 Vol. 2, sept. 2005. doi: 10.1109/PIMRC.2005.1651564.
- [82] A. Osseiran, E. Hardouin, A. Gouraud, M. Boldi, I. Cosovic, K. Gosse, J. Luo, S. Redana, W. Mohr, J. Monserrat, T. Svensson, A. Tolli, A. Mihovska, and M. Werner. The road to IMT-advanced communication systems: State-of-the- art and innovation areas addressed by the WINNER + project. *Communications Magazine, IEEE*, 47(6):38 –47, june 2009. ISSN 0163-6804. doi: 10.1109/MCOM.2009.5116799.
- [83] J.-E. Berg. A recursive method for street microcell path loss calculations. In *Personal, Indoor and Mobile Radio Communications, 1995. PIMRC'95. 'Wireless: Merging onto the Information Superhighway'.*, *Sixth IEEE International Symposium on*, volume 1, pages 140 –143 vol.1, sep 1995. doi: 10.1109/PIMRC.1995.476420.
- [84] M. Gudmundson. Correlation model for shadow fading in mobile radio systems. *Electronics Letters*, 27(23):2145 –2146, 1991. ISSN 0013-5194. doi: 10.1049/el:19911328.
- [85] V. Erceg, L.J. Greenstein, S. Tjandra, S.R. Parkoff, A. Gupta, B. Kulic, A. Julius, and R. Jastrzab. An empirically-based path loss model for wireless channels in suburban environments. In *Global Telecommunications Conference, 1998. GLOBECOM 98. The Bridge to Global Integration. IEEE*, volume 2, pages 922 –927 vol.2, 1998. doi: 10.1109/GLOCOM.1998.776865.

- [86] E. Perahia, D.C. Cox, and S. Ho. Shadow fading cross correlation between basestations. In *Vehicular Technology Conference, 2001. VTC 2001 Spring. IEEE VTS 53rd*, volume 1, pages 313 –317 vol.1, 2001. doi: 10.1109/VETECS.2001.944855.
- [87] F. Graziosi and F. Santucci. A general correlation model for shadow fading in mobile radio systems. *Communications Letters, IEEE*, 6(3): 102 –104, March 2002. ISSN 1089-7798. doi: 10.1109/4234.991146.
- [88] K. Yamamoto, A. Kusuda, and S. Yoshida. Impact of Shadowing Correlation on Coverage of Multihop Cellular Systems. In *Communications, 2006. ICC '06. IEEE International Conference on*, volume 10, pages 4538 –4542, june 2006. doi: 10.1109/ICC.2006.255354.
- [89] T.B. Sorensen. Slow fading cross-correlation against azimuth separation of base stations. *Electronics Letters*, 35(2):127 –129, jan 1999. ISSN 0013-5194. doi: 10.1049/el:19990085.
- [90] F. Graziosi, M. Pratesi, M. Ruggieri, and F. Santucci. Modeling of handover initiation algorithms with correlated co-channel interferers. In *Universal Personal Communications Record, 1997. Conference Record., 1997 IEEE 6th International Conference on*, pages 244 –248 vol.1, oct 1997. doi: 10.1109/ICUPC.1997.625558.
- [91] M. Pratesi, M. Ruggieri, F. Graziosi, and F. Santucci. Performance of signal strength handover algorithms with interference and correlated shadowings. In *Vehicular Technology Conference, 1997 IEEE 47th*, volume 2, pages 530 –534 vol.2, may 1997. doi: 10.1109/VETEC.1997.600383.
- [92] N. Gogate, D. Avidor, and S.S. Panwar. Simulation study of a fixed wireless access system. In *Universal Personal Communications, 1998. ICUPC '98. IEEE 1998 International Conference on*, volume 1, pages 209 –215 vol.1, oct 1998. doi: 10.1109/ICUPC.1998.732829.
- [93] D. Avidor, N. Hegde, and S. Mukherjee. On the impact of the soft handoff threshold and the maximum size of the active group on resource allocation and outage probability in the UMTS system. *Wireless Communications, IEEE Transactions on*, 3(2):565 – 577, march 2004. ISSN 1536-1276. doi: 10.1109/TWC.2004.825368.
- [94] D. Kaltakis, M.A. Imran, and R. Hoshyar. Uplink Capacity with Correlated Lognormal Shadow Fading. In *Vehicular Technology Confer-*

- ence, 2009. *VTC Spring 2009. IEEE 69th*, pages 1–5, april 2009. doi: 10.1109/VETECS.2009.5073895.
- [95] J.F. Monserrat, R. Fraile, and L. Rubio. Application of alternating projection method to ensure feasibility of shadowing cross-correlation models. *Electronics Letters*, 43(13):724–725, 21 2007. ISSN 0013-5194. doi: 10.1049/el:20070236.
- [96] J.F. Monserrat, R. Fraile, D. Calabuig, and N. Cardona. Complete Shadowing Modeling and its Effect on System Level Performance Evaluation. In *Vehicular Technology Conference, 2008. VTC Spring 2008. IEEE*, pages 294–298, may 2008. doi: 10.1109/VETECS.2008.73.
- [97] Wei Ni, Wei Zou, and Haifeng Wang. Modeling of Spatially Cross-Correlated Shadow Fading in Distributed Radio Access Networks. In *Communications, 2008. ICC '08. IEEE International Conference on*, pages 4472–4476, may 2008. doi: 10.1109/ICC.2008.839.
- [98] W. Lee and Y. Yeh. On the Estimation of the Second-Order Statistics of Log Normal Fading in Mobile Radio Environment. *Communications, IEEE Transactions on*, 22(6):869–873, jun 1974. ISSN 0090-6778. doi: 10.1109/TCOM.1974.1092290.
- [99] D. de la Vega, S. Lopez, J.M. Matias, U. Gil, I. Pena, M.M. Velez, J.L. Ordiales, and P. Angueira. Generalization of the Lee Method for the Analysis of the Signal Variability. *Vehicular Technology, IEEE Transactions on*, 58(2):506–516, feb. 2009. ISSN 0018-9545. doi: 10.1109/TVT.2008.926214.
- [100] J.W. Porter and J.A. Thweatt. Microwave propagation characteristics in the MMDS frequency band. In *Communications, 2000. ICC 2000. 2000 IEEE International Conference on*, volume 3, pages 1578–1582 vol.3, 2000. doi: 10.1109/ICC.2000.853761.
- [101] R.E. Badra and A. Zambrano. Street-level los/nlos model for urban macrocells based on observations. In *Wireless Communications and Networking Conference (WCNC), 2011 IEEE*, pages 1294–1297, march 2011. doi: 10.1109/WCNC.2011.5779316.
- [102] Bing Maps. <http://www.bing.com/maps>, .
- [103] Google Maps. <http://maps.google.fr>, .

-
- [104] C. Oestges, N. Czink, B. Bandemer, P. Castiglione, F. Kaltenberger, and A. Paulraj. Experimental characterization of indoor multi-link channels. In *Personal, Indoor and Mobile Radio Communications, 2009 IEEE 20th International Symposium on*, pages 2985–2989, sept. 2009. doi: 10.1109/PIMRC.2009.5450278.
- [105] C. Oestges, N. Czink, B. Bandemer, P. Castiglione, F. Kaltenberger, and A.J. Paulraj. Experimental characterization and modeling of outdoor-to-indoor and indoor-to-indoor distributed channels. *Vehicular Technology, IEEE Transactions on*, 59(5):2253–2265, jun 2010. ISSN 0018-9545. doi: 10.1109/TVT.2010.2042475.
- [106] Meifang Zhu, Fredrik Tufvesson, and Jonas Medbo. Correlation properties of large scale parameters from 2.66 ghz multi-site macro cell measurements. In *Vehicular Technology Conference (VTC Spring), 2011 IEEE 73rd*, pages 1–5, may 2011. doi: 10.1109/VETECS.2011.5956712.
- [107] T.B. Sorensen. Correlation model for slow fading in a small urban macro cell. In *Personal, Indoor and Mobile Radio Communications, 1998. The Ninth IEEE International Symposium on*, volume 3, pages 1161–1165 vol.3, sep 1998. doi: 10.1109/PIMRC.1998.731361.
- [108] I-Kang Fu, Chi-Fang Li, Ting-Chen Song, and Wern-Ho Sheen. Correlation models for shadow fading simulation. Technical report, IEEE TGM Technical report, 2007.